Studies Into Vibration-Signature-Based Methods for System Identification, Damage Detection and Health Monitoring of Civil Infrastructures

by

Reza Jafarkhani

A Dissertation Presented to the
FACULTY OF THE USC GRADUATE SCHOOL
UNIVERSITY OF SOUTHERN CALIFORNIA
In Partial Fulfillment of the
Requirements of the Degree
DOCTOR OF PHILOSOPHY
(Civil Engineering)

May 2013

Dedicated to my beloved family back in Iran and to my late grandma, who passed away just before my defense.

Acknowledgements

I would first and foremost like to express my deep and sincere gratitude to my advisor, Professor Sami F. Masri, for his invaluable guidance, support, and encouragement during the course of my long graduate studies and preparation of this work. His breath of knowledge, mentorship, and expertise have been invaluable resources for me in choosing the direction of my work and fulfilling my desire to study in a multi-disciplinary setting. I would also like to thank the other members of my Ph.D committee, Professor L. Carter Wellford, Professor James C. Anderson, Professor Erik A. Johnson, and Professor Roger G. Ghanem. I am particularly thankful to Professor Ghanem for his cooperation of providing the exclusive access to the CPU clusters on HPCC. The assistance of Professor M. Saiid Saiidi of the University of Nevada, Reno and Dr. Nathan Johnson, his former PhD student, is highly appreciated. I am also thankful to Professor Bin Xu, Dr. Jia He and Dr. Ren Zhou of the Hunan University, China for providing access to the experimental data set.

I would like to thank my colleagues in our research group for their friendship and hours of useful discussions. They are Dr. Farzad Tasbihgoo, Dr. Reza D. Nayeri, Dr. Mohammadreza Jahanshahi, Dr. Hae-Bum (Andrew) Yun, Ali Bolourchi, Miguel G. Hernandez, Vahid Keshavarzzadeh and Armen Derkevorkian.

Last but not least, I must thank my beloved family back in Iran, especially my parents for constantly encouraging and inspiring me throughout my studies since the first day I went to school 28 years ago, and my brothers and sister for their love and support.

Finally, I gratefully acknowledge the partial support by the National Science Foundation (NSF).

Table of Contents

List of Figures

Abstract

Civil infrastructures play a vital role in human societies. Recent catastrophic events due to the deficiency, failure or malfunction of these systems, claiming many lives and resulting in substantial economic loss, have attracted extensive attention focused on reviewing and amending the design and maintenance procedures of civil infrastructures. In addition to the possible failure of structural components, long-term forms of damage due to deterioration or fatigue may also necessitate regular monitoring of civil structures. Therefore, depending on the importance, use and risk, the structure of interest needs to be equipped with inspection, monitoring and maintenance systems. Structural Health Monitoring (SHM) is generally associated with any engineering methodology whose aim is to detect, locate and quantify the damage in the target system. Vibration-based techniques, as the most conventional SHM approaches, acquire and analyze the structural response using a variety of sensors mounted at different locations on the structure. The main goal of the study reported herein is to investigate and evaluate different vibration-signature-based methods for system identification, damage detection and health monitoring of civil structures. Various well-known techniques such as finite element model updating approach and damage detection methods based on artificial neural networks are studied and evaluated. Experimental data from two case studies, a quarter-scale two-span bridge system, tested at the University of Nevada, Reno, and a 1/20 scale 4-story building equipped with smart devices of magneto-rheological (MR) damper, are used for investigation and validation purposes. Guidelines are established for the optimum selection of the dominant control parameters involved in the application of some of the robust SHM approaches for achieving reliable SHM results under realistic conditions.

Chapter I

INTRODUCTION

I.1 Background

CIVIL infrastructures such as high-rise buildings, dams, bridges and lifelines play a vital role in human societies. The investment of the United States in civil infrastructure is estimated to be $20 trillion. Recent catastrophic events due to the deficiency, failure or malfunction of these systems, claiming many lives and resulting in substantial economic loss, have attracted extensive attention focused on reviewing and amending the design and maintenance procedures of civil infrastructures.

One of the challenging issues in designing civil infrastructures is the high initial cost of these assets. Performance-based design, as a trade-off approach, may allow the structure to undergo some ductile inelastic deformation with an acceptable level of damage. Such damage is component-based rather than system-based, meaning that the structure as a whole will still perform to a desired level, despite the failure in one or more isolated elements. This design philosophy results in a cost-effective design and higher system reliability, at the expense of possible localized damage. Therefore, depending on its importance, use and risk, the structure needs to be equipped with inspection, monitoring and maintenance systems. Furthermore, long-term forms of damage due to deterioration or fatigue may also necessitate regular monitoring of civil infrastructures. Consequently, the ability to continuously monitor the integrity of civil infrastructures provides the opportunity to reduce maintenance costs, while increasing the safety to the public.

The topic of Structural Health Monitoring (SHM) is generally associated with any engineering methodology whose aim is to detect, locate and quantify the damage in the target system. Vibration-based SHM techniques acquire and analyze the structural response using a variety of sensors mounted at different locations on the structure. Broadly speaking, SHM may be interpreted as a "continuous system identification of a physical or parametric model of the structure using time-dependent data" (Brownjohn (2007)).

Vibration-based methods are the most conventional approaches for SHM, but other methodologies such as optical or acoustic emission techniques have also been developed and employed in this field. While SHM is usually associated with on-line global damage detection in the structure, it is often followed by off-line local damage detection strategies (e.g., Non-Destructive Evaluation (NDE)) if any damage is detected. Meanwhile, it should be noted that damage is not the only source of variations in the measured dynamic response of the system. Hence, understanding and detecting (quantifying) the effects of other influencing parameters such as system nonlinearity, temperature variations, unobserved excitations, soil-structure interactions, and measurement noise, should also be carefully investigated and considered (Nayeri et al. (2008)).

Application areas of SHM may include, but are not to be limited to the following categorizes (Brownjohn (2007)):

- Structures subject to long-term movement or degradation of materials
- Feedback loop to improve future design
- Assessment of post-earthquake structural integrity
- Fatigue assessment
- Complementary to performance-based design philosophy
- Modifications to an existing structure
- Monitoring of structures affected by external works or during demolition

I.2 Literature Review

Qualitative and non-continuous methods of SHM have long been used to evaluate structures and machineries for their capacity to serve the intended purpose. For instance, since the beginning of the 19^{th} century, the sound of a hammer striking on the train wheel was a useful tool to detect if damage was present. In the last half a century, the development of quantifiable SHM approaches has been closely coupled with the evolution of digital computing hardware and inexpensive, fast networking technologies. Significant developments in the field have originated from major construction projects, such as offshore gas/oil production installations, large dams and highways bridges. During the 1970s and 1980s, the oil industry received the greatest attention and research effort to develop damage identification methods for offshore platforms. Applications of vibration-based methods of SHM in the aerospace community started during the late 1970s and early 1980s in conjunction with the development of the space shuttle. The development of a composite fuel tank for a reusable launch vehicle in mid-1990s motivated studies of damage identification for composite materials. Since the early 1980s, the vibration-based damage assessment of bridge structures and buildings has been of interest to the civil engineering community (Farrar and Worden (2007)).

Some representative publications that provide a comprehensive overview of the broad interdisciplinary field of SHM, the main technical challenges, as well as promising proposed approaches that have the potential of being useful tools for damage detection purposes in different classes of civil infrastructure systems, are available in the works of Doebling et al. (1996), Hou et al. (2000), Wang et al. (2001), Chang et al. (2003), Staszewski et al. (2004), Hera and Hou (2004), Ko and Ni (2005), Kim et al. (2007), Farrar and Worden (2007), Brownjohn (2007), Wang (2007) and Chandrashekhar and Ganguli (2009).

I.3 Motivation and Technical Challenges

Generally speaking, any SHM process may be defined in terms of the following four-step statistical pattern recognition paradigm (Farrar and Worden (2007)):

(i). Operational evaluation

(ii). Data acquisition, normalization and cleansing

(iii). Feature selection and information condensation

(iv). Statistical model development for feature discrimination

Each step is involved with many technical challenges to the adaptation of SHM that are common to all applications of this technology. These challenges include (Farrar and Worden (2007)):

- How to optimally define the number and location of the sensors?

- How to identify the appropriate features that are sensitive to small damage levels?
- How to discriminate the changes due to damage from those caused by other parameters such as changing environmental and/or test conditions?
- What are the appropriate statistical methods to discriminate features from undamaged and damaged structures?

Every civil infrastructure is usually unique and may require developing a special and customized SHM strategy. It should be noted that the chosen SHM strategy might be a trade-off solution to different aspects of the problem. For instance, one of the basic current technical challenges in SHM is that, with a minimum of optimally located sensors, any damage to be detected must have significant effects on the underlying structural dynamic properties (e.g., stiffness, mass or damping) of the system, which, in turn results in a measurable change in the observed dynamic response. Unfortunately, this is not usually the case in real operational structures, since typical localized damage will not significantly influence the dominant lower-frequency modes of the monitored structure. With increasing widespread availability of sensor networks and data acquisition and communication capabilities, one may think of a dense, fine-grained sensor architecture as an intuitive solution, but any increase in the size of the problem will introduce new impediments in the form of processing huge amounts of multi-faceted data sets with embedded mathematical and computational challenges.

I.4 Scope

The main goal of the study reported herein is to investigate and evaluate different vibration-signature-based methods for system identification, damage detection and health monitoring of civil structures. The following chapter reports the performance of two stochastic methods of global optimization for a subset of well-known benchmark functions. The application of these methods in finite element model updating approaches for damage detection purposes is investigated in Chapter 3. The case study is a quarter-scale, two-span bridge system, experimentally tested at the University of Nevada, Reno. Chapter 4 reports the performance of different system identification approaches for experimentally recorded data of a 1/20 scale 4-story building equipped with smart devices of magneto-rheological (MR) damper. This case study is also studied in Chapter 5 to investigate the application of artificial neural networks for identification of nonlinear structural models. The last chapter provides a brief overview of the whole dissertation and highlights the concluding remarks.

Chapter II

COMPARISON OF DIFFERENT GLOBAL OPTIMIZATION TECHNIQUES FOR HIGH-DIMENSIONAL PROBLEMS

II.1 Introduction

STRUCTURAL health monitoring through the use of finite element model updating techniques for dispersed civil infrastructures usually deals with minimizing a complex, nonlinear, non-convex, high-dimensional cost function with several local minima. Hence, global optimization algorithms with promising performance have received considerable attention for finite element model updating purposes. In recent years, different types of optimization algorithms have been designed and applied to solve real-life optimization problems, especially with engineering applications. Some of the most well-known approaches include classical deterministic methods such as quasi-Newton method as well as stochastic approaches such as genetic algorithms, evolutionary strategies, particle swarm optimization, hybrid evolutionary-classical methods, other non-evolutionary methods such as simulated annealing (SA), tabu search (TS) and others.

Global optimization methods can be categorized as follows:

(i). **Deterministic methods**, in which the computation is completely determined by previously sampled values . This group of optimization approaches are not generally successful on non-convex high-dimensional functions. Some examples are algorithms based on real algebraic geometry, interval optimization methods and branch and bound methods.

(ii). **Stochastic methods**, that incorporate probabilistic elements in the optimization procedure. Genetic algorithms, evolutionary strategies and particle swarm optimization belong to this group of optimization methods.

II.1.1 Scope

In this chapter, we empirically investigate the global search performance of some well-known optimization packages on a subset of standard test problems. The remainder is organized as follows: A brief explanation of each optimization method, definition of the benchmark functions, common termination criteria, size of problems and initialization scheme are presented. The results of statistical study based on an ensemble of 100 simulations for each case are provided and discussed. In particular, the effects of function order as well as population size on the performance of these methods are investigated, followed by the summary and concluding remarks.

II.2 Optimization Methods under Discussion

II.2.1 CMA-ES

Evolutionary Strategy based on Covariance Matrix Adaptation, abbreviated as CMA-ES, was proposed for the first time in 1994 (Ostermeier et al. (1994)) and has been considerably developed since then. In this method, any new population is generated based on the multivariate normal mutation distribution with adapted covariance matrix. The adaptation is based on increasing the likelihood of previously realized successful mutation steps, as well as exploiting the evolution path of the distribution mean of the strategy.

Theoretical concept behind CMA-ES can be summarized as follows (Akimoto et al. (2012)). If the probability density function of the multivariate normal distribution with mean vector m and covariance matrix $\sigma^2 C$ is represented as $N(x, m, \sigma^2 C)$, the CMA-ES starts with the initial parameters of m^0, σ^0, C^0, $p_\sigma^0 = 0$ and $p_C^0 = 0$ and repeats the following steps:

(i). Generate λ independent sample points $x_1, x_2, ..., x_\lambda$ from $N(x, m, \sigma^2 C)$.

(ii). Evaluate the function values at sample points $f(x_1), f(x_2), ..., f(x_\lambda)$.

(iii). Update the parameters of the algorithm as follows.

Mean vector:

$$m^{t+1} = \sum_{i=1}^{\lambda} W_{R_i} X_i \tag{II.1}$$

where R_i is the ranking of $f(x_i)$. W_{R_i} represents the weight for the ${R_i}^{th}$ highest point and has the following properties:

$$0 \leq W_i \leq W_j \leq 1 \forall i > j \qquad \& \qquad \sum_{i=1}^{\lambda} W_i = 1 \tag{II.2}$$

Global step-size:

$$\sigma^{t+1} = \sigma^t exp\left(\frac{c_\sigma}{d_\sigma} \frac{p_\sigma^{t+1} - \chi_d}{\chi_d}\right) \tag{II.3}$$

where c_σ and d_σ denote learning rate and the damping parameter, respectively. χ_d is the

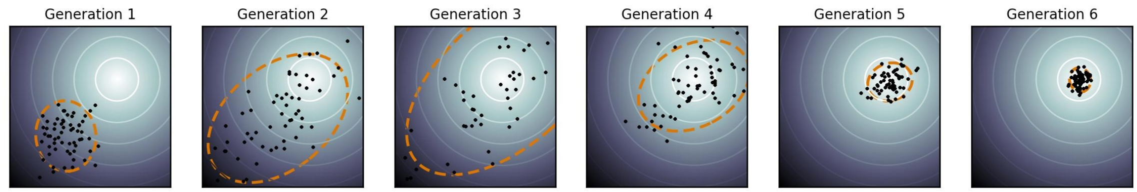

Figure II.1: Concept behind the covariance matrix adaptation for generation evolution. Two phenomena are observed as the generations develop: 1- The center of the new generation is shifted toward global minimum due to the weighting of the population for reproduction process. 2- The distribution shape adapts to an ellipsoidal or ridge-like landscape along the principle axis, which is the eigenvector corresponding to the largest eigenvalue of the covariance matrix. (figure adapted from http://en.wikipedia.org/wiki/CMA-ES).

expectation of the chi distribution with d degrees of freedom and p_σ is an evolution path being updated as

$$p_\sigma^{t+1} = (1-c_\sigma)p_\sigma^t + \sqrt{\frac{c_\sigma(2-c_\sigma)}{\sum_{i=1}^{\lambda} W_i^2}}\frac{(C^t)^{-\frac{1}{2}}(m^{t+1}-m^t)}{\sigma^t} \tag{II.4}$$

Covariance matrix:

$$C^{t+1} = (1-c_1-c_\mu)C^t + c_1 p_C^{t+1}(p_C^{t+1})^T + c_\mu \sum_{i=1}^{\lambda} W_{R_i}\frac{x_i-m^t}{\sigma^t}\left(\frac{x_i-m^t}{\sigma^t}\right)^T \tag{II.5}$$

where c_1 and c_μ are learning rate parameters and p_C is an evolution path, being updated as

$$p_C^{t+1} = (1-c_c)p_C^t + \sqrt{\frac{c_c(2-c_c)}{\sum_{i=1}^{\lambda} W_i^2}}\frac{(m^{t+1}-m^t)}{\sigma^t} \tag{II.6}$$

c_c represents the learning rate for the evolution path update.

Figure II.1 schematically illustrates the main concept behind the covariance matrix adaptation for a 2-D optimization problem. As shown, the search direction is modified such that the candidate solutions in the new generation are more likely to be sampled along the principle axis. Further details concerning this approach are available in Ostermeier et al. (1994). A module, written in MATLAB® by the developers of this optimization method, is used for this study.

II.2.2 Genetic algorithm

Genetic algorithms are considered as a computational analogy of adaptive systems. They are modeled based on the principles of the evolution of generations via natural selection, mutation and crossover. Evaluation of the individuals is performed using a fitness (cost) function. General paradigm of genetic algorithm methods involves:

(i). Initialization: Randomly generation of an initial population.

(ii). Selection: Selection a proportion of the existing population based on fitness to breed a new generation.

(iii). Reproduction: Production of the new generation population through genetic operators such as crossover and mutation.

(iv). Termination: Repeating step 2 and 3 until satisfying solution is obtained.

For this study, the **ga** module in the Optimization Toolbox of MATLAB® is exploited.

II.3 Test functions

In the field of global optimization methods, it is common to compare different algorithms using a large test set. Five well-known benchmark function are considered in this section to evaluate and compare the performance of global optimization methods under discussion. The benchmark functions include:

(i). **Rosenbrock function**: Function with a deep valley with the shape of a parabola.

(ii). **Schwefel function**: Function composed of a great number of peaks and valleys.

(iii). **Ackley function**: Function with an exponential term that covers its surface with numerous local minima.

(iv). **Rastrigin function**: Function made up of a large number of local minima whose value increases with the distance to the global minimum.

(v). **Griewank function**: Function with a product term that introduces interdependence among the variables.

Rosnebrock function is symmetric, uni-modal and non-separable with the global minimum at $\underset{\sim}{x} = 1.0$. The rest of the test problems have a high number of local optima (multi-modal), and are scalable in the problem dimension. The Rastrigin and Schwefel functions are additively separable, while Ackley function is separable, in that the global optimum can be located by optimizing each variable independently. Griewank is considered a partially separable function. The known global minimum is located at $\underset{\sim}{x} = 0.0$ for all functions, except for the Schwefel function, where the global minimum within $[-500; 500]^n$ resides at $\underset{\sim}{x} = 420.9687$. All the test problems have a global minimal function value of 0. Figure II.2 to II.6 show 2-D plots of the functions under investigation. The definition of each function as well as the range of interest and the global minimum are also provided in these figures. The termination criteria in the optimization process are defined as follows:

$$\mathbf{f} \leq 10^{-4} \qquad \Delta\mathbf{f} \leq 10^{-10}$$

$$\Delta\mathbf{x} \leq 10^{-10} \qquad Max_{eval} = \infty$$

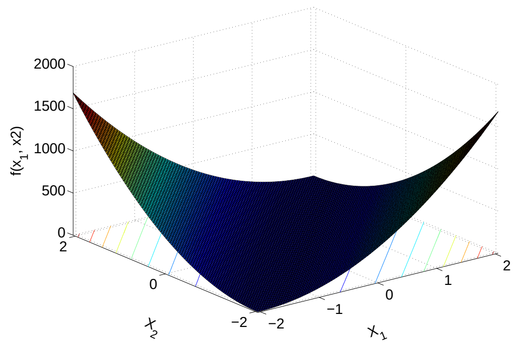

Full range plot

Figure II.2: Plot of 2-D Rosenbrock function.

$$\mathbf{f} = \sum_{i=1}^{n-1} \left(100(\mathbf{x}_{i+1} - \mathbf{x}_i^2)^2 + (1 - \mathbf{x}_i)^2\right)$$
$$-2.048 \leq \mathbf{x}_i \leq 2.048$$
$$Min \quad @ \quad \underset{\sim}{\mathbf{x}} = 1.0$$

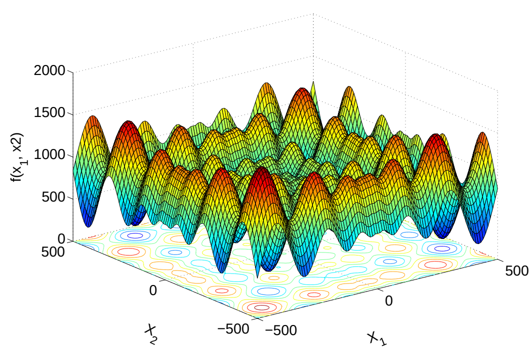

Full range plot

Figure II.3: Plot of 2-D Schwefel function.

$$\mathbf{f} = \sum_{i=1}^{n} \left(-\mathbf{x}_i \sin\left(\sqrt{|\mathbf{x}_i|}\right) + 418.9829\right)$$
$$-500 \leq \mathbf{x}_i \leq 500$$
$$Min \quad @ \quad \underset{\sim}{\mathbf{x}} = 420.9687$$

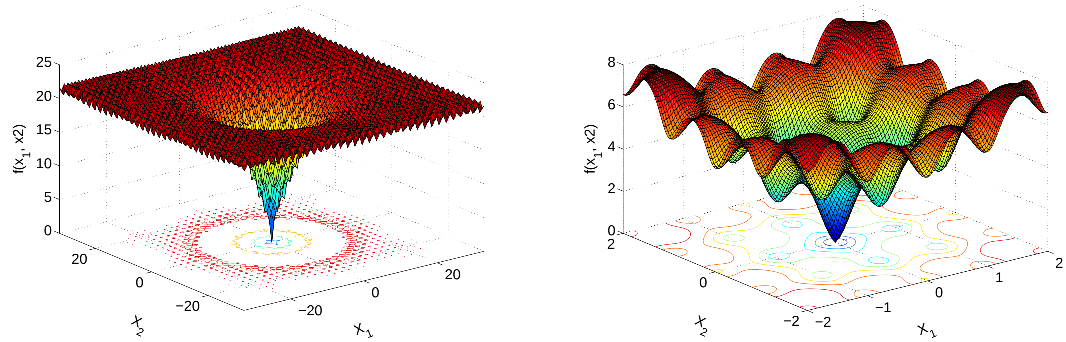

(a) Full range plot

(b) Focus around global minimum

Figure II.4: Plot of 2-D Ackley function.

$$\mathbf{f} = -a * e^{-b\sqrt{\frac{\sum_{i=0}^{n}\mathbf{x}_i^2}{n}}} - e^{\frac{\sum_{i=0}^{n} c.\cos(\mathbf{x}_i)}{n}} + a + e$$

$$-32.768 \leq \mathbf{x}_i \leq 32.768 \quad a = 20 \quad b = 0.2 \quad c = 2\pi$$

$$Min \quad @ \quad \underset{\sim}{\mathbf{x}} = 0.0$$

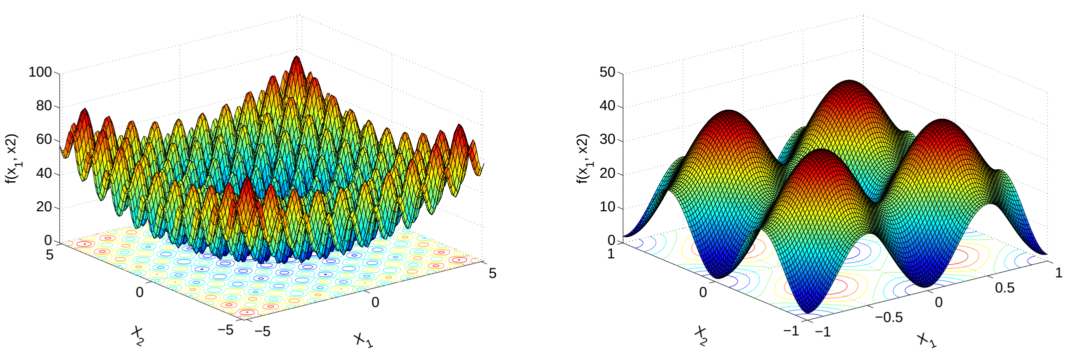

(a) Full range plot

(b) Focus around global minimum

Figure II.5: Plot of 2-D Rastrigin function.

$$\mathbf{f} = 10n + \sum_{i=1}^{n}\left(\mathbf{x}_i^2 - 10\cos(2\pi\mathbf{x}_i)\right)$$

$$-5.12 \leq \mathbf{x}_i \leq 5.12$$

$$Min \quad @ \quad \underset{\sim}{\mathbf{x}} = 0.0$$

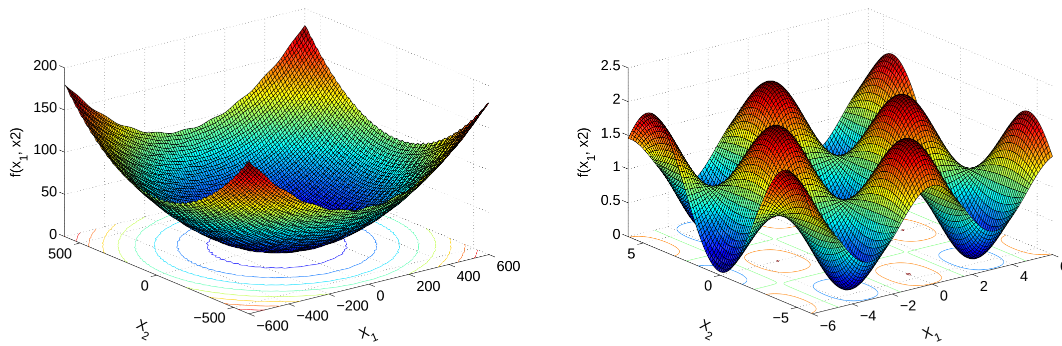

(a) Full range plot (b) Focus around global minimum

Figure II.6: Plot of 2-D Griewank function.

$$\mathbf{f} = \sum_{i=1}^{n} \frac{\mathbf{x}_i^2}{4000} - \prod_{i=1}^{n} \cos\left(\frac{\mathbf{x}_i}{\sqrt{i}}\right) + 1$$
$$-600 \leq \mathbf{x}_i \leq 600$$
$$Min \quad @ \quad \underset{\sim}{\mathbf{x}} = 0.0$$

II.4 Results and discussion

Preliminary investigation of optimization methods under discussion shows that the success rate to reach f_{stop} strongly depends on the population size and problem dimension with other parameters of less of influence. Therefore, it is decided to study the effects of these two parameters on the performance of global optimization methods. A statistical study based on an ensemble of 100 simulations for each case is conducted. The starting point x_0 is sampled uniformly within the initialization intervals. All the data history of each optimization process is recorded in a MAT file with double digit precision.

II.4.1 Problem-order effects

The dimensionality of the search space is an important factor in the complexity of the problem. In order to establish different degrees of difficulty in the problems, we have chosen a search space of dimensionality of $n = 5, 10, 25, 50, 100$ for each test functions. For both CMA-ES and GA

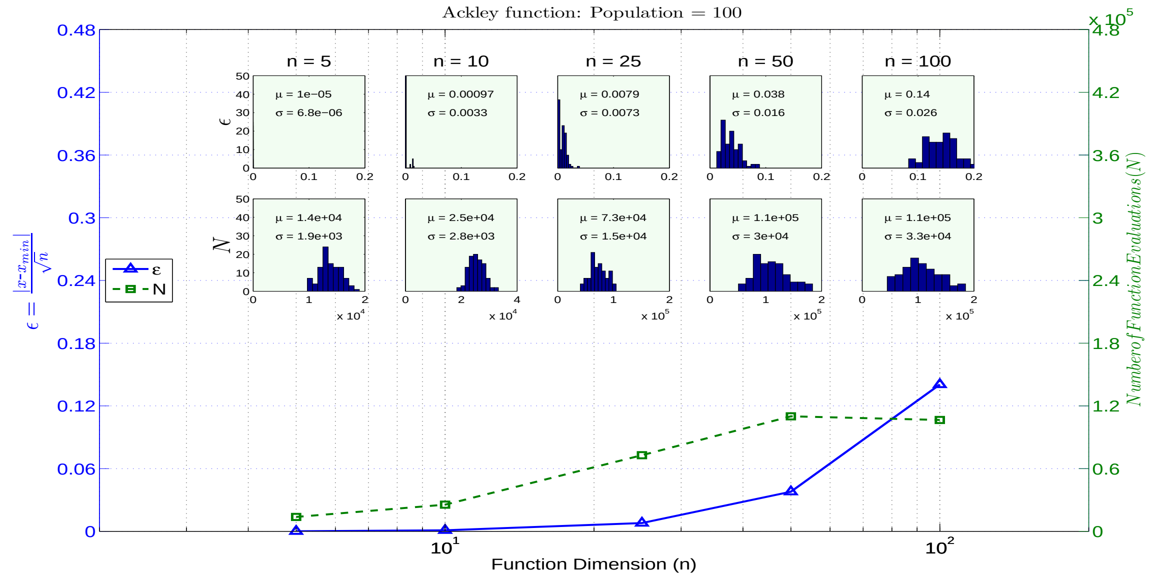

(a) GA

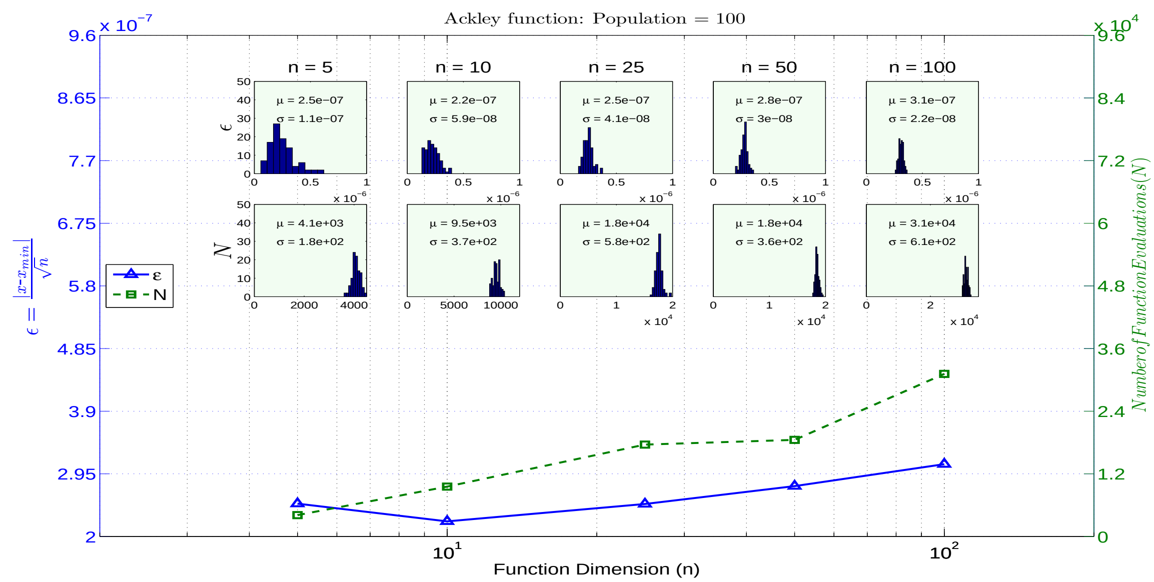

(b) CMA-ES

Figure II.7: Effects of problem-order on the performance of evolutionary optimization methods (GA and CMA-ES) for Ackley function. Population size in each generation is set as 100. The results are based on 100 simulations for each case. In each plot, the solid line shows the average of normalized error in the final solution vector while the dashed line indicates the average number of function evaluation to reach the solution. The statistical distribution for normalized error of the final solution and average number of function evolutions are also shown in small subplots. Note that the relatively small mean value and standard deviation of the normalized error (with respect to the dimension range = 32.768) shows the robustness and fidelity of these methods in solving high-order problems.

algorithms, all 100 runs in each case are performed with the default strategy parameter defined in the packages except for the population size, which is selected as $Pop = 100$.

The performance of optimization methods is highly influenced by the problem dimension. As shown in Figure II.7, where exemplary results are illustrated for Ackley function, normalized error of the solution vector slightly increases for higher function dimensions. As expected, both optimization methods require significantly more function evolutions to reach the solution for higher problem orders. The statistical distribution for normalized error of the final solution and average number of function evolutions are also plotted in this figure. For ease of comparison between different cases, the error is defined as the deviation of the final solution vector from exact global minimum, normalized with respect to the problem-order. Based on this definition, the error can be represented as:

$$\epsilon = \frac{|\underset{\sim}{x} - \underset{\sim}{x}_{min}|}{\sqrt{n}} \tag{II.7}$$

where ϵ is the normalized error, $\underset{\sim}{x}$ is the final solution found by the optimization method, $\underset{\sim}{x}_{min}$ is the exact global minimum, and n is the function dimension. Note that the relatively small mean value and standard deviation of the normalized error shows the robustness and fidelity of these methods in solving high order problems. Comparing Figure II.7(a) and Figure II.7(b) also shows that the average number of required function evaluations in CMA-ES to reach the solution increases almost linearly with the problem-order. On the other hand, the corresponding plot for GA illustrates superlinear behavior. The Ackley function represents the typical picture for the effects of problem-order on the performance of global optimization methods.

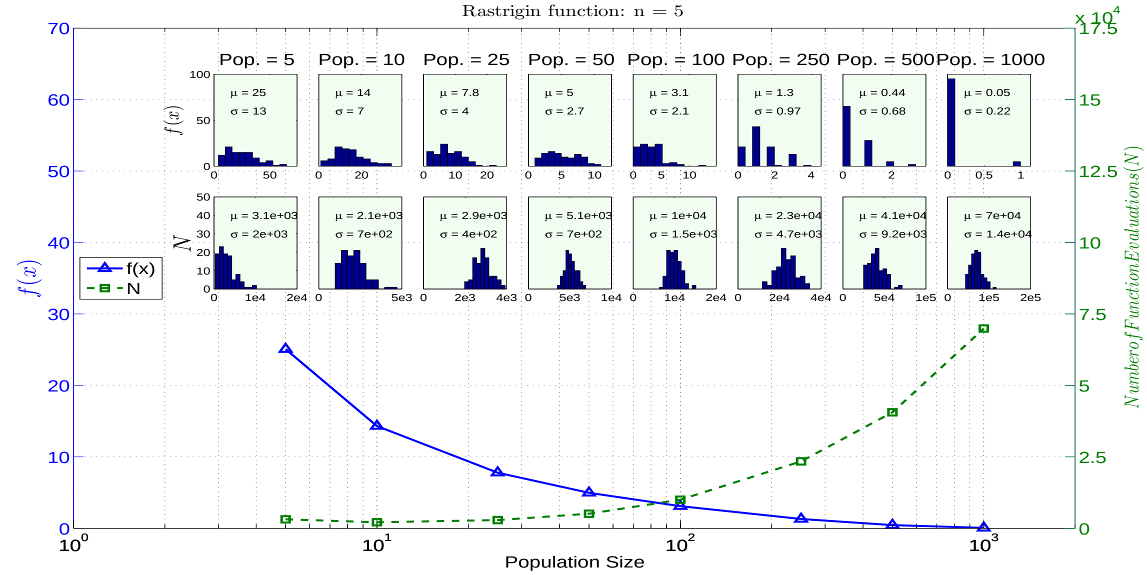

(a) GA

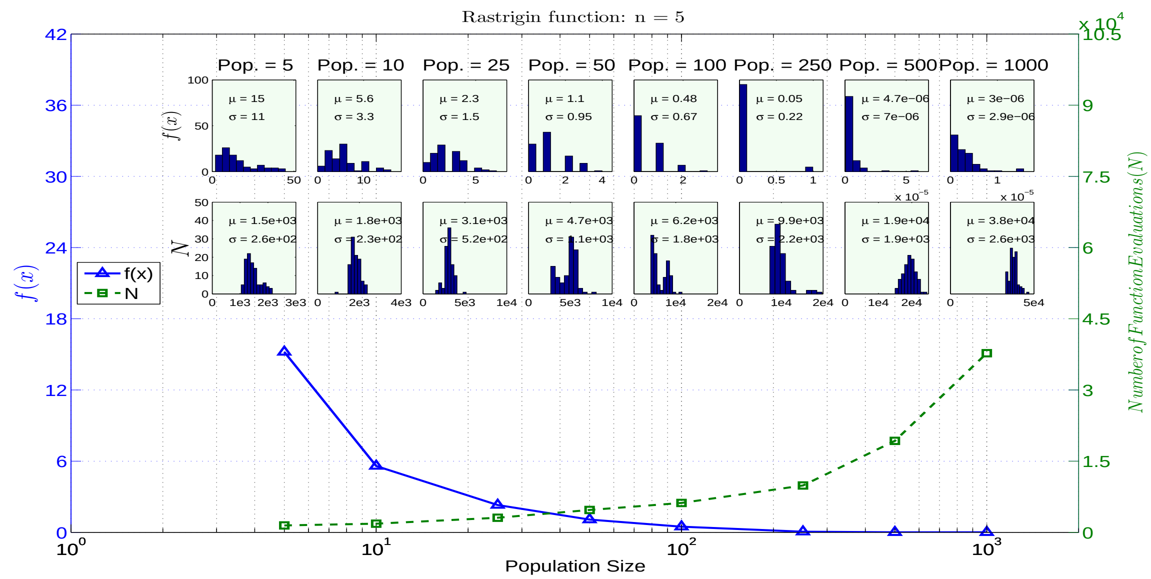

(b) CMA-ES

Figure II.8: Effects of population size on the performance of evolutionary optimization methods (GA and CMA-ES) for Rastrigin function of order $n = 5$. The population size of $Pop = 5, 10, 25, 50, 100, 250, 500, 1000$ is implemented. The results are based on 100 simulations for each case. In each plot, the solid line shows the final function value while the dashed line indicates the average number of function evaluation to reach the solution. The statistical distribution for the final function value and number of function evolutions are also shown in small subplots. Note that the success rate to reach better results (i.e., lower function value) strongly improves for larger population sizes, at the expense of higher computational effort (i.e., higher number of function evolutions).

II.4.2 Population size effects

The effects of the population size on the performance of evolutionary methods are also investigated in this study. To do so, the population sizes of $Pop = 5, 10, 25, 50, 100, 250, 500, 1000$ are implemented for a given problem size for each test function. Figure II.8 illustrates the performance versus population size for Rastrigin function of order $n = 5$, based on 100 simulations for each case. The statistical distribution for the final function value and average number of function evolutions are also shown in small subplots. As shown in this figure, the success rate to reach better results (i.e., lower function value) improves for larger population sizes, at the expense of higher computational effort (i.e., higher number of function evolutions).

II.5 Concluding Remarks

In this study, the performance of two global optimization methods are empirically investigated on a subset of well-known test functions. The global optimization algorithms under discussion were Genetic Algorithm (**ga** modules in MATLAB®) and an evolutionary strategy called CMA-ES. A suit of five standard test functions with a search space of dimensionality $n = 5, 10, 25, 50, 100$ was considered to study the effects of the problem-order on the performance of the optimization methods. In addition, the effects of population size on the performance of evolutionary methods are investigated for a subset of population sizes of $Pop = 5, 10, 25, 50, 100, 250, 500, 1000$. For each case, an ensemble of 100 simulations was generated to reach a reliable statistical data set. Based on the comparison of these results, the following conclusions can be made:

- Evolutionary stochastic optimization methods are generally successful in solving high-dimensional problems.

- As expected, both optimization methods require significantly more function evolutions to reach the solution for higher problem orders.

- Increasing the population size remarkably improves the performance of these methods at the expense of higher number of function evaluations. The study shows that the optimal population size takes a wide range of values depending on the cost function. For a given objective function, the optimum population size may be tuned through calibration process with the help of a statistical analysis.

- For multi-modal functions, CMA-ES shows better performance than GA in the sense that it returns smaller final function value with less average number of required function evaluations to reach the solution. For instance, while CMA-ES outperform GA on Ackley and Rastrigin functions (as shown in Figures II.7 and II.8), it significantly falls behind GA on Rosenbrock function. Noting that Rosenbrock is the only uni-modal non-separable test function of this study, this indicates that the performance of these optimization packages varies with the topography of the functions. This conclusion also agrees with the findings of the developers of CMA-ES, reported in Hansen and Kern (2004).

Chapter III

FINITE ELEMENT MODEL UPDATING USING EVOLUTIONARY STRATEGIES

III.1 Introduction

IN this chapter, the performance of global optimization methods which were discussed in the previous chapter is investigated for damage detection purposes, through the finite element model updating approach. The case study is a quarter-scale, two-span, reinforced concrete bridge system, which was investigated experimentally at the University of Nevada, Reno. The damage sequence in the structure was induced by a range of progressively-increasing excitations in the transverse direction of the specimen. Intermediate nondestructive white noise excitations and response measurements were used for system identification and damage detection purposes. It is shown that, when evaluated together with the strain gauge measurements and visual inspection results, the applied finite element model updating algorithm of this study could accurately detect, localize, and quantify the damage in the tested bridge columns throughout different phases of the experiment.

III.1.1 Literature Review

The finite element model updating method has been studied for many years as an important subject in the mechanical and aerospace engineering fields. It has also developed into a major research area within the field of SHM, responding to an increasing demand for evaluating the integrity of civil infrastructures. Many research projects have been conducted to develop a successful tool in structural health monitoring through finite element model updating methods. Most of these techniques are based on searching for an admissible set of structural parameters to minimize an error function involving the analytical and measured dynamic response. The success of these methodologies strongly depends on having a suitable definition for the cost function, an appropriate analytical model, an accurate system identification approach, and an effective robust optimization algorithm for global minimization.

Some representative publications that provide a comprehensive overview of the broad interdisciplinary field of finite element model updating for SHM, the main technical challenges, as well as promising proposed approaches that have the potential of being useful tools for damage detection purposes in different classes of civil infrastructure systems, are available in the works of Farhat and Hemez (1993), Adeli and Cheng (1994a), Zimmerman and Kaouk (1994), Adeli and Cheng (1994b), Friswell and Mottershead (1995), Doebling et al. (1996), Levin and Lieven (1998), Atalla and Inman (1998), Fritzen et al. (1998), Doebling et al. (1998), Hemez and Doebling (2001), Teughels et al. (2002), Jaishi and Ren (2005), Chu et al. (2008), Ni et al. (2008), and Cheung and Beck (2009).

III.1.2 Motivation and Technical Challenges

One of the basic current technical challenges in SHM is that, with a minimum of optimally located sensors, any damage to be detected must have significant effects on the underlying structural dynamic properties (e.g., stiffness, mass or damping) of the system, which, in turn results in a measurable change in the observed dynamic response. Unfortunately, this is not usually the case in real operational structures, since typical localized damage of interest in practical SHM applications may not induce significant influence on the dominant lower frequencies and the corresponding mode shapes of the monitored structure (unless it happens to occur at locations of high strain energy).

With increasing widespread availability of sensor networks and data acquisition and communication capabilities, one may think of a dense, fine-grained sensor architecture as an intuitive solution, but any increase in the size of the problem will introduce new impediments in the form of processing huge amounts of multi-faceted data sets with embedded mathematical and computational challenges. Of particular relevance to potential applications of finite element model updating approaches for SHM in conjunction with dispersed systems are issues dealing with minimization of a complex, non-linear, non-convex, high-dimensional cost function with several local minima. The more complicated the structure is with greater number of variables, the less likely the optimal solution is found by means of conventional deterministic optimization methods.

The major strides that have been achieved in the recent past with regard to the development of numerical optimization techniques for engineering applications, coupled with the tremendous increase of computational power, bring SHM through model updating approaches for large-scale structures within the realm of practicality. Specifically, the fact that stochastic optimization techniques, such as evolutionary algorithms, simulated annealing, and other random search methods have shown promising performance in solving global optimization problems is one of the main drivers for the growing interest in the investigation and implementation of these methods for large-scale finite element model updating approaches.

III.1.3 Scope

As a component of a collaborative multi-university, multi-disciplinary project utilizing the Network for Earthquake Engineering Simulation (NEES), a comprehensive series of experimental studies have been recently conducted at the University of Nevada, Reno (NEES@Reno) on large bridge systems. Recorded from densely-instrumented test specimens with a very large number of accelerometers, displacement transducers, and strain gauges at several locations and in different orientations, this collection of data provides a unique opportunity for applications in various fields of earthquake engineering, including the development and evaluation of structural health monitoring methodologies and damage detection techniques.

The main goal of the study reported here is to investigate the performance of two global optimization methods in finite element model updating approaches for damage detection purposes. The developed damage detection method was implemented on the NEES@Reno recorded data from the shake-table experiments conducted on a quarter-scale, two-span bridge system. The specimen was gradually damaged due to a sequence of low (Peak Ground Acceleration = 0.075g) to high (PGA = 2.11g) amplitude progressive excitations in the transverse direction. Intermediate nondestructive white noise excitations were also applied to the structure for system identification and damage detection purposes.

The remainder of this chapter is organized as follows. Section III.2 provides an overview of the system identification approach and finite element model updating technique used in this study; section III.3 describes the test bridge, data collection, and computational model; and section III.4 reports and discusses the damage-detection results and investigates the effectiveness of the proposed approach. Section III.5 highlights the concluding remarks.

III.2 Overview of Identification Approach

III.2.1 Subspace Method for System Identification

The subspace state-space system identification algorithm (**n4sid** module in the System Identification Toolbox of MATLAB®) was employed for this study. Subspace algorithms have been shown to be computationally very efficient and robust, specially for large data sets and large-scale systems. The two main steps in the subspace system identification methods can be summarized as follows (De Cock and De Moor (2003)):

(i). Estimating the Kalman filter state sequence of the dynamical system without any prior knowledge of the mathematical model, through an orthogonal or oblique projections of row spaces of data block Hankel matrices, and then determining the order, the observability matrix and/or the state sequence, by applying a singular value decomposition.

(ii). State space model realization through the solution of a linear least-squares problem.

Various linear algebra algorithms such as QR and singular value decomposition may be implemented in different stages of this procedure. The main principles of subspace identification methods with related mathematical derivations are available in De Cock and De Moor (2003).

The k^{th} time step in the discrete-time state-space representation of a Linear, Time-Invariant (LTI) model can be expressed as:

$$\begin{aligned} x_{k+1} &= \mathbf{A}x_k + \mathbf{B}u_k + w_k \\ y_k &= \mathbf{C}x_k + \mathbf{D}u_k + v_k \end{aligned} \tag{III.1}$$

where x, y and u represent the state, output and input vectors, respectively. Process noise (w) and measurement noise (v) are assumed to be zero-mean, stationary, white-noise vector sequences. The state space realization to estimate matrices $\mathbf{A}$ (dynamical system matrix), $\mathbf{B}$ (input matrix), $\mathbf{C}$ (output matrix) and $\mathbf{D}$ (feedthrough matrix) can be achieved by means of the subspace system identification algorithm (Ljung (1986)). It is impossible to measure the input term u in the case of ambient vibration; however, it can be modeled as white noise in the following form:

$$\begin{aligned} x_{k+1} &= \mathbf{A}x_k + w_k \\ y_k &= \mathbf{C}x_k + v_k \end{aligned} \tag{III.2}$$

This simplified model is suitable as long as the input does not contain some dominant frequency components in addition to white noise; otherwise, those frequency components cannot be separated from the eigenfrequencies of the system (Skolnik et al. (2006)). If eigendecomposition of the state matrix ($\mathbf{A}$) is represented in the form of:

$$\mathbf{A} = \mathbf{\Psi}\mathbf{\Lambda}\mathbf{\Psi}^{-1} \tag{III.3}$$

where $\mathbf{\Psi}$ and $\mathbf{\Lambda}$ are eigenvector and eigenvalue matrices respectively, the modal properties of a continuous-time structural system can be subsequently derived from (Nayeri (2007)):

$$\begin{aligned}
\mathbf{\Lambda} &= diag(\overline{\sigma}_i \pm j\overline{\Omega}_i) && \text{(III.4)}\\
\sigma_i \pm j\Omega_i &= \frac{\ln(\overline{\sigma}_i \pm j\overline{\Omega}_i)}{\Delta t} && \text{(III.5)}\\
\omega_i &= \sqrt{\sigma_i^2 + \Omega_i^2} && \text{(III.6)}\\
\zeta_i &= -\cos\left[\tan^{-1}(\frac{\Omega_i}{\sigma_i})\right] && \text{(III.7)}\\
\underset{\sim}{\Phi}_i &= \mathbf{C}\underset{\sim}{\Psi}_i && \text{(III.8)}
\end{aligned}$$

where ω_i, ζ_i and $\underset{\sim}{\Phi}_i$ represent the natural frequency, damping ratio, and the mode shape of the i^{th} mode of the system, respectively. Through the use of stability diagrams, the physical modal properties of the structure can be accurately identified and distinguished from the spurious ones usually generated due to the sensor noise and measurement errors.

III.2.2 Formulation of Cost Function

The cost function describes a Potential Energy Surface (PES) in the parameter space, and its global minimum optimizes the desired objective. One of the most common feature-extraction methods in finite element model updating is based on correlating the measured system response, in the frequency or time domain, with the corresponding quantities in the analytical model. For the study reported herein, the cost function to be minimized in the model updating process is calculated by cumulatively summing over the first n dominant modes of the structure. Each term, corresponding to one of the structural modes, is the summation of two weighted, normalized values which quantify the deviation of the analytical frequency and mode shape from the corresponding measured ones. From this definition, the cost function can be written as follows:

$$J(\underset{\sim}{\alpha}) = \sum_{i=1}^{n}\left[W_{f_i}|\frac{f_i^{(e)} - f_i^{(a)}}{f_i^{(e)}}|^2 + W_{\underset{\sim}{\Phi}_i}\left(1 - \frac{|\underset{\sim}{\Phi}_i^{(e)T}\underset{\sim}{\Phi}_i^{(a)}|^2}{(\underset{\sim}{\Phi}_i^{(e)T}\underset{\sim}{\Phi}_i^{(e)})(\underset{\sim}{\Phi}_i^{(a)T}\underset{\sim}{\Phi}_i^{(a)})}\right)\right] \qquad \text{(III.9)}$$

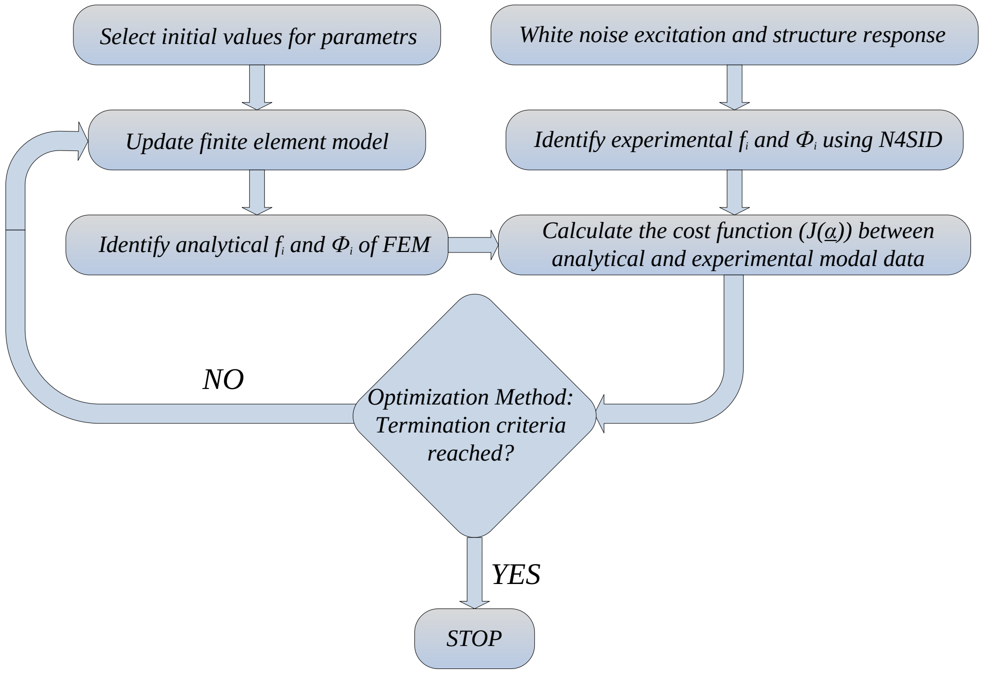

Figure III.1: Flowchart of finite element model updating process.

where $\underset{\sim}{\alpha}$ is the set of input parameters to be identified, f_i and $\underset{\sim}{\Phi}_i$ represent the natural frequency and the mode shape of the i^{th} mode, and W_i denotes the corresponding weight. Superscripts (e) and (a) stand for experimental and analytical results, respectively. The flowchart in Figure III.1 illustrates the steps in finite element model updating process.

III.3 Experimental Case Study

III.3.1 Description of Test Bridge Structure

The case study to illustrate the application of the method under discussion is a two-span reinforced concrete bridge tested experimentally at the University of Nevada, Reno. The quarter-scale specimen has equal span-length of 30 ft (9.14 m) and three double-column bents with variable column heights of 6 ft (1.83 m), 8 ft (2.44 m), and 5 ft (1.52 m) respectively. The column section is a

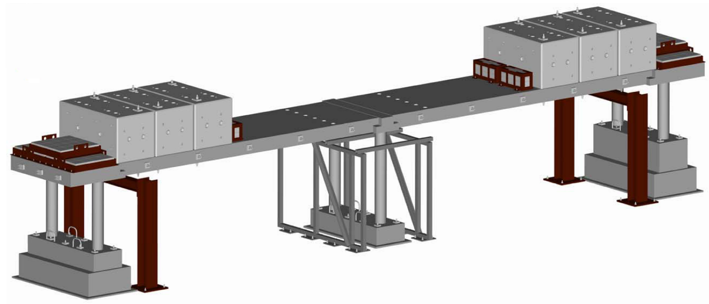

Figure III.2: Rendering of the bridge structure (adapted from Johnson et al. (2006)).

1 ft diameter circular reinforced concrete with 1.56% longitudinal steel ratio. The deck of the bridge is a precast slab with post-tensioned reinforcement in both the longitudinal and transverse directions. It consists of six superstructure beams (three on each span) resting on the ledges at the top of the columns. An amount of 280 kip (1245 kN) of additional mass is also provided on the slab to consider scaling effects. More detailed information about this structure and the related experimental study are available in Johnson et al. (2006). Figure III.2 shows a rendering of the bridge structure.

III.3.2 Destructive Shaking Procedure

The bridge was tested under simulated excitations based on records from the Century City Country Club (1994 Northridge earthquake). Different levels of shaking amplitude, covering the range of PGA = 0.075g $\sim$ 2.11g, were conducted on the structure. Intermediate, white-noise excitations were also applied for system identification purposes (Johnson et al. (2006)). Although the specimen underwent these excitations at different times, a combined 390-sec time-history for each record was used in this paper. The corresponding combined time-history record for the sequence of excitations in the transverse direction is shown in Figure III.3, and its specifications are presented in Table III.1.

Table III.1: NEES@Reno information of the combined time-history record for the excitations in the transverse direction as shown in Figure III.3.

Test	Ground Motion	T_{start} (sec)	T_{end} (sec)	PGA(g)
WN-1	White Noise	0	60	0.07
Test-13	Low Earthquake	60	75	0.18
Test-14	Moderate Earthquake	75	90	0.31
WN-2	White Noise	90	150	0.07
Test-15	High Earthquake	150	165	0.68
Test-17	High Earthquake	165	180	1.26
WN-3	White Noise	180	240	0.07
Test-18	Severe Earthquake	240	255	1.65
WN-4	White Noise	255	315	0.07
Test-19	Extreme Earthquake	315	330	2.11
WN-5	White Noise	330	390	0.07

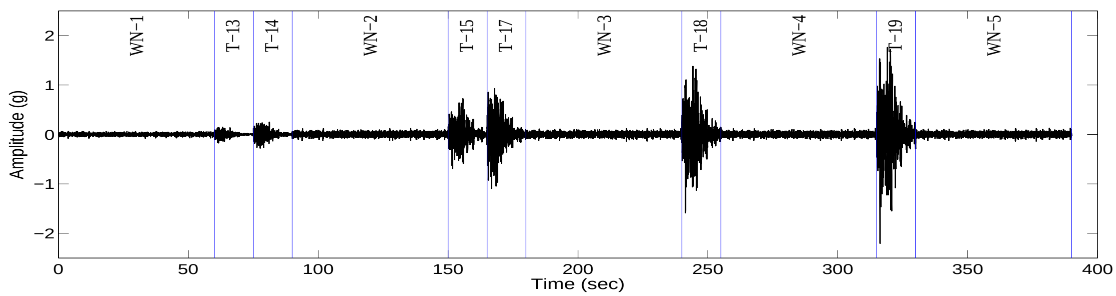

Figure III.3: NEES@Reno combined time-history record for the sequence of the excitations applied to the bridge model in the transverse direction. Windows indicated by WN-i represent the ith white noise excitation test, and windows designated by T-n denote earthquake-like test number n. Note the significant difference in test levels covering the 390-sec record.

III.3.3 Instrumentation, Data Acquisition and Filtering

Extensive instrumentation consisting of 298 channels (25 for slab displacements, 3 for footing slip, 68 for column curvatures, 15 for column shear, 14 for slab accelerations, 1 for support frame acceleration, 104 for longitudinal reinforcement strain, 56 for transverse reinforcement strain, and 12 for shake table response) were used to record the data at the frequency rate of 100 Hz (Johnson et al. (2006)). From a practical point of view, real structures outside of the lab environment do not generally enjoy such a comprehensive level of instrumentation. Consequently, it was decided for the purposes of the study reported here, to also investigate a case under the assumption that only

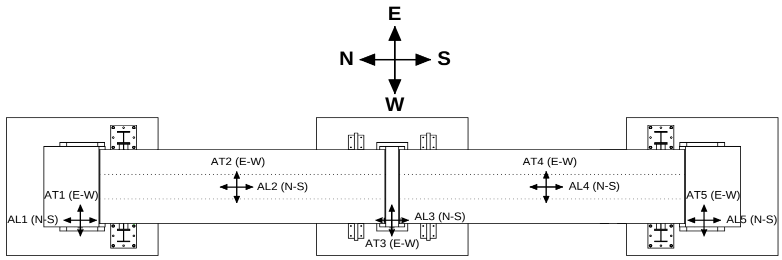

(a) Top View

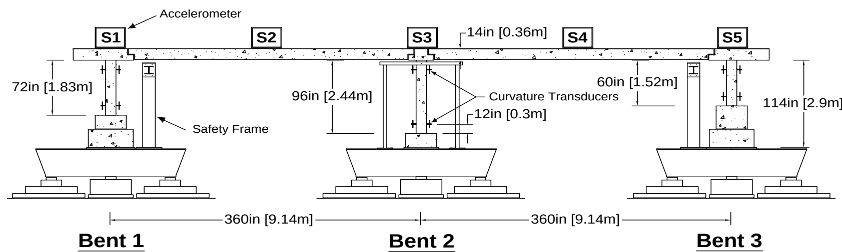

(b) Elevation View

Figure III.4: Top View (a) and Elevation View (b) of the NEES@Reno bridge, together with selected sensor locations for this study. S1 to S5 denote the location of accelerometers on the bridge deck. (adapted from Johnson et al. (2006)).

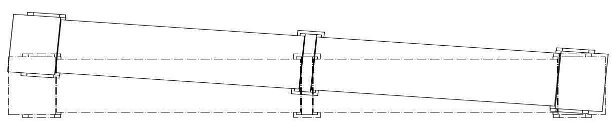

(a) 1^{st} Transverse mode shape (f = 3.09 Hz)

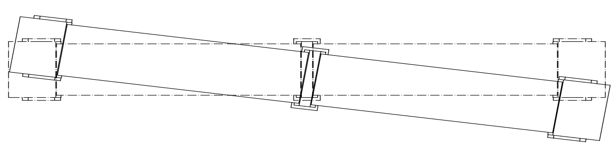

(b) 2^{nd} Transverse mode shape (f = 4.15 Hz)

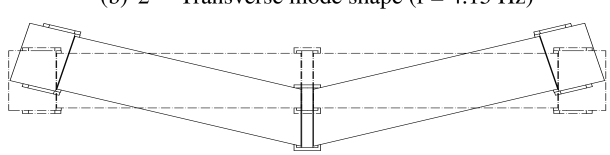

(c) 3^{rd} Transverse mode shape (f = 12.90 Hz)

Figure III.5: First three identified transverse mode shapes of the tested structure in the undamaged state.

a limited number of sensors is available. The following two scenarios were considered:

(i). Only time-history records in both the longitudinal and transverse directions of the bridge obtained from the five accelerometers on the deck are available.

(ii). Time-history records of the accelerometers on the deck as well as column curvature transducers are available.

Figure III.4 illustrates the location of the selected instrumentation for this study, deployed by the NEES@Reno team on the tested bridge structure.

The first three transverse modes, in addition to the first longitudinal mode, were considered in the calculation of the cost function. Note that, since the deck of the bridge is rigid, considering the physics of the problem, it is impossible to evaluate the stiffness of the structure and detect damage in the column level by just using the data from the sensors on the superstructure. Therefore the second scenario requires more data from the curvature transducers on the top and the bottom of the columns. In the definition of mode shapes for the cost function in the second scenario, the measurements from the curvature transducers were used to determine the rotational degrees of freedom about the longitudinal axis of the structure at the distance of 8.5 in (21.6 cm) from the end of the columns. As illustrated in Figure III.5, based on the data processing conducted for this study, the first transverse mode was identified as a dominant deck translation with slight in-plane rotation (f = 3.09 Hz); the second mode as a dominant deck in-plane rotation with slight translation (f = 4.15 Hz), and the third one as a deck bending (f = 12.90 Hz). The first longitudinal mode was in translation and dominated the longitudinal response (f = 2.99 Hz). System identification results for the aforementioned modes with low-pass filtered data at 25 Hz or at any higher range were found to be identical. Consequently, a low-pass filter of 25 Hz was applied to all the processed records.

III.3.4 NASTRAN® Finite Element Model

With the assumption that the behavior of the tested bridge would stay in the linear region when it underwent low amplitude white-noise excitation, a NASTRAN® computer model was developed using linear beam column elements. The NASTRAN® model emulated the SAP2000 model provided by the NEES@Reno research team who conducted the bridge test. Gross section properties were used for all of the elements, but the stiffness of the reinforced columns were calibrated and updated to represent the equivalent cracked moment of inertia.

As mentioned earlier, two scenarios were considered for investigating the model updating procedure:

- **Scenario 1**: Modal properties were identified based on the records from the 5 accelerometers on the deck. Based on system identification results from white-noise excitation records after each destructive shaking test, a 4-dimensional cost function (3 parameters for the stiffness of the bents in the transverse direction + 1 parameter for the longitudinal stiffness of all bents) was optimized to quantify the overall damage in the bents.

- **Scenario 2**: Modal properties were identified based on the records from 17 sensors (5 accelerometers on the deck + 12 curvature transducers on the top and bottom of the columns). A 13-dimensional cost function (12 parameters for the stiffness on the top and bottom of the columns in the transverse direction + 1 parameter for the longitudinal stiffness of all columns) was optimized to detect and quantify the overall and localized damage for each column, after each destructive shaking test.

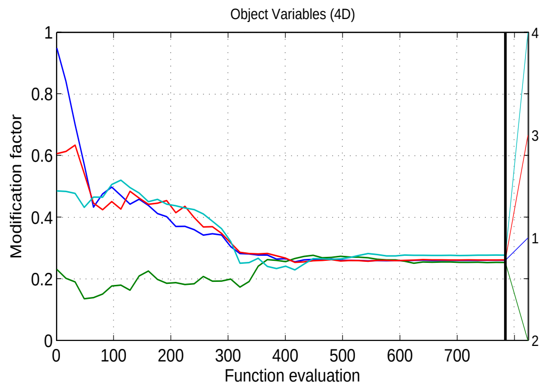

(a) Scenario 1 - CMA-ES

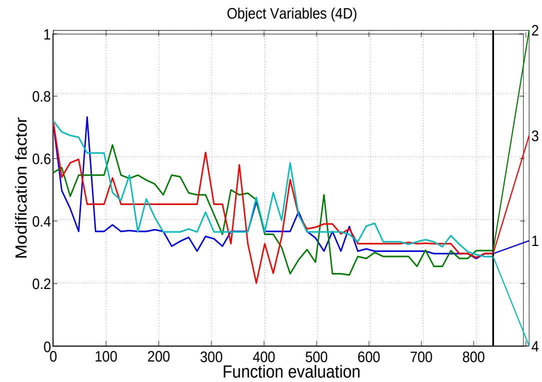

(b) Scenario 1 - GA

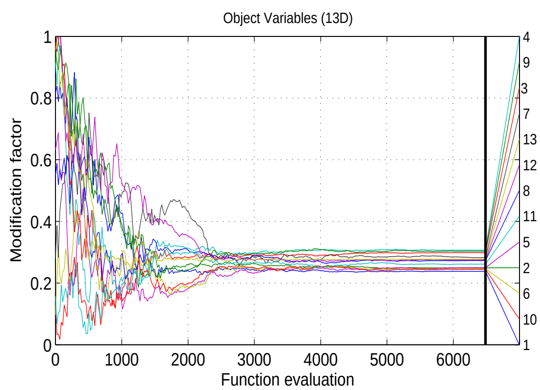

(c) Scenario 2 - CMA-ES

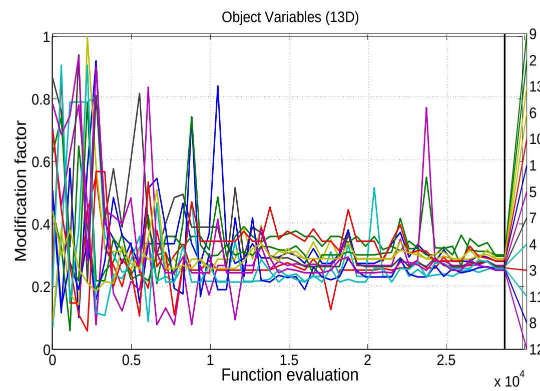

(d) Scenario 2 - GA

Figure III.6: Finite element model updating results for the calibration study. Plots (a) and (b) show the variation of the modification factors with function evaluation through the optimization procedure for Scenario 1 while plots (c) and (d) corresponds to Scenario 2. Each function evaluation consists of a finite element analysis to find the modal properties of the analytical model for the given set of input parameters and then computation of the cost function. The dark thick vertical line on the Right-Hand-Side (RHS) indicates the end of optimization process. In each plot, the RHS small panel provides a high-resolution plot of the modification factors when the identification procedure converged. Numbers on the RHS indicate the index of the system parameter being identified and the straight lines point to the corresponding curve. The correspondence of these parameters to the physical properties of the tested structure is available in Table III.7.

Table III.2: Calibration results for analytical finite element model based on the identified experimental modal properties of the undamaged state of the bridge using subspace method. S1 to S5 represent the location of the accelerometers on the deck as shown in Figure III.4.

Mode	**Method**	**Freq. (Hz)**	**MAC**	**Mode Shape Values**				
				S1	**S2**	**S3**	**S4**	**S5**
1^{st} Transverse	Experimental	3.09	0.995	0.67	0.57	0.38	0.26	0.08
	Analytical	3.10		0.63	0.55	0.43	0.30	0.15
2^{nd} Transverse	Experimental	4.15	0.995	0.42	0.16	-0.23	-0.50	-0.70
	Analytical	4.22		0.38	0.07	-0.23	-0.51	-0.73
3^{rd} Transverse	Experimental	12.90	0.996	0.42	-0.42	-0.61	-0.36	0.39
	Analytical	13.83		0.41	-0.35	-0.64	-0.34	0.42
1^{st} Longitudinal	Experimental	2.99	1.00	0.44	0.44	0.45	0.45	0.46
	Analytical	2.94		0.45	0.45	0.45	0.45	0.45

For calibration purposes, as shown in Figure III.6, finite element model updating for both scenarios was conducted to reproduce the response of the bridge specimen in the undamaged state. The identified parameters through the model updating process were modification factors to be applied to the gross section properties of the columns in the finite element model, eventually representing the equivalent cracked reinforced concrete. For Scenario 1, shown in Figure III.6(a) and Figure III.6(b), parameters 1-3 represent the modification factors for the stiffness of the bents in the transverse direction and parameter 4 for the longitudinal stiffness of all bents. For Scenario 2, illustrated in Figure III.6(c) and Figure III.6(d), parameters 1-12 correspond to the stiffness in the transverse direction on the bottom and top of the columns and parameter 13 to the longitudinal stiffness of all bents. The correspondence of these parameters to the physical properties of the tested structure is available in Table III.7. The resulting set of modification factors agreed fairly well with the factor (33% of the gross moment of inertia) calculated by the NEES@Reno researchers (Johnson et al. (2006)) using the slope of the elastic region in the elasto-plastic idealized moment-curvature relationship obtained from an analysis performed through a computer program called RCMC (Moment-Curvature analysis of confined and unconfined Reinforced Concrete sections).

Calibration results including obtained analytical and experimental frequencies as well as Modal Assurance Criterion (MAC) values for the corresponding mode shapes are listed in Table III.2. MAC values greater than 99.5% with frequency differences less than 2% (except the third transverse mode which is of less importance) clearly indicate that there is a satisfactory agreement between the modeled and the observed modal properties.

III.3.5 Choice of Initial Parameters and Weights

Parameter selection is a key issue in model updating procedures. The confidence in different measured test values and initial parameter estimations can be expressed through the weights in the cost function. Proper weighting factors can improve the optimization results significantly; however, this requires a good deal of knowledge about the assumptions made in the finite element modeling of the system, as well as the possible error sources in the analysis.

For typical structures, the system response is generally dominated by the low frequency modes. In general, the higher the number of parameters is to be identified, the more modes are required to be included in the cost function. On the other hand, using higher modes may not be reliable due to not only the measurement noise but also the discretization effect in analytical finite element modeling. Consequently, a plausible choice leads to setting higher weighting on the dominant modes, while avoiding too little weighting factors for higher modes to preserve their embedded information in the cost function (e.g., the inverse of the natural frequency). Nevertheless, model updating results cannot be considered unique since they ultimately depend on user-defined weights and constraints, as well as incorporating all the well-known limitations associated with inverse problems.

Upon implementing all of the aforementioned considerations, different sets of weighting factors in the model updating algorithm used in this study were evaluated for a synthetic damage detection scenario in the structure. To this end, a randomly damaged computer finite element model was generated for each simulation and the original undamaged model was updated to capture the modal properties of the damaged state through the optimization of the cost function. Scenario 2 (availability of data from 17 sensors) with a cost function involving a parameter vector of order 13 was considered for the simulation. Statistical data based on an ensemble of 100 simulations, with a maximum of 5000 iterations for each test (needed due to the stochastic nature of the algorithm), were investigated to determine the proper selection of the identification parameters. Despite the fact that even the accurate computational simulation of realistic damage phenomena is a challenging problem in its own right, random initial parameter choice was employed for each run in order to evaluate the robustness of the algorithm under discussion. Figure III.7 illustrates the probability density function of the random error in each parameter estimation for the weighting set of $W_{\underset{\sim}{f}} = W_{\underset{\sim}{\Phi}} = \{4\ 2\ 1\ 1\}$ (4, 2 and 1 for the first three transverse modes, and 1 for the first longitudinal mode). For the weighting set of $\{4\ 2\ 1\ 1\}$, the model updating algorithm was found to be capable of detecting, localizing, and quantifying the damage in all sections of the structure, with a high level of confidence (95% level of confidence with an error margin of less than 4% for all parameters). Therefore, this weighting set was adopted in the rest of the study.

III.4 Results and discussion

III.4.1 Preliminary Damage Tracking

Finite element model updating is inherently a time-consuming process which makes it impractical for on-line prediction of system parameters. On the other hand, change-detection in modal

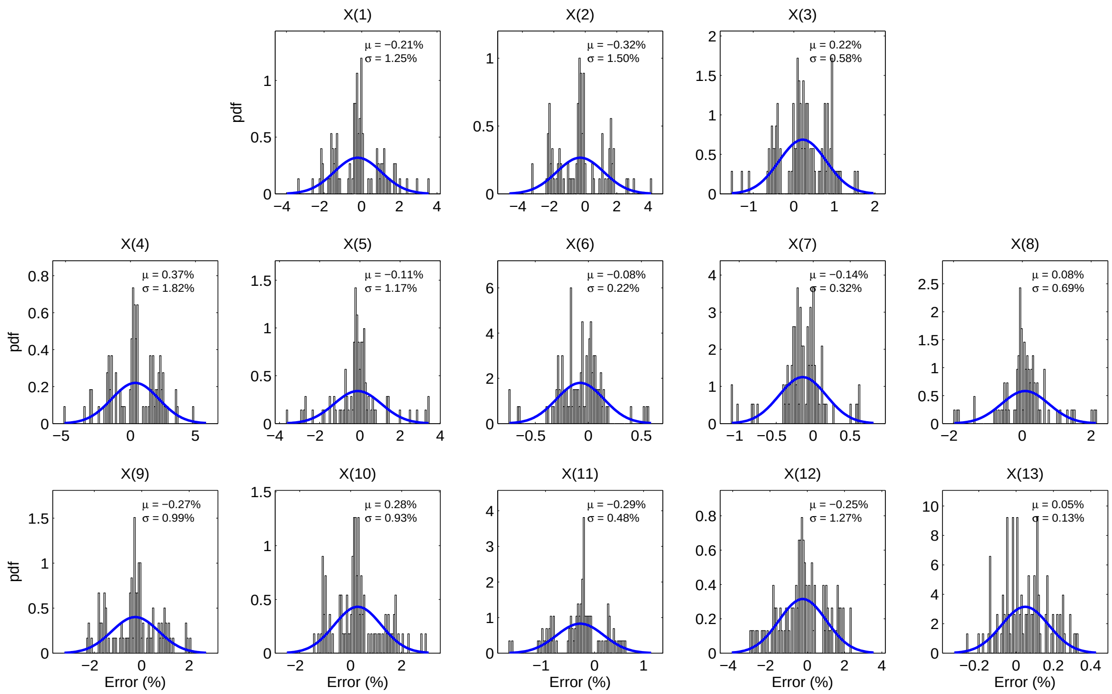

Figure III.7: Probability density function (pdf) of the parameters estimation error. A total of 100 simulations for scenario 2, with maximum of 5000 iterations for each test, were conducted for this study using CMA-ES. The cost function to be optimized consisted a parameter vector of order 13. X(1) to X(12) represent the stiffness on the top and bottom of the columns in the transverse direction and X(13) denotes the longitudinal stiffness of the bents. The correspondence of these parameters to the physical properties of the tested structure is available in Table III.7. Initial parameters set was selected randomly for each simulation to evaluate the robustness of the algorithm. In each plot panel, a thin line indicates the outline of the histogram of the parameter estimation error, and the solid line represents the estimated Gaussian pdf having a matching mean (σ) and standard deviation (μ) to the corresponding histogram. Note that the abscissa and ordinate ranges are not identical.

properties (i.e., frequencies, mode shapes, and system damping) is quite well known as an easily quantifiable structural damage index in the field of SHM (Masri et al. (2008)). Hence, a preliminary damage tracking technique that relies on detection of any shift in these quantities to trigger the model updating procedure may drastically increase its efficacy. Notice that, actual damage in real structures manifests itself in different complex forms (Masri et al. (2008)) and therefore, one of the practical challenges in conjunction with damage detection in physical systems is the monitoring indicators. For example, it is well recognized in the structural dynamics community that, solely detecting frequency shifts is a poor precursor of damage in realistic systems, due to its relative insensitivity to small changes (Nayeri et al. (2008), Peeters and De Roeck (2001), Sohn et al. (1999), Cornwell et al. (1999)). Therefore, a reliable change-detection scheme should provide a meaningful correlation between the estimated system parameters and physical measures of the structural dynamic properties of the monitored system.

Considering all the above mentioned aspects, a preliminary damage tracking technique was developed for this study using a recursive autoregressive moving average model (Recursive ARMA) to produce a near-real-time (on-line) monitoring method to detect any significant change in the system response. The first order single-output recursive ARMA structure to predict the value of the cost function is defined as:

$$(1 + \phi L)J(t) = (1 + \theta L)\epsilon(t) \tag{III.10}$$

where J is the real-time cost function value (defined by Equation III.9) based on extracted modal properties from a given window size of the past response record. ϕ and θ are Autoregressive (AR) and Moving Average (MA) parameters, ϵ represents the white noise disturbance value and

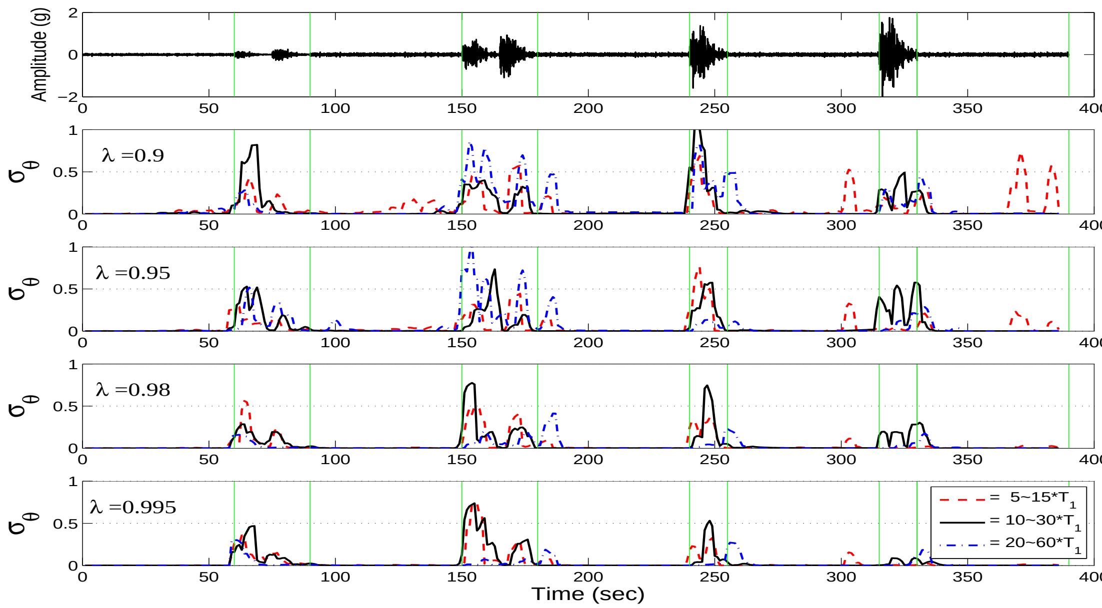

Figure III.8: Preliminary damage detection through tracking of the standard deviation of the moving average parameter (θ) in the ARMA model. Four typical values of the forgetting factor (λ = 0.90, 0.95, 0.98 and 0.995) and different window sizes for system identification were considered in this study. The first row illustrates the synchronized plot of the excitation to the structure in the transverse direction.

L denotes the lag operator in time series analysis. Any change in the dynamic system throughout the experiment, resulting in the fluctuation of the value of the cost function, would be presumably reflected in the estimated parameters by the ARMA model. This procedure was implemented in MATLAB® (using the **rarmax** module) for the response of the structure to the combined excitation in the transverse direction.

Successive values of the standard deviation of the MA parameter (θ) in the recursive ARMA model over a 5-second window size is shown in Figure III.8. The plot illustrates the effects of different lengths of the response record used for system identification, as well as the forgetting factor variant, λ, which weighs past information exponentially less as time goes on. As expected, using a short-length of response ($5T_1 \sim 15T_1$, where T_1 is the fundamental period of the linearized system) for system identification would result in fast damage detection at the expense of a possible false-positive damage indication (indication of damage when none is present), while employing a too-long window size ($20T_1 \sim 60T_1$) would increase the possibility of false-negative damage indication (no indication of damage when damage is present). Both types of these errors are clearly undesirable, since the former would cause unnecessary downtime and consequent economic disruption, while the latter would bring safety issues to the system.

Figure III.8 also compares the effects of four typical values for the forgetting factor (λ = 0.90, 0.95, 0.98 and 0.995). Similar to the system identification window size, the forgetting factor value showed a significant effect on the reaction time to changing system parameters, and an inverse effect on ignoring noise. The smaller forgetting factor was more robust in detection of instantaneous damage to the system, but also more vulnerable to noise. A window size of ($10T_1 \sim 30T_1$) for system identification, and a forgetting factor of λ = 0.95 were found to be suitable for reliable instantaneous damage tracking of the investigated structure and therefore implemented in this study. To simulate the real-time continuous monitoring of the structure, this proposed preliminary damage tracking method was used to trigger the model updating procedure whenever the monitored quantity settled down to a steady-state near-zero value after exceeding a predefined threshold.

III.4.2 Model Updating Results

Damage detection using input-output data

The finite element model updating procedure was employed for both scenarios at different levels of damage to the structure. Table III.3 to Table III.6 display the identified frequencies and the corresponding mode shapes (measured at the location of the accelerometers on the deck) of the structure in the various time windows depicted in Figure III.3 (WN-2 to WN-5) for the first longitudinal and the first three transverse modes. These identified quantities were used in the calculation of the cost function for the finite element model updating procedures illustrated in Figures III.9 to III.12.

Figure III.9 and Figure III.10 show the finite element model updating results using CMA-ES for scenario 1 and 2, respectively. Similar results using GA optimization algorithm in the finite element updating procedure are illustrated in Figure III.11 and Figure III.12. As shown in Figure III.9 and Figure III.11, based on system identification results using recorded response measurements by 5 sensors, a 4-dimensional cost function was optimized to detect and quantify the overall damage in each bent. Parameters 1-3 represent the remaining stiffness of the bents in the transverse direction and parameter 4 is the corresponding value for the longitudinal stiffness of all bents. As illustrated in Figure III.10 and Figure III.12 for scenario 2, based on system identification results using recorded response measurements by 17 sensors, a 13-dimensional cost function was optimized to detect and quantify the overall and localized damage for each column. Parameters 1-12 indicate the remaining stiffness in the transverse direction on the bottom and top of the columns and parameter 13 represents the corresponding value for the longitudinal stiffness of all bents. The correspondence of these parameters to the physical properties of the tested structure is available in Table III.7. In each figure, plots (a) to (d) show the variation of the modification factors with function evaluation through the optimization procedure for white-noise excitation windows WN-2 to WN-5, respectively. Diminishing fluctuation of the parameters being identified through the optimization process indicates the convergence of these quantities to their final values. The dark thick vertical line denotes the end of optimization process. In each plot, the RHS small panel

Table III.3: System identification results for test window WN-2. S1 to S5 represent the location of the accelerometers on the deck as shown in Figure III.4. These values were used for the finite element model updating procedures illustrated in Figures III.9(a), III.10(a), III.11(a), and III.12(a).

Mode	**Freq. (Hz)**	**Mode Shape Values**				
		S1	**S2**	**S3**	**S4**	**S5**
1^{st} Transverse	2.46	0.68	0.54	0.40	0.26	0.08
2^{nd} Transverse	3.44	0.34	-0.04	-0.25	-0.51	-0.75
3^{rd} Transverse	12.33	0.40	-0.41	-0.62	-0.37	0.38
1^{st} Longitudinal	2.82	0.44	0.44	0.44	0.45	0.45

Table III.4: System identification results for test window WN-3. These values were used for the finite element model updating procedures illustrated in Figures III.9(b), III.10(b), III.11(b), and III.12(b).

Mode	**Freq. (Hz)**	**Mode Shape Values**				
		S1	**S2**	**S3**	**S4**	**S5**
1^{st} Transverse	1.53	0.69	0.54	0.40	0.26	0.10
2^{nd} Transverse	1.82	0.31	0.01	-0.23	-0.50	-0.78
3^{rd} Transverse	11.95	0.39	-0.43	-0.62	-0.38	0.37
1^{st} Longitudinal	2.02	0.44	0.44	0.45	0.45	0.45

Table III.5: System identification results for test window WN-4. These values were used for the finite element model updating procedures illustrated in Figures III.9(c), III.10(c), III.11(c), and III.12(c).

Mode	**Freq. (Hz)**	**Mode Shape Values**				
		S1	**S2**	**S3**	**S4**	**S5**
1^{st} Transverse	1.39	0.55	0.48	0.45	0.39	0.34
2^{nd} Transverse	1.57	0.39	0.11	-0.18	-0.47	-0.77
3^{rd} Transverse	11.94	0.42	-0.41	-0.62	-0.39	0.34
1^{st} Longitudinal	1.82	0.44	0.45	0.45	0.44	0.45

Table III.6: System identification results for test window WN-5. These values were used for the finite element model updating procedures illustrated in Figures III.9(d), III.10(d), III.11(d), and III.12(d).

Mode	**Freq. (Hz)**	**Mode Shape Values**				
		S1	**S2**	**S3**	**S4**	**S5**
1^{st} Transverse	1.34	0.61	0.53	0.42	0.33	0.22
2^{nd} Transverse	1.56	0.45	0.12	-0.16	-0.44	-0.75
3^{rd} Transverse	11.81	0.40	-0.41	-0.62	-0.40	0.35
1^{st} Longitudinal	2.05	0.45	0.44	0.45	0.44	0.45

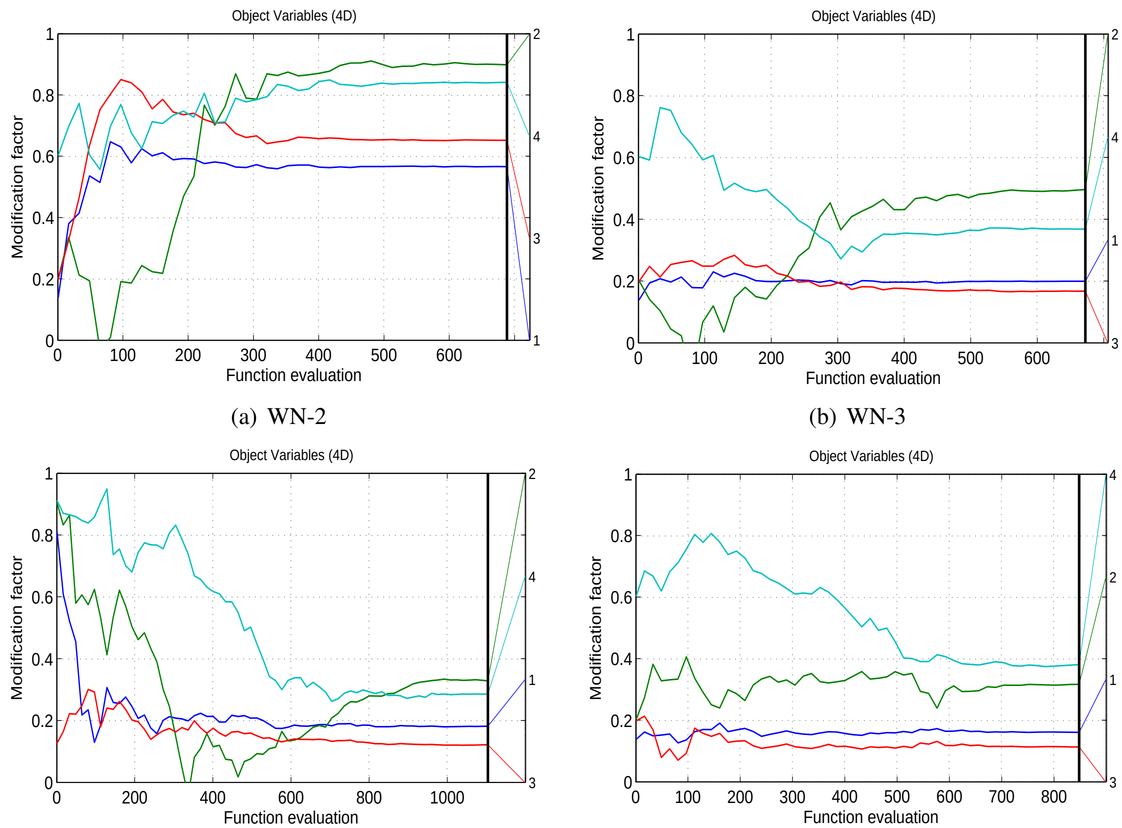

(a) WN-2 (b) WN-3

(c) WN-4 (d) WN-5

Figure III.9: Finite element model updating results for Scenario 1, using CMA-ES. Plots (a) to (d) show the variation of the modification factors with function evaluation through the optimization procedure for white-noise excitation windows WN-2 to WN-5, respectively. Based on system identification results using recorded response measurements by 5 sensors, a 4-dimensional cost function was optimized to detect and quantify the overall damage in each bent. Parameters 1-3 represent the remaining stiffness of the bents in the transverse direction and parameter 4 is the corresponding value for the longitudinal stiffness of all bents (Please also see the caption of Figure III.6 for further details).

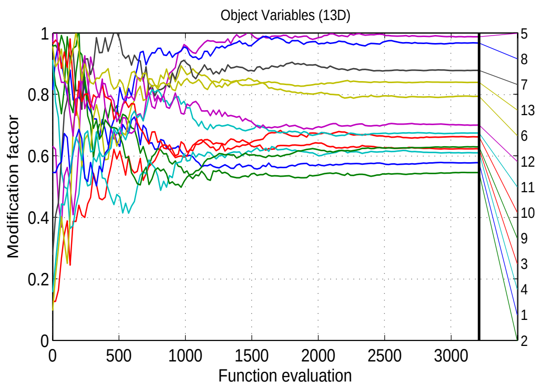

(a) WN-2

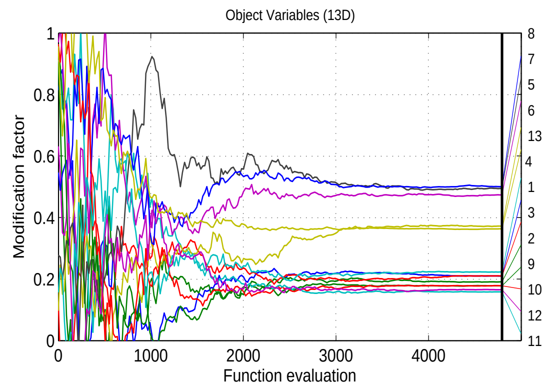

(b) WN-3

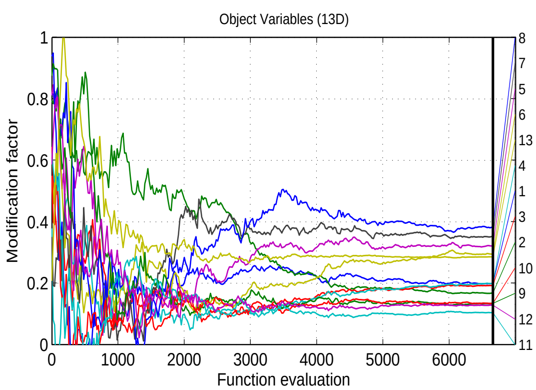

(c) WN-4

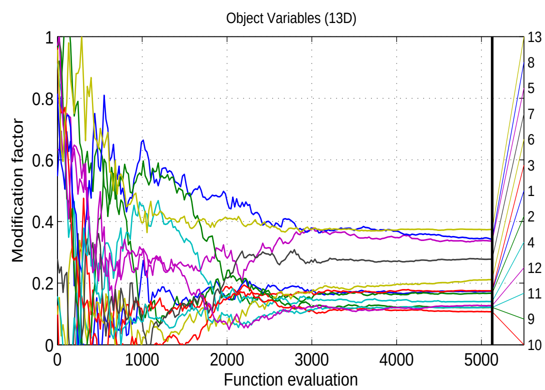

(d) WN-5

Figure III.10: Finite element model updating results for Scenario 2, using CMA-ES. Plots (a) to (d) show the variation of the modification factors with function evaluation through the optimization procedure for white-noise excitation windows WN-2 to WN-5, respectively. Based on system identification results using recorded response measurements by 17 sensors, a 13-dimensional cost function was optimized to detect and quantify the overall and localized damage for each column. Parameters 1-12 represent the remaining stiffness in the transverse direction on the bottom and top of the columns and parameter 13 is the corresponding value for the longitudinal stiffness of all bents (Please also see the caption of Figure III.6 for further details).

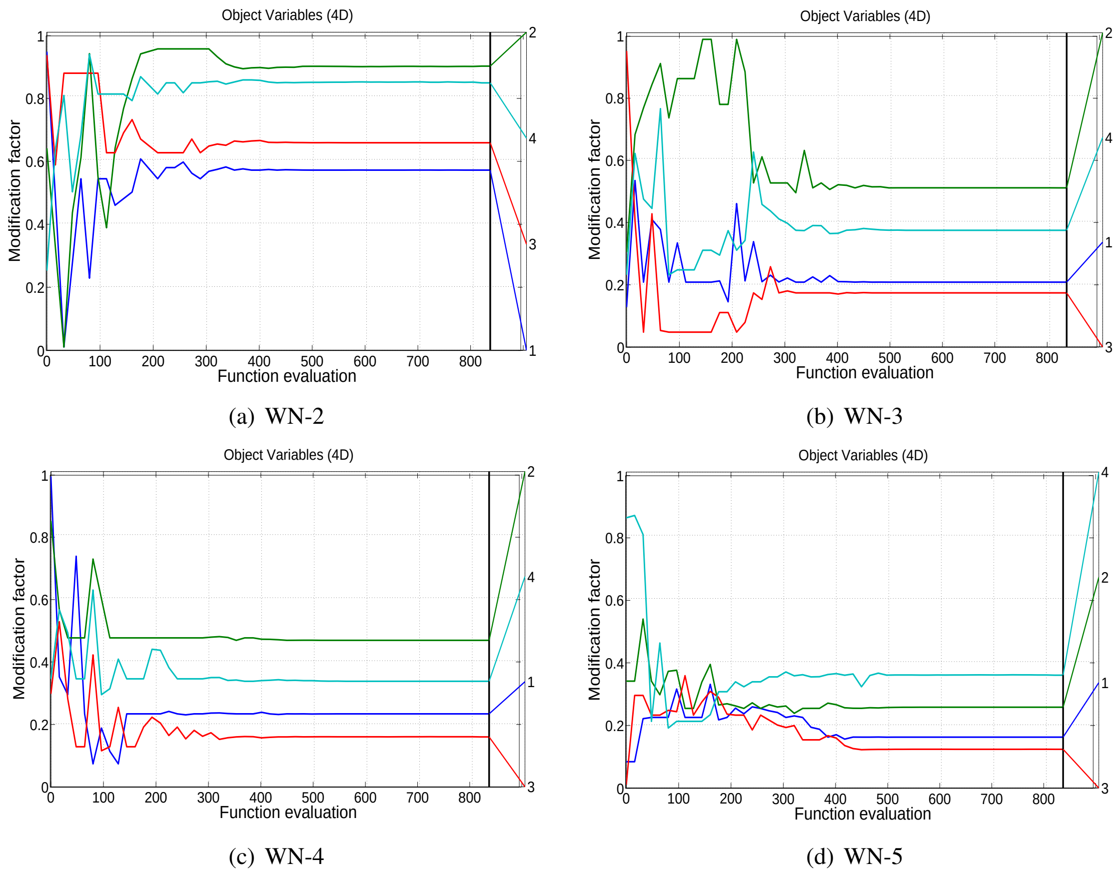

(a) WN-2

(b) WN-3

(c) WN-4

(d) WN-5

Figure III.11: Finite element model updating results for Scenario 1, using GA. Plots (a) to (d) show the variation of the modification factors with function evaluation through the optimization procedure for white-noise excitation windows WN-2 to WN-5, respectively. Based on system identification results using recorded response measurements by 5 sensors, a 4-dimensional cost function was optimized to detect and quantify the overall damage in each bent. Parameters 1-3 represent the remaining stiffness of the bents in the transverse direction and parameter 4 is the corresponding value for the longitudinal stiffness of all bents (Please also see the caption of Figure III.6 for further details).

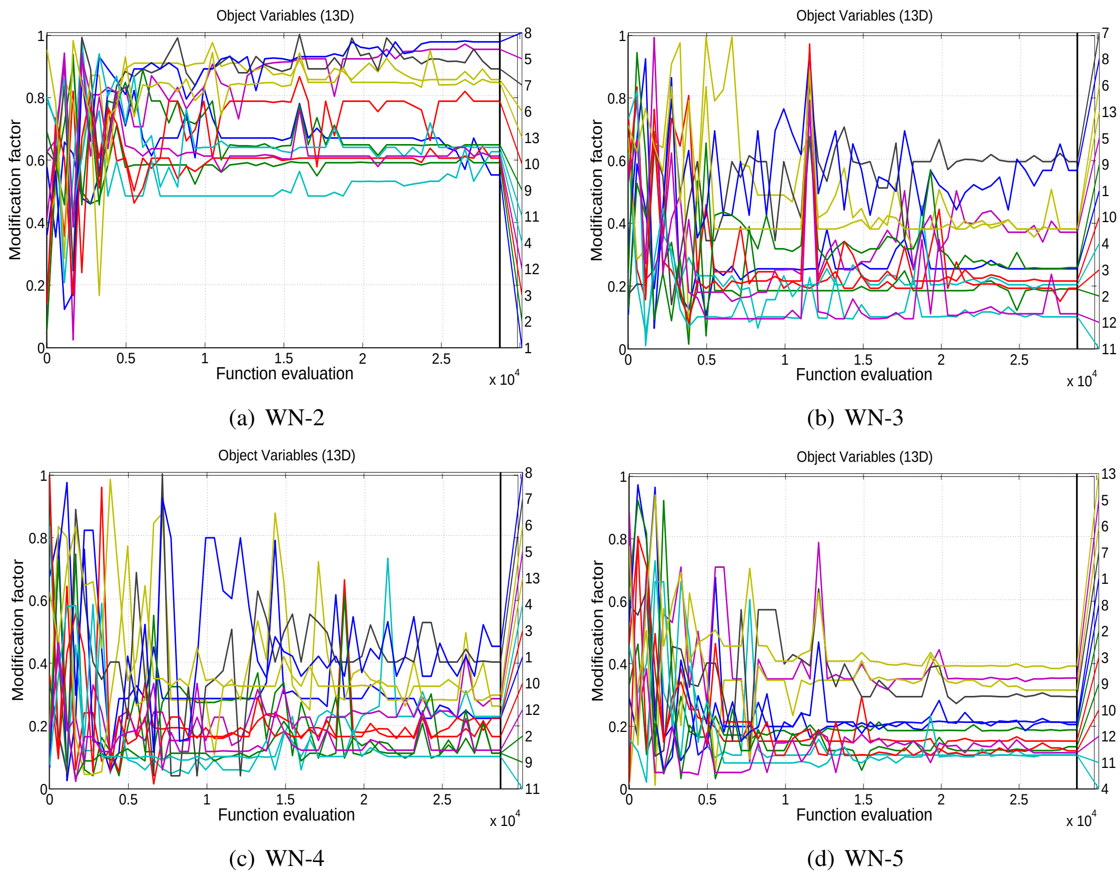

(a) WN-2

(b) WN-3

(c) WN-4

(d) WN-5

Figure III.12: Finite element model updating results for Scenario 2, using GA. Plots (a) to (d) show the variation of the modification factors with function evaluation through the optimization procedure for white-noise excitation windows WN-2 to WN-5, respectively. Based on system identification results using recorded response measurements by 17 sensors, a 13-dimensional cost function was optimized to detect and quantify the overall and localized damage for each column. Parameters 1-12 represent the remaining stiffness in the transverse direction on the bottom and top of the columns and parameter 13 is the corresponding value for the longitudinal stiffness of all bents (Please also see the caption of Figure III.6 for further details).

provides a high-resolution plot of the modification factors when the identification procedure converged. Numbers on the RHS indicate the index of the system parameter being identified and the straight lines point to the corresponding curve. As shown in these figures, both CMA-ES and GA converge to pretty close global minimums; however, GA may take more computational effort to reach the solution, especially for higher order problem.

Note that, as the damage induced in the test structure escalates in response to increasing levels of shaking in the test windows WN-2 through WN-5, the measure of damage provided by the modification factors assures a diminishing value (since a value of 1.00 for modification factor indicates an undamaged state, whereas 0.00 represents a completely damaged state). Damage detection results for the test windows WN-2 to WN-5 are also tabulated in Table III.7 to Table III.10, respectively. In each table, the identified damage quantities ((1.00 - Modification Factor)$\times$100%) through the optimization process for both scenarios as well as their correspondence to the physical properties of the tested structure are presented. Please note that in the second scenario, the average of four obtained damage values for each bent (last two columns in Table III.7 to Table III.10) represents the overall damage to that bent. Comparing this average to the damage value obtained in the first scenario for each bent (column #4 and column #5 in Table III.7 to Table III.10) indicates a fair agreement between the results of two scenarios. The damage indices calculated by the NEES@Reno test team for the bents are also listed for comparison and validation purposes.

Table III.7: Damage detection results for test window WN-2. Damage values show the percentage of the loss of stiffness in the columns with respect to the intact stage. The damage indices calculated by the NEES@Reno test team for the bents using strain gauge records are also listed. The corresponding finite element model updating procedures, resulting in these quantities, are illustrated in Figures III.9(a) , III.10(a), III.11(a), and III.12(a).

Bent no.	Damage Index	Scenario 1			Scenario 2			
	(NEES@Reno)	X(i)	CMA-ES	GA	X(i)	Location	CMA-ES	GA
Bent-1$_T$	**0.28**	X(1)	43%	43%	X(1)	East Column Bottom	42%	45%
					X(2)	East Column Top	45%	41%
					X(3)	West Column Bottom	38%	40%
					X(4)	West Column Top	39%	38%
Bent-2$_T$	**0.14**	X(2)	10%	11%	X(5)	East Column Bottom	1%	5%
					X(6)	East Column Top	21%	15%
					X(7)	West Column Bottom	12%	12%
					X(8)	West Column Top	3%	3%
Bent-3$_T$	**0.18**	X(3)	35%	35%	X(9)	East Column Bottom	37%	36%
					X(10)	East Column Top	34%	22%
					X(11)	West Column Bottom	36%	36%
					X(12)	West Column Top	30%	39%
All Bents$_L$	-	X(4)	16%	16%	X(13)	All Col. Longitudinal	16%	16%

Table III.8: Damage detection results for test window WN-3. The corresponding finite element model updating procedures, resulting in these quantities, are illustrated in Figures III.9(b) , III.10(b), III.11(b), and III.12(b).

Bent no.	Damage Index	Scenario 1			Scenario 2			
	(NEES@Reno)	X(i)	CMA-ES	GA	X(i)	Location	CMA-ES	GA
Bent-1$_T$	**1.19**	X(1)	80%	79%	X(1)	East Column Bottom	79%	75%
					X(2)	East Column Top	81%	81%
					X(3)	West Column Bottom	79%	81%
					X(4)	West Column Top	78%	80%
Bent-2$_T$	**0.61**	X(2)	50%	49%	X(5)	East Column Bottom	53%	63%
					X(6)	East Column Top	63%	62%
					X(7)	West Column Bottom	50%	41%
					X(8)	West Column Top	50%	44%
Bent-3$_T$	**0.99**	X(3)	83%	83%	X(9)	East Column Bottom	82%	74%
					X(10)	East Column Top	82%	79%
					X(11)	West Column Bottom	84%	90%
					X(12)	West Column Top	83%	89%
All Bents$_L$	-	X(4)	63%	63%	X(13)	All Col. Longitudinal	63%	62%

Table III.9: Damage detection results for test window WN-4. The corresponding finite element model updating procedures, resulting in these quantities, are illustrated in Figures III.9(c) , III.10(c), III.11(c), and III.12(c).

Bent no.	Damage Index (NEES@Reno)	Scenario 1			Scenario 2			
		X(i)	CMA-ES	GA	X(i)	Location	CMA-ES	GA
Bent-1_T	**1.63**	X(1)	82%	77%	X(1)	East Column Bottom	80%	78%
					X(2)	East Column Top	83%	89%
					X(3)	West Column Bottom	81%	78%
					X(4)	West Column Top	80%	77%
Bent-2_T	**0.86**	X(2)	67%	54%	X(5)	East Column Bottom	68%	72%
					X(6)	East Column Top	70%	70%
					X(7)	West Column Bottom	65%	60%
					X(8)	West Column Top	62%	55%
Bent-3_T	**1.38**	X(3)	88%	84%	X(9)	East Column Bottom	87%	89%
					X(10)	East Column Top	87%	84%
					X(11)	West Column Bottom	90%	90%
					X(12)	West Column Top	87%	88%
All Bents_L	-	X(4)	71%	67%	X(13)	All Col. Longitudinal	71%	74%

Table III.10: Damage detection results for test window WN-5. The corresponding finite element model updating procedures, resulting in these quantities, are illustrated in Figures III.9(d) , III.10(d), III.11(d), and III.12(d).

Bent no.	Damage Index (NEES@Reno)	Scenario 1			Scenario 2			
		X(i)	CMA-ES	GA	X(i)	Location	CMA-ES	GA
Bent-1_T	**2.15**	X(1)	84%	84%	X(1)	East Column Bottom	83%	79%
					X(2)	East Column Top	83%	81%
					X(3)	West Column Bottom	82%	85%
					X(4)	West Column Top	86%	89%
Bent-2_T	**1.15**	X(2)	68%	74%	X(5)	East Column Bottom	66%	65%
					X(6)	East Column Top	79%	69%
					X(7)	West Column Bottom	72%	71%
					X(8)	West Column Top	66%	80%
Bent-3_T	**1.87**	X(3)	89%	88%	X(9)	East Column Bottom	88%	87%
					X(10)	East Column Top	89%	88%
					X(11)	West Column Bottom	88%	89%
					X(12)	West Column Top	87%	89%
All Bents_L	-	X(4)	63%	64%	X(13)	All Col. Longitudinal	63%	61%

The changes in the stiffness of the columns after WN-5 are generally insignificant. Interestingly, an increase in the stiffness of the structure in transverse direction is also observed after WN-5 (71% damage after WN-4 and 63% after WN-5). Note that such an outcome is not uncommon when dealing with experimental data. Meanwhile, this may be attributed to some extent to the self-healing behavior of concrete cracks.

Damage detection using output-only data

In continuous monitoring of a large-scale system, it is usually infeasible to excite the structure by a measurable artificial source, and even if possible, it will require expensive input devices such as shakers. Moreover, during real operation, the loading conditions may be substantially different from the ones used in the modal test. Therefore there is a considerable tendency toward the use of freely available ambient excitation sources for system identification and damage detection purposes. Various output-only system identification methods for operational modal analysis have been proposed in the frequency domain (e.g, Peak-Picking method (PP), Complex Mode Indication Function (CMIF), etc) and time domain (e.g, Instrumental Variable method (IV), Covariance-Driven Stochastic Subspace Identification (SSI-COV), Data-Driven Stochastic Subspace Identification (SSI-DATA), etc) and have successfully been applied to real-life vibration data (Peeters and Roeck (2001)).

To evaluate the proposed finite element model updating approach for output-only data analysis, the damage detection procedures for both scenarios are conducted in window test WN-2 and the results are presented in Figure III.13 and tabulated in Table III.11. Again, subspace method is applied for modal identification of the structure. As expected, comparison of these results with the corresponding quantities which are obtained from input-output data analysis (presented in Table

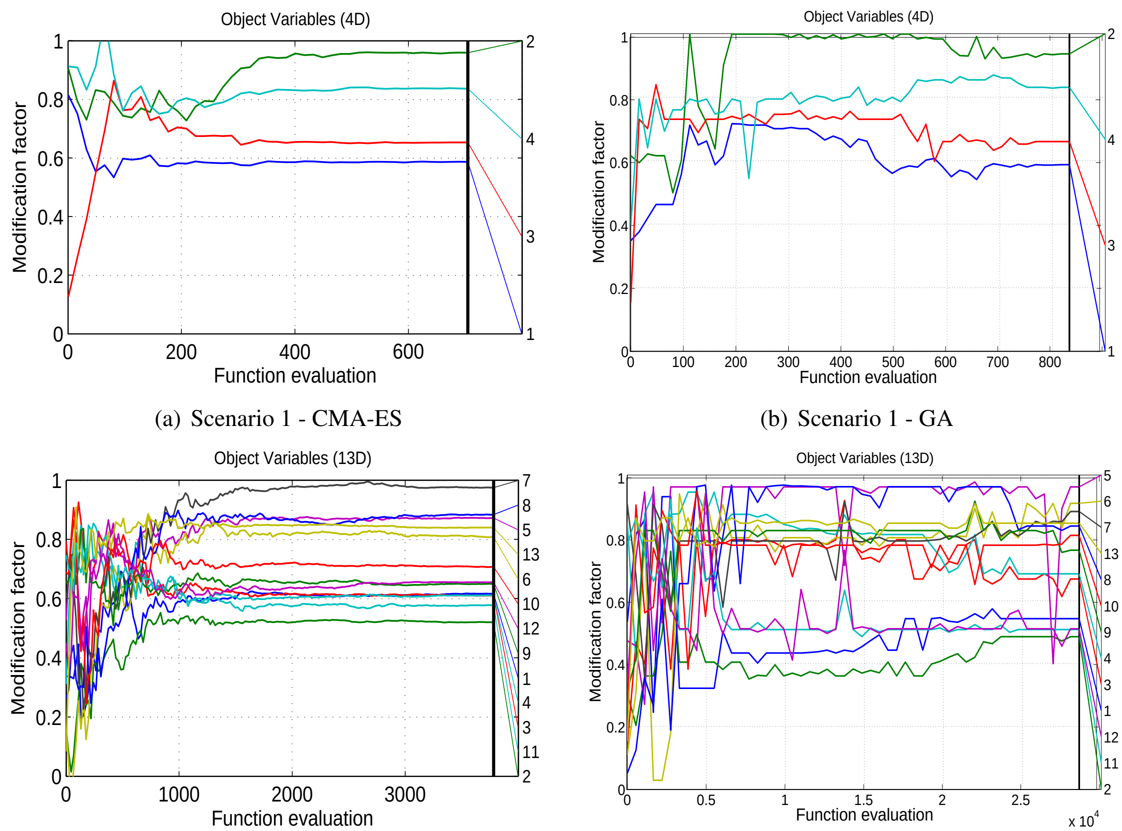

(a) Scenario 1 - CMA-ES

(b) Scenario 1 - GA

(c) Scenario 2 - CMA-ES

(d) Scenario 2 - GA

Figure III.13: Finite element model updating results using output-only data for test window WN-2. Plots (a) and (b) show the variation of the modification factors with function evaluation through the optimization procedure for Scenario 1 while plots (c) and (d) corresponds to Scenario 2. The correspondence of these parameters to the physical properties of the tested structure is available in Table III.11. For comparison purposes, the reader is referred to the corresponding figures using input-output data for damage detection in test window WN-2 which are illustrated in Figures III.9(a), III.10(a), III.11(a), and III.12(a).

III.7; see also Figures III.9(a), III.10(a), III.11(a), and III.12(a)) shows an acceptable agreement, primarily due to the white-noise nature of the excitations. Of course, the performance of the method for real-life situations will highly depend on the accuracy of the important modal features of the structure extracted from output-only vibration measurements.

Table III.11: Damage detection results for test window WN-2 using output-only data. The corresponding finite element model updating procedures, resulting in these quantities, are illustrated in Figure III.13.

Bent no.	Damage Index (NEES@Reno)	Scenario 1			Scenario 2			
		X(i)	CMA-ES	GA	X(i)	Location	CMA-ES	GA
Bent-1_T	**0.28**	X(1)	41%	41%	X(1)	East Column Bottom	38%	46%
					X(2)	East Column Top	48%	51%
					X(3)	West Column Bottom	39%	33%
					X(4)	West Column Top	39%	31%
Bent-2_T	**0.14**	X(2)	4%	6%	X(5)	East Column Bottom	13%	4%
					X(6)	East Column Top	19%	9%
					X(7)	West Column Bottom	2%	12%
					X(8)	West Column Top	12%	16%
Bent-3_T	**0.18**	X(3)	35%	34%	X(9)	East Column Bottom	35%	24%
					X(10)	East Column Top	29%	19%
					X(11)	West Column Bottom	42%	49%
					X(12)	West Column Top	34%	49%
All Bents$_L$	-	X(4)	16%	17%	X(13)	All Col. Longitudinal	16%	15%

III.4.3 Validation Results

To quantitatively estimate the amount of damage to the structure, the NEES@Reno research team calculated a damage index for each bent and for each test motion using strain gauge records. This damage index, developed by Park and Ang (1985) for reinforced concrete, is a practical measure of damage based on a combination of the amount of dissipated hysteretic energy, and the maximum displacement demand over ultimate displacement ratio. For validation purposes, these damage indices are also listed in Table III.7 to Table III.10. Values greater than 1.00 indicate collapse. However, the probability of collapse at this threshold is approximately 50 percent with a standard deviation of $\sigma = 0.54$. Damage indices greater than 1.00 represent a higher probability of collapse (Johnson et al. (2006)).

The index represents a mechanistic damage model through the following equation:

$$DI = \frac{\delta_M}{\delta_u} + \frac{\beta}{Q_y \delta_u} \int dE \tag{III.11}$$

in which δ_M, δ_u, Q_y and dE represent maximum deformation under earthquake, ultimate deformation under monotonic loading, calculated yield strength and incremental absorbed hysteretic energy, respectively. Coefficient β is defined as follows:

$$\beta = \left(-0.447 + 0.073\frac{l}{d} + 0.24n_0 + 0.314p_t\right) \times 0.7^{\rho_\omega} \tag{III.12}$$

where $\frac{l}{d}(\geq 1.7)$, $n_0(\geq 0.2)$, p_t and ρ_ω indicate shear span ratio, normalized axial stress, longitudinal steel ratio and confinement ratio respectively (Park and Ang (1985)). More detailed information regarding the calculation of these indices is available in Johnson et al. (2006).

Figure III.14 illustrates the linear regression relating the damage index and the quantified damage through the model updating procedure. Computed correlation factors ($\rho_{cmaes} = 0.956, \rho_{ga} = 0.946$) strongly confirm the accuracy of the detected damage values qualitatively and quantitatively. Unfortunately, such a validation is not possible for detected localized damages on the top and the bottom of the columns; hence, the reliability of these results highly depends upon the accuracy of the identified modal properties of the structure in the different stages of the experiment.

In order to gauge the damage detection results of this study, it is useful to compare them with

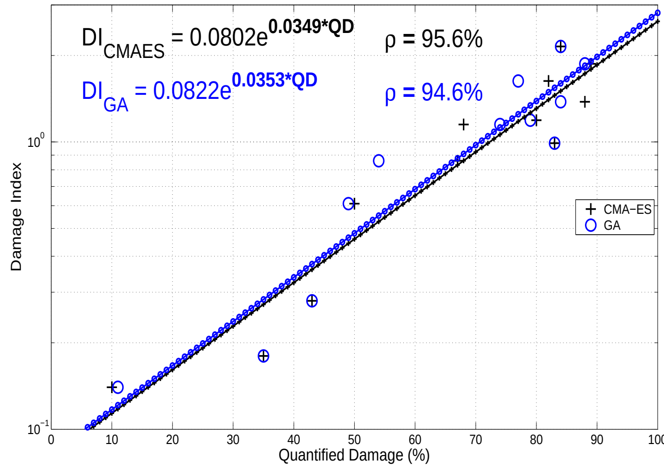

Figure III.14: Linear regression plot relating the damage index and the quantified damage. The abscissa shows the quantified damage, identified through the model updating procedure in the first scenario (column #4 and column #5 in Table III.7 to Table III.10), and the ordinate is the damage index introduced by Park and Ang (1985) (column #2 in Table III.7 to Table III.10), which is a practical measure of damage based on dissipated hysteretic energy and ductility demand.

the observations of the NEES@Reno team throughout the experiment. Table III.12 compares the finite element model updating results with the visual inspections reported in Johnson et al. (2006). As explained in the last column of this table, there is a fair agreement between the qualitative reported visual inspections and the quantitative identified damage indices through the model updating approach.

III.5 Concluding Remarks

The underlying objective of this study is to evaluate the performance of two global optimization methods in the finite element model updating approaches for damage detection in dispersed structural systems, which usually deals with minimization of a complex, non-linear, non-convex, high-dimensional cost function. The case study was a two-span reinforced concrete bridge, experimentally tested at the University of Nevada, Reno. The subspace method for system identification

Table III.12: Comparison of finite element model updating results with NEES@Reno observations

Test Window	**NEES@Reno Observation (Johnson et al. (2006))**	**Model Updating Results**
WN-2	"No damage was observed in the bridge until after test 13. During test 13, initial hairline flexural cracks developed in Bent-1."	The higher detected damage value in Bent-1 (43% and 43%) agrees with the reported visual inspection. (Table III.7)
WN-3 	"Flexural cracking began in Bent-3 and became significant in the columns of both Bents-1 and 3 during test 15. Also during test 15, initial hairline cracks began to develop in Bent-2. During test 17, significant concrete spalling exposed the column lateral reinforcement in both Bents-1 and 3."	Significant detected damage values in Bent-1 (80% and 79%) and Bent-3 (83% and 83%) are in complete agreement with visual observations. Lower value in Bent-2 (50% and 49%) shows the incipient stages of damage in the middle of the structure. (Table III.8)
WN-4 	"Significant spalling and exposure of lateral column reinforcement in Bent-2 became evident during test 18. Also during test 18, the longitudinal reinforcement of Bent-3, the shortest of the bents, became exposed and initial buckling was observed on the bottom west side of the west column."	Very high detected damage value in Bent-3 (88% and 84%) indicates severe situation in the shortest bent. Damage values of (82% and 77%) in Bent-1 and (67% and 54%) in Bent-2 confirm the visual inspection results. (Table III.9)
WN-5 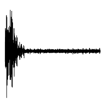	"Both columns of Bent-3 failed in flexure during test 19. The top and bottom of Bent-3 columns experienced significant plastic hinging and crushing of the core concrete. Four Bent-3 spirals fractured, and 36 longitudinal bars buckled."	Complete failure in Bent-3 is clearly reflected in its significant detected damage value (89% and 88%). Bent-1 is also in severe condition with more than 84%/84% loss of stiffness. As predicted, since Bent-2 would be the most unlikely bent to fail during the experiment, it has the least damage index of 68%/74%. (Table III.10)

was used to extract the modal parameters (natural frequencies, mode shapes, and modal damping) of the bridge system. A NASTRAN® computer model was developed based on the previous SAP2000 model provided by the NEES@Reno team and validated with the system identification results from the measured data. A simple on-line damage detection method, using an ARMA model, was proposed and employed to trigger the finite element model updating process. Two scenarios, assuming the availability of limited or large number of sensors were investigated for the finite element model updating procedure. The feasibility of the proposed finite element model updating algorithm to accurately detect, localize, and quantify the damage in the columns of the tested bridge throughout the experiment was investigated and validated by comparison to experimental measurements and visual inspections.

Based on the comparison of the results from the application of the finite element model updating algorithm under discussion with the strain gauge measurements and visual observations, the following conclusions can be made:

(i). The simple ARMA model proposed for preliminary on-line damage detection can significantly increase the efficacy of the model updating process.

(ii). The finite element model updating algorithm presented and applied in this study could accurately detect and quantify the overall damage in the tested bridge bents throughout the experiment.

(iii). The proposed method also showed very promising results for damage detection in the system using output-only data. This reveals the potential of the technique to provide a useful tool for SHM purposes in conjunction with promising methods for the identification of modal properties using available ambient vibration data.

(iv). The finite element model updating algorithm used in this study was shown to be robust and accurate to detect, localize and quantify the damage in the columns in synthetic simulations; however, the experimental results could not be completely validated. The reliability of these results highly depends upon the accuracy of the identified (equivalent) modal properties of the (damaged, nonlinear) structure in different stages of the experiment.

(v). Detected damage values are highly correlated ($\rho_{cmaes} = 0.956, \rho_{ga} = 0.946$) with the damage index developed by Park and Ang (1985), which is a practical measure of damage based on dissipated hysteretic energy and ductility demand.

(vi). Both CMA-ES and GA converge to pretty close global minimums; however, GA may take more computational effort to reach the solution, especially for higher-order problem.

Even though the cost function to be optimized in this study was not relatively high-dimensional (13-D), considering the promising performance of the optimization method under discussion in solving well-known benchmark problems of global optimization, the general conclusions from this study are useful in providing guidelines for the application of stochastic optimization methods to real-world search problems, especially in the implementation of structural health monitoring for complex, nonlinear distributed systems.

Chapter IV

EVALUATION AND APPLICATION OF SOME DATA-DRIVEN APPROACHES FOR THE DEVELOPMENT OF EQUIVALENT LINEAR SYSTEM FOR NONLINEAR STRUCTURES

IV.1 Introduction

THE performance of six different system identification methods is studied in this section. The fidelity of the methods under discussion in identifying the structural dynamic properties of a nonlinear system is evaluated by using the experimental data from a 4-story model building.

IV.1.1 Vibration-Signature-Based Nonlinear System Identification Methods: A Literature Review

The large family of system identification methods for estimation of nonlinear models based on experimental measurements can be classified in several different approaches. The current presentation gives an overview on some essential features in the area which includes a summary of a comprehensive literature review and classification of methods presented by Kerschen et al. (2006), variants and developments in each class, and their possible advantages and limitations.

Linearization

Several studies have attempted to find an equivalent linear model that can predict the response of a nonlinear system. Caughey (1963) generalized the equivalent linearization method of Kryloff and Bogoliubov to the case of nonlinear dynamic systems with random excitation. The method operates directly on the equations of motion of a nonlinear oscillator under external Gaussian excitation and replaces the nonlinear structure by a linear model based on minimizing a statistical error function between the outputs of two systems. Many developments have been proposed since to address the drawbacks of the technique such as the requirement of partially knowing the system or its limitation to specific excitations. More works in this field can be found in Iwan (1973), Wen (1980), Iwan and Mason (1980), Bruckner and Lin (1987), Roberts and Spanos (1990), Socha and Soong (1991), Bouc (1994), Rice (1995), Soize and Le Fur (1997), Proppe et al. (2003), Bellizzi and Defilippi (2003), Belendez et al. (2008), and Socha (2008).

Time-domain methods

Time-domain system identification methods have the advantage of taking direct measurements as input, resulting in no loss of embedded information about the system in the recorded data, as well as less time and effort to spend on data acquisition and processing. A fundamental time-domain approach, called “Restoring Force Surface” (RFS), was proposed by Masri and Caughey (1979) and Masri et al. (1982) that initiated the analysis of nonlinear structural systems in terms of their internal RFSs. The original method was extremely appealing for its simplicity of concept; however, it suffered from complicated numerical analysis. It also required all vibration-signatures (acceleration, velocity, displacement) data at all DOFs. Many researchers tried to improve the method and overcome these demands in the following years including Masri et al. (1987a), Masri et al. (1987b), Worden (1990a), Worden (1990b), Mohammad et al. (1992), Duym and Schoukens (1995), Kerschen et al. (2001), Haroon et al. (2005), Nayeri et al. (2008), and Allen et al. (2008). Another interesting time-domain technique for nonlinear system identification based on the generalization of the multivariable ARMAX models for linear systems, called NARMAX (Nonlinear Auto-Regressive Moving Average models with eXogeneous input), has been proposed by Leontaritis and Billings (1985a) and Leontaritis and Billings (1985b) and received considerable attention in the structural dynamics community.

Frequency-domain methods

Frequency-domain system identification methods study the data mainly in the form of spectra or Frequency Response Functions (FRF). Easier computation and more intuitive interpretation are key advantages of these methods over time-domain approaches. Early frequency-domain methods for nonlinear system identification were based upon the use of functional series such as Volterra and Wiener series (Schetzen (1980)). An example of the application of these methods in the field of structural dynamics was presented by Gifford (1989) in his doctoral dissertation. His proposed method was based on extracting nonlinear parameters by fitting surfaces or hyper-surfaces to the Higher Order Frequency Response Functions (HOFRF). The method was later improved and expanded in various works such as Storer and Tomlinson (1993), Khan and Vyas (2001), and Chatterjee and Vyas (2004). Other frequency-domain approaches have been developed for identification of nonlinear systems, including methods using nonlinear resonances (e.g., Nayfeh (1985)), spectral methods based on the reverse path analysis (e.g., Rice and Fitzpatrick (1988));

methods using higher-order spectra (e.g., Roberts et al. (1995)); techniques using associated linear equations (e.g., Feijoo et al. (2004)), or those developed for Hammerstein models (e.g., Bai (2010)). For a comprehensive overview of this field of research, readers may consult Pintelon and Schoukens (2001).

Modal methods

Modal analysis represents a dynamic system in the form of its modal parameters. Despite the popularity and suitability of this traditional method for linear models, its application to highly-nonlinear systems usually leads to erroneous results. Seminal work of Rosenberg (1962) and Rosenberg (1966) on the concept of Nonlinear Normal Mode (NNM) has provided an excellent theoretical foundation for developing nonlinear system identification methods based on modal analysis; however, new complications will arise due to the amplitude-dependency of NNMs and their periods. Among many techniques that have been developed based on this methodology is an early attempt by Szemplinska-Stupnicka (1979) and Szemplinska-Stupnicka (1983) to approximate NNMs using the mode of vibration in resonant conditions.

Investigators have also proposed other modal methods for identification of nonlinear systems. Masri et al. (1982) introduced a low-order regression analysis in modal space using the classical RFS method. Bellizzi et al. (2001) proposed an identification method based on comparing experimental coupled nonlinear modes to the predicted ones. Representatives of recent applications of modal analysis for nonlinear system identification can be found in He et al. (2008) and Platten et al. (2009).

Time-frequency analysis

Time-frequency analysis is based on studying the time-varying nature of the vibrational characteristics of the nonlinear system by decomposing the signal into a set of simpler components. Spina et al. (1996) studied the application of time-frequency analysis using Gabor transform on nonlinear oscillations. The Gabor transform identifies a time-variant matrix to decouple the transient response into a set of quasi-harmonic components. Kitada (1998) proposed a method based on expanding the response and excitation of the nonlinear system in terms of scaling functions using wavelet transform. Ghanem and Romeo (2001) presented a wavelet-based approach using orthogonal Daubechies scaling functions for model and parameter identification of nonlinear systems. Kareem and Kijewski (2002) studied the use of the wavelet transform for time-frequency analysis of wind effects on structures. Pai et al. (2008) proposed a methodology that uses the Hilbert-Huang transform (HHT) and a Sliding-Window Fitting (SWF) technique to drive time-dependent dynamic characteristics of nonlinear systems through perturbation analysis.

Black-box modeling

Black-box modeling is a practical data-only-based system identification method that makes no a priori assumption about the model. When physical insight about the system or the source of nonlinearity is not available, nonlinear black-box modeling can be considered for system identification purposes; however, the identified model parameters may not be specifically attributed to physical information of the structure. Artificial neural network is among the most popular approaches that have been used for nonlinear mapping between recorded input and output data of the system. The fundamental paper of Narendra and Parthasarathy (1990) demonstrated that neural networks can be used effectively for the identification and control of nonlinear dynamical systems. Masri et al. (1992) and Masri et al. (1993) used "dynamic neurons" in a multi-layer perceptron neural networks structure to represent nonlinear systems. Chen and Billings (1992), Chassiakos and Masri (1996), Masri et al. (2000), Kosmatopoulos et al. (2001), and Chen (2009) have also studied using artificial neural networks for black-box nonlinear system identification purposes. Other methods for non-parametric identification of nonlinear systems include splines models (e.g. Peifer et al. (2003)), and dynamic fuzzy wavelet neural networks models (e.g. Adeli and Jiang (2006)).

Structural model updating

Structural model updating techniques compute and update the model parameters through minimizing an objective function that measures the deviation of simulated response of the model from the corresponding real measurement. One of the main applications of these techniques is to make corrections to the initial finite element model of complex structures which usually suffers from modeling, parameter, and testing errors. Berman and Flannelly (1971) and Baruch (1978) were among the first researchers to introduce finite element model updating for linear structures. Schmidt (1994) used the method of modal state observers to update the parameters of nonlinear dynamic systems. Dippery and Smith (1998) employed the minimum model error estimation algorithm for updating nonlinear models. Kyprianou et al. (2001) used differential evolution algorithm for minimizing the objective function in the method. Meyer and Link (2003) defined the objective function based on the difference between the measured and predicted displacement response in the frequency domain. Yuen and Beck (2003) proposed a model updating method to quantify the uncertainties in the model parameters. Kerschen and Golinval (2005) proposed a two-step methodology for decoupling the estimation of the linear and nonlinear parameters of the finite element model. Muto and Beck (2008) developed an identification method for hysteretic systems using Bayesian updating. For a detailed description of model updating methods, the readers are referred to Friswell and Mottershead (1995).

IV.1.2 Scope

In this study, the performance of six different system identification methods is investigated, using experimental data obtained from a 4-story model building. The six methods under discussion are:

(i). Linear System Using Least-Squares Method

(ii). Symmetric Linear System Using Least-Squares Method

(iii). Restoring Force Surface (RFS) Method for Chain-Like Systems

(iv). Model Updating Method

(v). Sub-Space Identification Method

(vi). Iterative Prediction-Error Minimization Method

It is not the intention of this research to compare these methods in detail, but rather to study their performance in identifying the structural dynamic properties of the system. Comparison of different system identification techniques on operational data is potentially a subjective matter for several reasons. Firstly, due to the lack of a reliable reference system, the methods can only be compared relative to one another rather than to the exact solution. Furthermore, the comparison criterion is also a highly subjective choice depending on the actual application. Some researchers may suggest that the accuracy of the identified modal properties or the regenerated response is the critical parameter for comparison of the methods, while others might emphasize the significance of other factors such as robustness, computational efficiency, etc (Andersen et al. (1999)).

Considering the relatively small size of the structural model under discussion (4 DOF system), emphasis in this study is placed on studying the identified structural matrices (mass, damping, and stiffness matrices), and modal properties (frequencies, damping, and mode-shapes) for the purpose of detecting, localizing and quantifying the nonlinearity in the system throughout the experiment.

The theory behind each method is briefly reviewed in section IV.2. In section IV.3, the test structure, a 4-story model building which was investigated experimentally at Hunan University in China, as well as the test procedure are explained. Section IV.4 presents the results and discussion, and section IV.5 highlights the concluding remarks.

IV.2 Overview of System Identification Methods Under Discussion

IV.2.1 Linear System Using Least-Squares Method

Consider a discrete nonlinear MDOF system that is subjected to directly applied excitation forces $f_1(t)$ as well as prescribed support motions $x_0(t)$. The governing equations of motion for this multi-input/multi-output nonlinear system can be written as

$$\mathbf{M}^e_{11}\ddot{\mathbf{x}}_1(t)+\mathbf{C}^e_{11}\dot{\mathbf{x}}_1(t)+\mathbf{K}^e_{11}\mathbf{x}_1(t)+\mathbf{M}^e_{10}\ddot{\mathbf{x}}_0(t)+\mathbf{C}^e_{10}\dot{\mathbf{x}}_0(t)+\mathbf{K}^e_{10}\mathbf{x}_0(t)+\mathbf{f}_{NL}(t)=\mathbf{f}_1(t) \quad \text{(IV.1)}$$

where the coefficients are defined as follows:

- $f_1(t)$ = column vector of order n_1, representing directly applied forces;
- $x(t) = (x_1^T(t), x_0^T(t))^T$ = system displacement vector of order $n_1 + n_0$;
- $x_1(t)$ = active DOF displacement vector of order n_1;

- $x_0(t)$ = prescribed support displacement vector of order n_0;
- $\mathbf{M}_{11}^e$, $\mathbf{C}_{11}^e$, $\mathbf{K}_{11}^e$ = constant matrices that characterize the equivalent inertia, damping, and stiffness forces associated with the unconstrained DOFs of the system, each of order $n_1 \times n_1$;
- $\mathbf{M}_{10}^e$, $\mathbf{C}_{10}^e$, $\mathbf{K}_{10}^e$ = constant matrices that characterize the inertia, damping, and stiffness forces associated with the support motions, each of order $n_1 \times n_0$;
- $f_{NL}(t)$ = an n_1 column vector of nonlinear nonconservative forces.

The governing equation of the linearized version of this system can be presented as

$$\mathbf{M}_{11}^e\ddot{\mathbf{x}}_1(t) + \mathbf{C}_{11}^e\dot{\mathbf{x}}_1(t) + \mathbf{K}_{11}^e\mathbf{x}_1(t) + \mathbf{M}_{10}^e\ddot{\mathbf{x}}_0(t) + \mathbf{C}_{10}^e\dot{\mathbf{x}}_0(t) + \mathbf{K}_{10}^e\mathbf{x}_0(t) = \mathbf{f}_1(t) \qquad \text{(IV.2)}$$

For clarity of presentation, let the six matrices appearing in Equation IV.2 be denoted by ${}^1A$, ${}^2A$, ..., ${}^6A$, respectively. If the i^{th} row of a generic matrix ${}^jA$ is shown as $\langle {}^jA_i \rangle$, the parameter vector α_i, that constitutes all of these elements in six matrices, can be introduced as:

$$\alpha_{\mathbf{i}} = (\langle {}^1A_i \rangle, \langle {}^2A_i \rangle, \langle {}^3A_i \rangle, \langle {}^4A_i \rangle, \langle {}^5A_i \rangle, \langle {}^6A_i \rangle)^T \qquad \text{(IV.3)}$$

Let the response vector $r(t)$ of order $3(n_1 + n_0)$ be defined as

$$\mathbf{r}(t) = (\ddot{\mathbf{x}}_1^T(t), \dot{\mathbf{x}}_1^T(t), \mathbf{x}_1^T(t), \ddot{\mathbf{x}}_0^T(t), \dot{\mathbf{x}}_0^T(t), \mathbf{x}_0^T(t))^T \qquad \text{(IV.4)}$$

If the excitation and the response of this linear system is measured at time steps $t = t_1, t_2, ..., t_N$, then at every t_k

$${}^1A\ddot{\mathbf{x}}_1(t_k) + {}^2A\dot{\mathbf{x}}_1(t_k) + {}^3A\mathbf{x}_1(t_k) + {}^4A\ddot{\mathbf{x}}_0(t_k) + {}^5A\dot{\mathbf{x}}_0(t_k) + {}^6A\mathbf{x}_0(t_k) = \mathbf{f}_1(t_k) \qquad k = 1, 2, ..., N \qquad \text{(IV.5)}$$

With introduction of matrix $\mathbf{R}$ as

$$\mathbf{R} = \begin{bmatrix} \mathbf{r}^T(t_1) \\ \mathbf{r}^T(t_2) \\ \vdots \\ \mathbf{r}^T(t_N) \end{bmatrix} \quad \text{(IV.6)}$$

the grouping of the measurements can be expressed concisely as

$$\hat{\mathbf{R}}\hat{\alpha} = \hat{\mathbf{b}} \quad \text{(IV.7)}$$

where $\hat{\mathbf{R}}$ is a block diagonal matrix whose diagonal elements are equal to R, $\hat{\alpha} = (\hat{\alpha}_{\mathbf{1}}^{\mathbf{T}}, \hat{\alpha}_{\mathbf{2}}^{\mathbf{T}}, ..., \hat{\alpha}_{\mathbf{n_1}}^{\mathbf{T}})^T$ and $\hat{\mathbf{b}}$ is the corresponding vector of excitation measurements. It should be noted that $\hat{\mathbf{R}}$ is of order $m \times n$ where $m = Nn_1$, and $n = 3n_1(n_1 + n_0)$, and therefore, if a sufficient number of measurements is taken, it will result in $m > n$. Under these conditions, least-squares procedures can be used to solve for all the system parameters that constitute the entries in $\hat{\alpha}$:

$$\hat{\alpha} = \hat{\mathbf{R}}^{\dagger}\hat{\mathbf{b}} \quad \text{(IV.8)}$$

where $\hat{\mathbf{R}}^{\dagger}$ is the pseudo-inverse of $\hat{\mathbf{R}}$. In the more general case where the measurements associated with certain DOFs are more reliable than others and/or measurements accumulated over certain time periods are to be emphasized differently from the others, a symmetric, nonsingular, usually diagonal error weighting matrix $\mathbf{W}$ can be used with the overdetermined set of equations in Equation IV.7. Let the deviation error $\underline{\hat{e}}$ be

$$\underline{\hat{e}} = \hat{\mathbf{b}} - \hat{\mathbf{R}}\hat{\alpha} \quad \text{(IV.9)}$$

Using the weighted least-squares method to minimize the cost function J,

$$J = \underline{\hat{e}}^T W \underline{\hat{e}} \tag{IV.10}$$

results in the following approximate solution

$$\hat{\alpha} = (\mathbf{\hat{R}^T W \hat{R}})^{-1} \mathbf{\hat{R}^T W \hat{b}} \tag{IV.11}$$

Considering the diagonal nature of partitioned matrix $\mathbf{\hat{R}}$, the solution of Equation IV.7 can be simplified into a set of n_1 decoupled matrix equations, each of the form:

$$\mathbf{R}\hat{\alpha}_\mathbf{i} = \mathbf{\hat{b}_i} \qquad i = 1, 2, ..., n_1 \tag{IV.12}$$

Comparing the orders of $\mathbf{\hat{R}}$ to $\mathbf{R}$ shows that the order of $\mathbf{R}$ is smaller by a factor of n_1^2, making Equation IV.12 much more computationally efficient. Least-squares techniques can again be used to find the components of the n_1 parameter vectors $\hat{\alpha}_i$:

$$\hat{\alpha}_\mathbf{i} = \mathbf{\hat{R}}^\dagger \mathbf{\hat{b}_i} \tag{IV.13}$$

Note that $\mathbf{\hat{R}}^\dagger$ needs to be computed only once (Masri et al. (1987a)).

IV.2.2 Symmetric Linear System Using Least-Squares Method

When dealing with structural systems, it is a legitimate assumption that structural matrices possess symmetric properties. For a special case of linear system with symmetric matrices, the i^{th} (row) component of the n_1 system of equations in Equation IV.2 is presented as

$$\sum_{j=i}^{n_1} \left({}^{1}A_{ij}\ddot{\mathbf{x}}_{1_j} + {}^{2}A_{ij}\dot{\mathbf{x}}_{1_j} + {}^{3}A_{ij}\mathbf{x}_{1_j} + {}^{4}A_{ij}\ddot{\mathbf{x}}_{0_j} + {}^{5}A_{ij}\dot{\mathbf{x}}_{0_j} + {}^{6}A_{ij}\mathbf{x}_{0_j} \right) +$$
$$\sum_{j=1}^{i-1} \left({}^{1}A_{ij}\ddot{\mathbf{x}}_{1_j} + {}^{2}A_{ij}\dot{\mathbf{x}}_{1_j} + {}^{3}A_{ij}\mathbf{x}_{1_j} \right) = \mathbf{f}_{1_i}(t) \qquad i = 1, 2, ..., n_1 \tag{IV.14}$$

Let $\langle {}^{j}A_i^l \rangle$ denote the elements of a square matrix ${}^{j}A$ that reside in row i and lie below the diagonal of the partitioned matrix. For example $\langle {}^{j}A_i^l \rangle = 0$ and $\langle {}^{j}A_k^l \rangle = ({}^{j}A_{k,1}, {}^{j}A_{k,2}, ..., {}^{j}A_{k,k-1})$. Similarly, let $\langle {}^{j}A_i^u \rangle$ denote the complement of $\langle {}^{j}A_i^l \rangle$ associated with row i. In other words, $\langle {}^{j}A_i^u \rangle$ corresponds to the diagonal and above the diagonal elements of row i. For example, in a matrix ${}^{j}A$ of order n, $\langle {}^{j}A_k^u \rangle = ({}^{j}A_{k,k}, {}^{j}A_{k,k+1}, ..., {}^{j}A_{k,n})$. Using this notation, the following quantities are defined:

$$\underline{\alpha}_{\mathbf{i}} = (\langle {}^{1}A_i^u \rangle, \langle {}^{2}A_i^u \rangle, \langle {}^{3}A_i^u \rangle, \langle {}^{4}A_i \rangle, \langle {}^{5}A_i \rangle, \langle {}^{6}A_i \rangle)^T \tag{IV.15}$$

$$\underline{\beta}_{\mathbf{i}} = (\langle {}^{1}A_i^l \rangle, \langle {}^{2}A_i^l \rangle, \langle {}^{3}A_i^l \rangle)^T \tag{IV.16}$$

$$\begin{aligned} \underline{\mathbf{r}}_i(t) = {} & (\ddot{\mathbf{x}}_{1_i}^T(t), \ddot{\mathbf{x}}_{1_{i+1}}^T(t), ..., \ddot{\mathbf{x}}_{1_{n_1}}^T(t), \dot{\mathbf{x}}_{1_i}^T(t), \dot{\mathbf{x}}_{1_{i+1}}^T(t), ..., \dot{\mathbf{x}}_{1_{n_1}}^T(t), \\ & \mathbf{x}_{1_i}^T(t), \mathbf{x}_{1_{i+1}}^T(t), ..., \mathbf{x}_{1_{n_1}}^T(t), \ddot{\mathbf{x}}_0^T(t), \dot{\mathbf{x}}_0^T(t), \mathbf{x}_0^T(t))^T \end{aligned} \tag{IV.17}$$

$$\begin{aligned} \underline{\mathbf{v}}_{\mathbf{i}}(t) = {} & (\ddot{\mathbf{x}}_{1_1}^T(t), \ddot{\mathbf{x}}_{1_2}^T(t), ..., \ddot{\mathbf{x}}_{1_{i-1}}^T(t), \dot{\mathbf{x}}_{1_1}^T(t), \dot{\mathbf{x}}_{1_2}^T(t), ..., \dot{\mathbf{x}}_{1_{i-1}}^T(t), \\ & \mathbf{x}_{1_1}^T(t), \mathbf{x}_{1_2}^T(t), ..., \mathbf{x}_{1_{i-1}}^T(t))^T \end{aligned} \tag{IV.18}$$

With the definition of $\alpha_{\mathbf{i}}$, $\beta_{\mathbf{i}}$, $\mathbf{r}_{\mathbf{i}}(t)$ and $\mathbf{v}_{\mathbf{i}}(t)$, Equation IV.14 can be expressed as:

$$\underline{\mathbf{r}}_{\mathbf{i}}{}^T(t)\underline{\alpha}_{\mathbf{i}} + \underline{\mathbf{v}}_{\mathbf{i}}{}^T(t)\underline{\beta}_{\mathbf{i}} = \mathbf{f}_{1_i}(t) \tag{IV.19}$$

which can be rewritten in the form:

$$\underline{\mathbf{r}}_{\mathbf{i}}{}^{T}(t)\underline{\alpha}_{\mathbf{i}} = \mathbf{f}_{i}(t) - \underline{\mathbf{v}}_{\mathbf{i}}{}^{T}(t)\underline{\beta}_{\mathbf{i}} \tag{IV.20}$$

Starting from the first row ($i = 1$), $\underline{\mathbf{v}}_{\mathbf{i}}(t)$ is a null vector and elements of $\underline{\alpha}_{\mathbf{1}}$ can be computed as in general method. For the next rows, system parameters in $\underline{\beta}_{\mathbf{i}}$ have been determined in the previous stage of the calculation and the term on the RHS of Equation IV.20 is known or can be measured. Thus a system with symmetric matrices can be identified for the given measurements (Masri et al. (1987a)).

IV.2.3 Restoring Force Surface (RFS) Method for Chain-Like Systems

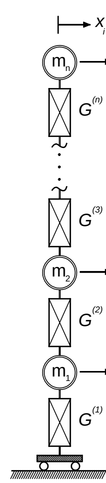

Figure IV.1: Model of a MDOF chain-like system.

Consider the MDOF chain-like structure shown in Figure IV.1 which consists of n elements, each with a lumped mass m_i, and an arbitrary (unknown) nonlinear restoring function $G^{(i)}$. The structure may be subjected to a base excitation $\mathbf{x_0}(t)$, and/or directly applied forces $F_i(t)$. In the context of civil structures, this system would be analogous to an n-story building with rigid floor slabs under ambient forces or ground motion excitation. It is assumed that the absolute acceleration at each element, $\ddot{\mathbf{x}}_i(t)$, is directly available from measurement. The other state variables, $\dot{\mathbf{x}}_i(t)$ and $\mathbf{x}_i(t)$, can be computed through integration of acceleration records. At this stage, we also need to assume that the applied force $F_i(t)$ are measurable. The relative motion between two consecutive elements can be computed as follows:

$$\mathbf{z_i}(t) = \mathbf{x_i}(t) - \mathbf{x_{i-1}}(t) \qquad i = 1, 2, ..., n \tag{IV.21}$$

A reasonable assumption in the field of structural dynamics is that the restoring force at each element is only dependent on the relative displacement and velocity across the terminals of that element:

$$\mathbf{G^{(i)}} = \mathbf{G^{(i)}}(\mathbf{z_i}, \dot{\mathbf{z}}_\mathbf{i}) \tag{IV.22}$$

Therefore the equations of motion for such a system can be written as

$$\begin{aligned} m_n\ddot{\mathbf{x}}_\mathbf{n} &= \mathbf{F_n}(t) - \mathbf{G^{(n)}}(\mathbf{z}_n, \dot{\mathbf{z}}_\mathbf{n}) \\ m_i\ddot{\mathbf{x}}_\mathbf{i} &= \mathbf{F_i}(t) - \mathbf{G^{(i)}}(\mathbf{z}_i, \dot{\mathbf{z}}_\mathbf{i}) + \mathbf{G^{(i+1)}}(\mathbf{z}_{i+1}, \dot{\mathbf{z}}_\mathbf{i+1}) \qquad i = n-1, n-2, ..., 1 \end{aligned} \tag{IV.23}$$

Equation IV.23 can be rewritten to express the unknown restoring force functions as

$$\begin{aligned} \mathbf{G^{(n)}}(\mathbf{z}_n, \dot{\mathbf{z}}_n) &= \mathbf{F_n}(t) - m_n\ddot{\mathbf{x}}_\mathbf{n} \\ \mathbf{G^{(i)}}(\mathbf{z}_i, \dot{\mathbf{z}}_i) &= \mathbf{F_i}(t) - m_i\ddot{\mathbf{x}}_\mathbf{i} + \mathbf{G^{(i+1)}}(\mathbf{z}_{i+1}, \dot{\mathbf{z}}_\mathbf{i+1}) \qquad i = n-1, n-2, ..., 1 \end{aligned} \tag{IV.24}$$

which can be presented in the more compact form of

$$\mathbf{G}^{(\mathbf{i})}(\mathbf{z}_i, \dot{\mathbf{z}}_i) = \sum_{j=i}^{n} (\mathbf{F}_\mathbf{j}(t) - m_j \ddot{\mathbf{x}}_\mathbf{j}) \qquad i = 1, 2, ..., n \tag{IV.25}$$

Thus, starting from the tip of the chain, one can sequentially determine the time-histories of all the inter-story restoring forces within the chain. The advantage of this formulation is that the identification problem of a MDOF system is converted to a set of decoupled SDOF problems. For the very top element, the restoring force is directly computed by subtracting the inertia force from the external force measured at the top element. Then, starting from the element right before the very last, the restoring force can be calculated by subtracting the inertia force from the external force at that element, plus the restoring force of the previous element which has been computed in the previous step. It should be noted that since the identification of the restoring force for each element within the chain is dependent on the restoring force of the previous element, there is an error accumulation effect, in which the error propagates down the chain and leads to a bigger error for the lower elements of the chain.

Once the time-history of the restoring functions for all the elements is determined, one can use suitable basis functions to approximate a nonparametric model for each element. A suitable choice of basis functions would be a power series expansion in the doubly indexed series as follows:

$$\mathbf{Basis} = \mathbf{\Phi} = \sum_{q=0}^{q_{max}} \sum_{r=0}^{r_{max}} \mathbf{z}^q \dot{\mathbf{z}}^r \tag{IV.26}$$

A third-order expansion is usually sufficient for most of practical applications in structural dynamics. Thus, for $q_{max} = r_{max} = 3$, the set of basis functions becomes

$$\mathbf{\Phi} = \left\{1, \dot{\mathbf{z}}, \dot{\mathbf{z}}^2, \dot{\mathbf{z}}^3, \mathbf{z}, \mathbf{z}\dot{\mathbf{z}}, \mathbf{z}\dot{\mathbf{z}}^2, \mathbf{z}\dot{\mathbf{z}}^3, \mathbf{z}^2, \mathbf{z}^2\dot{\mathbf{z}}, \mathbf{z}^2\dot{\mathbf{z}}^2, \mathbf{z}^2\dot{\mathbf{z}}^3, \mathbf{z}^3, \mathbf{z}^3\dot{\mathbf{z}}, \mathbf{z}^3\dot{\mathbf{z}}^2, \mathbf{z}^3\dot{\mathbf{z}}^3\right\} \tag{IV.27}$$

Standard least-squares methods can then be used to find the individual coefficients associated with each basis function

$$\begin{aligned} \mathbf{G^{(i)}} &= \sum_{q=0}^{q_{max}} \sum_{r=0}^{r_{max}} \mathbf{p}_{qr}^{(i)} \mathbf{z}_i^q \dot{\mathbf{z}}_i^r \\ \mathbf{G^{(i)}} &= \mathbf{\Phi}^{(i)} \mathbf{p}^{(i)} \\ \mathbf{p}^{(i)} &= [\mathbf{\Phi}^{(i)}]^{\dagger} \mathbf{G^{(i)}} \end{aligned} \tag{IV.28}$$

where $\mathbf{G^{(i)}}$ is an $N \times 1$ vector whose elements are the time history samples of the i^{th} restoring function; $\mathbf{p}^{(i)}$ is a $((1+q_{max})(1+r_{max}))\times 1$ vector of the unknown parameters $\mathbf{p}_{qr}^{(i)}$ to be identified in the process, $\mathbf{\Phi}^{(i)}$ is an $N \times ((1 + q_{max})(1 + r_{max}))$ matrix of the known time-histories of the basis functions (Equation IV.26), N is the number of time samples, and the superscript † denotes the pseudo-inverse. Note that identified damping and stiffness matrices for chain-like systems will be in symmetric tridiagonal form while the mass matrix is in diagonal form (Masri et al. (1982)).

IV.2.4 Model Updating Method

As discussed earlier, one of the most popular feature-extraction methods in finite element model updating is based on correlating the measured system response, in the frequency or time domain, with the corresponding quantities in the analytical model. For the study reported herein, the cost function to be minimized in the model updating process was similar to the one in the least-squares method for linear systems. The defined cost function quantifies the deviation of the analytical response from the corresponding measured ones and cumulatively sums them over the N data points. In other words, for the linear MDOF system governed by Equation IV.2, model updating procedure was applied for each unconstrained degree of freedom to minimize the following cost function:

$$J(\hat{\alpha}_{\mathbf{i}}) = \|\mathbf{R}\hat{\alpha}_{\mathbf{i}} - \hat{\mathbf{b}}_{\mathbf{i}}\| \qquad i = 1, 2, ..., n_1 \tag{IV.29}$$

where $\| \quad \|$ measures the Euclidian norm of the vector. The CMA-ES optimization package was used to minimize the cost function and achieve an optimal set of elements for the structural dynamic matrices of the system.

IV.2.5 Sub-Space Identification Method

The last two methods under discussion are based on identifying the state-space representation of the structural system. In control engineering, a state-space representation is a mathematical model of a physical system as a set of input, output and state variables related by first-order differential equations. For an LTI dynamical system, these differential and algebraic equations can be written in matrix form, which provides a convenient and compact way to model and analyze multi-input, multi-output (MIMO) systems. Continuous-time state-space representation of an LTI model is presented as:

$$\begin{aligned} \dot{X}(t) &= \mathbf{A}_c X(t) + \mathbf{B}_c U(t) + v(t) \\ Y(t) &= \mathbf{C}_c X(t) + \mathbf{D}_c U(t) + w(t) \end{aligned} \tag{IV.30}$$

where X, Y, and U represent the state, output, and input vectors, respectively. Process noise (v) and measurement noise (w) are assumed to be zero-mean, stationary, white-noise vector sequences. The state-space realization will result in estimation of matrices $\mathbf{A}_c$ (dynamical system matrix), $\mathbf{B}_c$ (input matrix), $\mathbf{C}_c$ (output matrix) and $\mathbf{D}_c$ (feedthrough matrix). For the discrete-time state-space representation of this model, the k^{th} time step can be expressed as:

$$\begin{aligned} X((k+1)T) &= \mathbf{A}X(kT) + \mathbf{B}U(kT) + v(kT) \\ Y(kT) &= \mathbf{C}X(kT) + \mathbf{D}U(kT) + w(kT) \end{aligned} \tag{IV.31}$$

where T is the sampling interval. The relationships between the discrete-time state-space matrices A, B, C, and D and the continuous-time state-space matrices A_c, B_c, C_c, and D_c are given for piece-wise-constant input as follows:

$$\mathbf{A} = e^{\mathbf{A_c}T} \qquad \mathbf{B} = \int_0^T e^{\mathbf{A}_c\tau}\mathbf{B}_c \, \mathrm{d}\tau \qquad \mathbf{C} = \mathbf{C}_c \qquad \mathbf{D} = \mathbf{D}_c \tag{IV.32}$$

To form the state-space representation of the MDOF dynamic system governed by Equation IV.2, state, output, and input vectors are defined as:

$$X(t) = \begin{bmatrix} x_1(t) \\ \dot{x}_1(t) \end{bmatrix} \tag{IV.33}$$

$$Y(t) = x_1(t) \tag{IV.34}$$

$$U(t) = f_1(t) \tag{IV.35}$$

These definitions will result in the following state-space representation

$$\mathbf{A}_c = \begin{bmatrix} \underline{\mathbf{0}} & \underline{\mathbf{I}} \\ -\mathbf{M}^{-1}\mathbf{K} & -\mathbf{M}^{-1}\mathbf{C} \end{bmatrix} \qquad \mathbf{B}_c = \begin{bmatrix} \underline{\mathbf{0}} \\ \mathbf{M}^{-1} \end{bmatrix} \qquad \mathbf{C}_c = \begin{bmatrix} \underline{\mathbf{I}} & \underline{\mathbf{0}} \end{bmatrix} \qquad \mathbf{D}_c = \begin{bmatrix} \underline{\mathbf{0}} \end{bmatrix} \tag{IV.36}$$

This state-space representation is not unique in the sense that we get an equivalent equation by introducing a non-singular transformation matrix T as follows

$$
\begin{aligned}
\mathbf{T}\dot{X}(t) &= \mathbf{T}\mathbf{A}_c\mathbf{T}^{-1}X(t) + \mathbf{T}\mathbf{B}_cU(t) + v(t) \\
Y(t) &= \mathbf{C}_c\mathbf{T}^{-1}X(t) + \mathbf{D}_cU(t) + w(t)
\end{aligned}
\tag{IV.37}
$$

Equations IV.30 and IV.37 are said to be equivalent because they describe the same system and have the same transform function. On the other hand, care must be taken because two state-space equations might have the same transfer function without being equivalent.

Inversely, in order to extract the mass, stiffness, and damping matrices of the structure from its state-space representation, it is necessary to have the identified state-space matrices in the form of Equation IV.36. Since the identification process usually leads to an estimate of the state-space matrices up to a similarity transformation $\mathbf{T}$ ($\mathbf{A}_T = \mathbf{T}\mathbf{A}_c\mathbf{T}^{-1}, \mathbf{B}_T = \mathbf{T}\mathbf{B}_c, \mathbf{C}_T = \mathbf{C}_c\mathbf{T}^{-1}$), the abstraction of $\mathbf{M}$, $\mathbf{C}$, and $\mathbf{K}$ is not straightforward as from $[\mathbf{A}_c, \mathbf{B}_c, \mathbf{C}_c]$. It can be shown that there exists a unique similarity transformation P that transforms $[\mathbf{A}_T, \mathbf{B}_T, \mathbf{C}_T]$ to the form of $[\mathbf{A}_c, \mathbf{B}_c, \mathbf{C}_c]$ in Equation IV.36. A similarity transformation P that satisfies

$$
\begin{aligned}
\mathbf{A}_c &= \mathbf{P}\mathbf{A}_T\mathbf{P}^{-1} \\
\mathbf{B}_c &= \mathbf{P}\mathbf{B}_T \\
\mathbf{C}_c &= \mathbf{C}_T\mathbf{P}^{-1}
\end{aligned}
\tag{IV.38}
$$

is obtained as follows:

$$\mathbf{P} = \begin{bmatrix} \mathbf{C}_T \\ \mathbf{C}_T \mathbf{A}_T \end{bmatrix} \tag{IV.39}$$

The mass, damping, and stiffness matrices can then be determined as (Jezequel (1997)):

$$\mathbf{M} = (\mathbf{C}_T \mathbf{A}_T \mathbf{B}_T)^{-1} \qquad [\mathbf{K} \ \ \mathbf{C}] = \mathbf{M} \mathbf{C}_T \mathbf{A}_T^2 \begin{bmatrix} \mathbf{C}_T \\ \mathbf{C}_T \mathbf{A}_T \end{bmatrix}^{-1} \tag{IV.40}$$

The **n4sid** module in the System Identification Toolbox of MATLAB® was employed for this study.

IV.2.6 Iterative Prediction-Error Minimization Method

The iterative Prediction-Error Minimization algorithm (the **pem** module in the System Identification Toolbox of MATLAB®) was used to estimate model parameters of the structure. For the linear model defined in Equation IV.30, the general symbolic transfer function description is given by:

$$Y(t) = \mathbf{G}U(t) + \mathbf{H}e(t) \tag{IV.41}$$

where $\mathbf{G}$ is a transfer function that takes the input **U** to the output Y. $\mathbf{H}$ is a transfer function that describes the properties of the additive output noise model. PEM uses optimization to minimize the cost function, defined as follows, to find $\mathbf{G}$ and $\mathbf{H}$:

$$V_N(\mathbf{G}, \mathbf{H}) = \sum_{t=t_1}^{t_N} e(t)^2 \tag{IV.42}$$

where $e(t)$ is the difference between the measured output and the predicted output of the model. For a linear model, this error is defined by the following equation:

$$e(t) = \mathbf{H}^{-1}(q)\left[Y(t) - \mathbf{G}(q)U(t)\right] \quad \text{(IV.43)}$$

where q is the lag operator. The subscript N indicates that the cost is a function of the number of data samples and becomes more accurate for larger values of N. As with any nonlinear optimization algorithm, there is a chance that the model might find a local minimum that is not accurate for a specific system. When matrices $\mathbf{G}$ and $\mathbf{H}$ are estimated, one of many available methods can then be used to derive a minimal state-space realization of the system from the transfer function matrix.

IV.3 Experimental Case Study: Hunan University Building Model Structure

IV.3.1 Description of Test Building Model

The case study is a 4-story frame structure which was investigated experimentally at Hunan University, China. The steel-frame building model is $40cm \times 30cm$ in plan and $120cm$ in height with a total mass of $\simeq 52.4kg$. All the junctions between the floors (each made of a $10mm$ thick steel plate) and the column elements (each made of a $120cm$ long steel bar with a cross section of $30mm \times 5mm$) are connected by bolts. In the second phase of the experiment, the structure is also equipped with a magneto-rheological (MR) damper between the third and the fourth floor to simulate nonlinear behavior in the system, and the actual nonlinear hysteretic restoring force is measured by a force transducer. The building model was equipped with one accelerometer at

(a) Building without MR damper

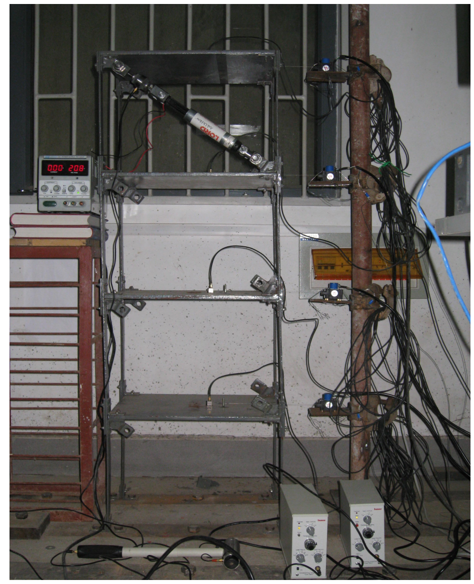

(b) Building with MR damper

Figure IV.2: Experimental case study building model before and after the installation of the MR damper.

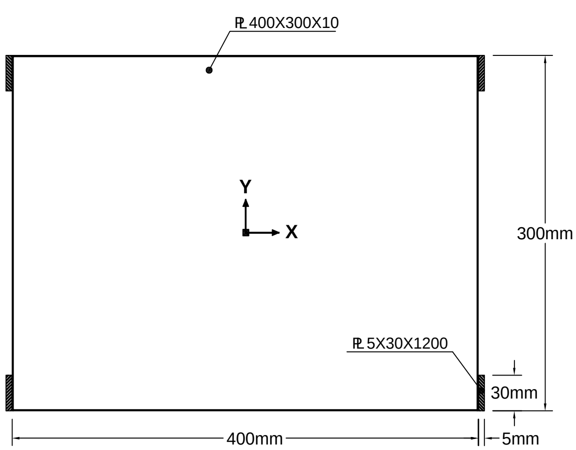

(a) Top view

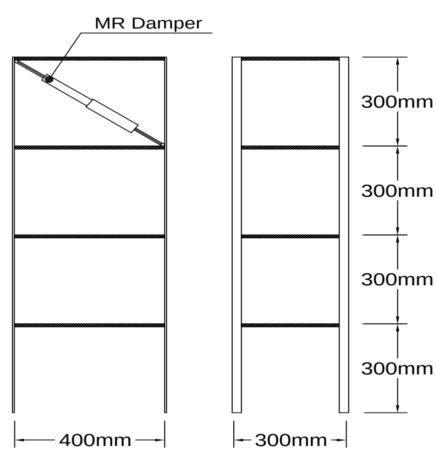

(b) Elevation view

Figure IV.3: (a) Top view and (b) Elevation view of the tested building structure each floor to record the data at the frequency rate of 1000 Hz throughout the experiment. Figure IV.2 shows photos of the building model before and after the installation of the MR damper on the structure. The top view and elevation view of the structure are also illustrated in Figure IV.3.

IV.3.2 Test Cases

For the purpose of nonlinear behavior identification, the experiment was conducted in two stages: (1) before and (2) after adding the MR damper. The behavior of the structure is assumed to be linear before it is equipped with the MR damper. In the second stage, four different nonlinearity scenarios based on the electric current input to the MR damper (0.00A, 0.05A, 0.10A and 0.15A) were considered. In each of these five cases, the structure was excited at each floor by means of an impact hammer, and the corresponding accelerations were measured simultaneously by the accelerometers mounted on each floor, while the velocity and the displacements of the structure were obtained from the integration of the measured accelerations. Figure IV.4 to Figure IV.8 show the applied force on the structure and the corresponding measurements for Case 0 to Case 4, respectively. The description of these tests are also tabulated in Table IV.1 (Xu et al. (2010)).

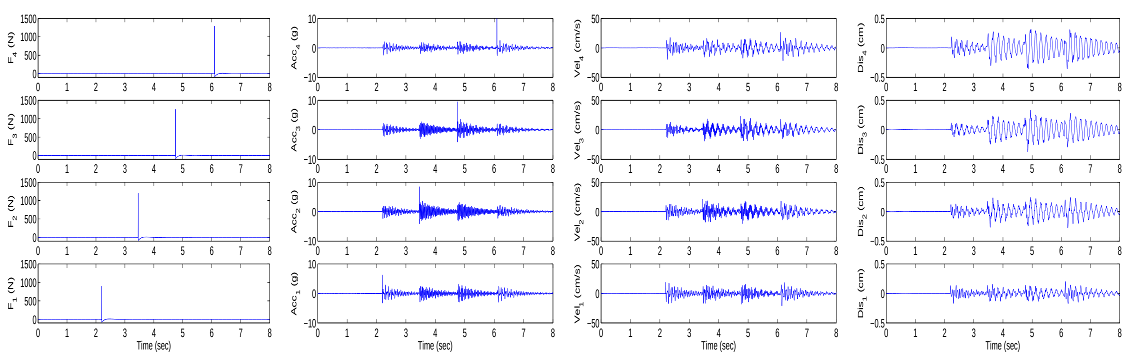

(a) Force (b) Acceleration (c) Velocity (d) Displacement

Figure IV.4: (a) Applied forces and the corresponding recorded (b) Acceleration, (c) Velocity and (d) Displacement at each floor for Case 0 (No MR damper)

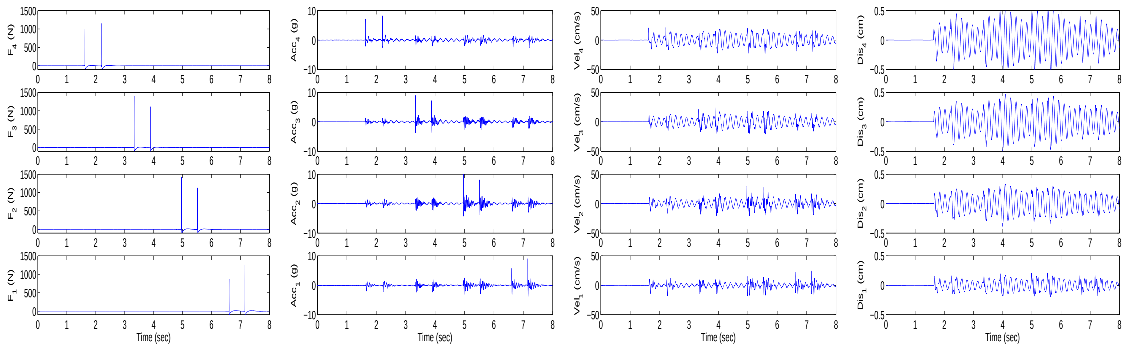

(a) Force (b) Acceleration (c) Velocity (d) Displacement

Figure IV.5: (a) Applied forces and the corresponding recorded (b) Acceleration, (c) Velocity and (d) Displacement at each floor for Case 1 (MR damper with 0.00A input current)

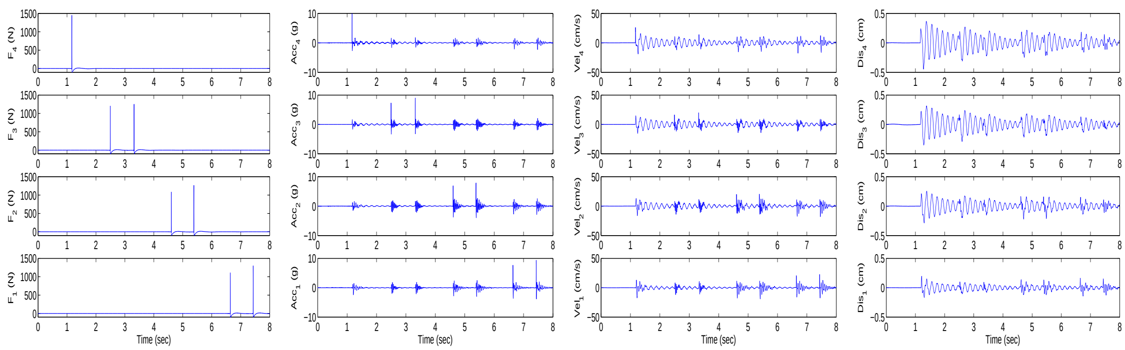

(a) Force (b) Acceleration (c) Velocity (d) Displacement

Figure IV.6: (a) Applied forces and the corresponding recorded (b) Acceleration, (c) Velocity and (d) Displacement at each floor for Case 2 (MR damper with 0.05A input current)

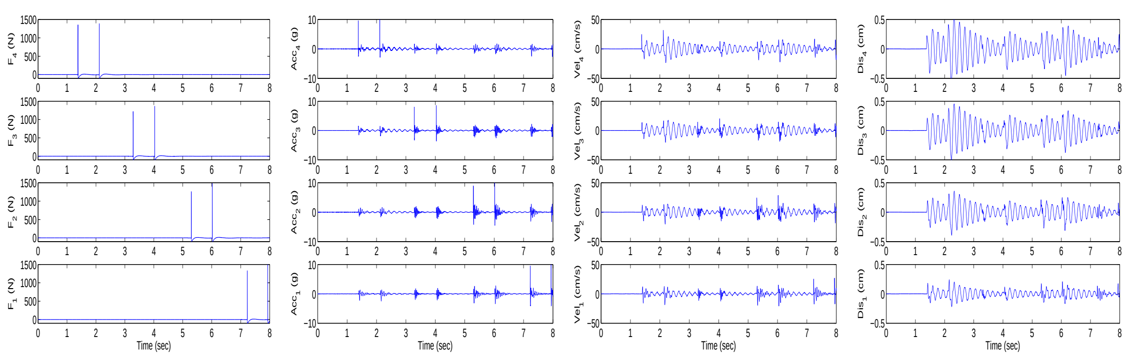

(a) Force (b) Acceleration (c) Velocity (d) Displacement

Figure IV.7: (a) Applied forces and the corresponding recorded (b) Acceleration, (c) Velocity and (d) Displacement at each floor for Case 3 (MR damper with 0.10A input current)

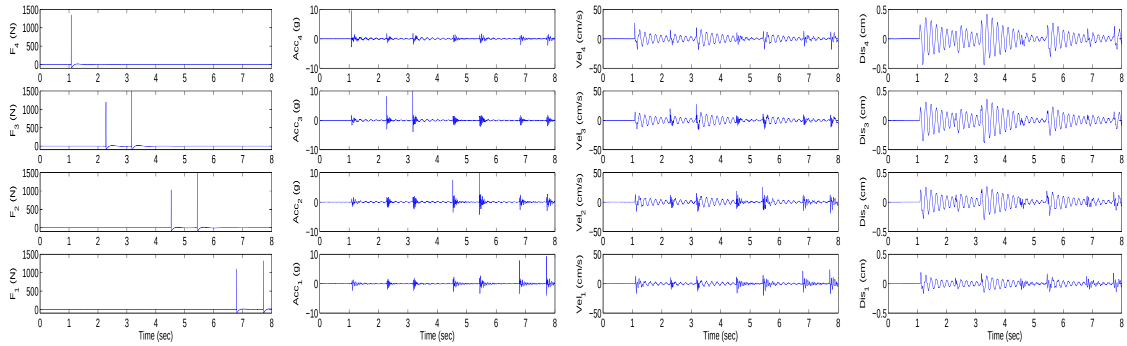

(a) Force (b) Acceleration (c) Velocity (d) Displacement

Figure IV.8: (a) Applied forces and the corresponding recorded (b) Acceleration, (c) Velocity and (d) Displacement at each floor for Case 4 (MR damper with 0.15A input current)

Table IV.1: Description of the conducted experiments

Case #	Input current	Impact forces	Sequence of excitations
Case 0	No MR damper	Single impact force on each floor	1-2-3-4
Case 1	0.00A	Two impact forces on each floor	4-3-2-1
Case 2	0.05A	Single impact force on the 4th floor and two impact forces on others	4-3-2-1
Case 3	0.10A	Two impact forces on each floor	4-3-2-1
Case 4	0.15A	Single impact force on the 4th floor and two impact forces on others	4-3-2-1

IV.4 Results

No information about the structure was assumed for the identification of the system, and only the applied excitations and corresponding system response measurements were used to implement each of the methods under discussion. Therefore the mass, damping, and stiffness coefficients for each test case were identified independently with no priori knowledge about the system. The building model was equipped with one accelerometer at each floor to record the response of the system. From a practical point of view, real structures outside of the lab environment might not enjoy such a comprehensive level of instrumentation on all key degrees-of-freedom. Consequently, it was decided for the purposes of this study, to also investigate a situation under the assumption that only a limited number of sensors is available. The following two scenarios were considered:

(i). **Full Instrumentation Recordings:** Time-history records obtained from all four accelerometers are available.

(ii). **Partial Instrumentation Recordings (Model Order Reduction):** Only time-history records obtained from the accelerometers on the top two floors are available. Considering the sequence and timing of the applied impact forces on the structure, this scenario is only contemplated for cases 1 to 4, using the first 4.0 seconds of the recorded data to avoid the effects of missing excitations on the system.

The recorded data was processed and high pass filtered with the lowest cut-off frequency of 1 Hz.

IV.4.1 Identified Mass, Damping and Stiffness Matrices

Full Instrumentation Recordings

Tables IV.2 and IV.3 present the obtained mass, damping and stiffness matrices from different system identification methods for case 0 and 4, respectively. Comprehensive results for all case studies are tabulated and presented in Appendix A. As expected, other than elements corresponding to the MR damper in the damping matrix (bolded values), no significant change is detected in other structural dynamic matrices throughout the experiment. The identified values in the damping matrix corresponding to the location of MR damper (between the third and fourth floors) monotonically increase as the input current to the MR damper is intensified. Furthermore, there is a reasonable agreement among the identified matrices obtained from different methods.

Table IV.2: Identified mass, damping, and stiffness matrices of the system: Case 0

Method \ Matrix	**M**	**C**	$\mathbf{K}_{(\times 10^{-5})}$
Linear System Method	$\begin{bmatrix} 11.10 & 0.74 & -0.17 & 0.71 \\ 0.63 & 11.99 & 0.27 & 0.29 \\ -0.63 & 0.49 & 12.83 & 0.58 \\ 0.88 & 0.54 & 0.55 & 11.67 \end{bmatrix}$	$\begin{bmatrix} 42.74 & -2.85 & -16.22 & -4.11 \\ -8.20 & 29.61 & -9.55 & -7.29 \\ -15.17 & -7.47 & \mathbf{48.23} & 5.33 \\ -0.96 & -3.69 & -8.70 & \mathbf{12.05} \end{bmatrix}$	$\begin{bmatrix} 2.60 & -1.44 & 0.02 & 0.14 \\ -1.63 & 3.27 & -1.80 & 0.11 \\ 0.06 & -1.72 & 3.08 & -1.45 \\ 0.15 & 0.07 & -1.58 & 1.43 \end{bmatrix}$
Sym. Linear System Method	$\begin{bmatrix} 11.10 & 0.74 & -0.17 & 0.71 \\ 0.74 & 11.06 & 0.38 & 0.30 \\ -0.17 & 0.38 & 12.13 & 0.53 \\ 0.71 & 0.30 & 0.53 & 10.44 \end{bmatrix}$	$\begin{bmatrix} 42.74 & -2.85 & -16.22 & -4.11 \\ -2.85 & 29.60 & -10.26 & -6.55 \\ -16.22 & -10.26 & \mathbf{48.45} & 5.80 \\ -4.11 & -6.55 & 5.80 & \mathbf{9.61} \end{bmatrix}$	$\begin{bmatrix} 2.60 & -1.44 & 0.02 & 0.14 \\ -1.44 & 2.96 & -1.64 & 0.09 \\ 0.02 & -1.64 & 2.97 & -1.39 \\ 0.14 & 0.09 & -1.39 & 1.25 \end{bmatrix}$
RFS Method for Chain-Like Systems	$\begin{bmatrix} 11.34 & 0 & 0 & 0 \\ 0 & 11.15 & 0 & 0 \\ 0 & 0 & 13.06 & 0 \\ 0 & 0 & 0 & 12.55 \end{bmatrix}$	$\begin{bmatrix} 39.60 & -20.83 & 0 & 0 \\ -20.83 & 47.78 & -26.95 & 0 \\ 0 & -26.95 & \mathbf{38.05} & -11.10 \\ 0 & 0 & -11.10 & \mathbf{11.10} \end{bmatrix}$	$\begin{bmatrix} 2.53 & -1.27 & 0 & 0 \\ -1.27 & 2.79 & -1.52 & 0 \\ 0 & -1.52 & 3.07 & -1.55 \\ 0 & 0 & -1.55 & 1.55 \end{bmatrix}$
Model Updating Method	$\begin{bmatrix} 11.12 & 0.72 & -0.21 & 0.74 \\ 0.60 & 11.94 & 0.28 & 0.30 \\ -0.65 & 0.52 & 12.83 & 0.59 \\ 0.85 & 0.51 & 0.54 & 11.65 \end{bmatrix}$	$\begin{bmatrix} 44.00 & -2.63 & -16.23 & -3.96 \\ -7.94 & 29.87 & -10.59 & -7.57 \\ -15.03 & -6.55 & \mathbf{47.25} & 4.83 \\ -2.66 & -2.71 & -7.56 & \mathbf{11.69} \end{bmatrix}$	$\begin{bmatrix} 2.60 & -1.44 & 0.01 & 0.14 \\ -1.63 & 3.26 & -1.80 & 0.11 \\ 0.05 & -1.71 & 3.08 & -1.45 \\ 0.15 & 0.07 & -1.58 & 1.43 \end{bmatrix}$
Sub-Space Method	$\begin{bmatrix} 14.93 & 0.13 & -0.56 & -0.28 \\ 0.01 & 14.10 & 0.02 & -0.17 \\ -0.29 & 0.03 & 13.81 & -0.04 \\ -0.15 & -0.10 & 0.02 & 12.56 \end{bmatrix}$	$\begin{bmatrix} 49.99 & -2.91 & -21.66 & -4.20 \\ -10.07 & 29.36 & -10.09 & -7.75 \\ -16.39 & -7.61 & \mathbf{50.46} & 7.16 \\ -2.36 & -3.02 & -5.95 & \mathbf{12.07} \end{bmatrix}$	$\begin{bmatrix} 3.60 & -2.14 & 0.25 & 0.06 \\ -2.10 & 3.98 & -2.13 & 0.09 \\ 0.23 & -2.05 & 3.49 & -1.64 \\ -0.01 & 0.14 & -1.77 & 1.60 \end{bmatrix}$
Iterative PEM Method	$\begin{bmatrix} 14.50 & 0.10 & -0.50 & -0.18 \\ 0.05 & 14.09 & 0.18 & 0.02 \\ -0.25 & 0.10 & 14.15 & -0.14 \\ 0.11 & 0.04 & 0.09 & 12.78 \end{bmatrix}$	$\begin{bmatrix} 46.97 & -6.92 & -26.79 & 1.39 \\ -16.36 & 24.06 & -5.17 & -6.10 \\ 0.41 & -8.17 & \mathbf{34.47} & 11.28 \\ -5.53 & 0.99 & -0.64 & \mathbf{6.06} \end{bmatrix}$	$\begin{bmatrix} 3.47 & -2.08 & 0.26 & 0.05 \\ -2.06 & 3.92 & -2.13 & 0.12 \\ 0.24 & -2.07 & 3.56 & -1.69 \\ 0.03 & 0.13 & -1.78 & 1.61 \end{bmatrix}$

Table IV.3: Identified mass, damping, and stiffness matrices of the system: Case 4

Method \ Matrix	**M**	**C**	$\mathbf{K}_{(\times 10^{-5})}$
Linear System Method	$\begin{bmatrix} 13.72 & 0.53 & -0.14 & 0.37 \\ 0.55 & 13.00 & 0.67 & -0.12 \\ -0.43 & 1.06 & 13.17 & 2.27 \\ 0.27 & -0.16 & 1.43 & 10.84 \end{bmatrix}$	$\begin{bmatrix} 54.46 & -9.98 & -36.75 & 12.84 \\ -32.06 & 52.49 & 15.33 & -46.34 \\ 25.80 & -84.01 & \mathbf{326.03} & -295.32 \\ -19.19 & 55.89 & -295.02 & \mathbf{323.97} \end{bmatrix}$	$\begin{bmatrix} 3.17 & -1.85 & 0.16 & 0.08 \\ -1.75 & 3.39 & -1.70 & -0.01 \\ 0.10 & -1.47 & 2.62 & -1.22 \\ 0.03 & -0.14 & -1.01 & 1.12 \end{bmatrix}$
Sym. Linear System Method	$\begin{bmatrix} 13.72 & 0.53 & -0.14 & 0.37 \\ 0.53 & 13.26 & 0.67 & -0.14 \\ -0.14 & 0.67 & 13.68 & 2.53 \\ 0.37 & -0.14 & 2.53 & 11.93 \end{bmatrix}$	$\begin{bmatrix} 54.46 & -9.98 & -36.75 & 12.84 \\ -9.98 & 47.69 & 1.55 & -38.42 \\ -36.75 & 1.55 & \mathbf{337.10} & -342.98 \\ 12.84 & -38.42 & -342.98 & \mathbf{424.73} \end{bmatrix}$	$\begin{bmatrix} 3.17 & -1.85 & 0.16 & 0.08 \\ -1.85 & 3.50 & -1.74 & -0.02 \\ 0.16 & -1.74 & 2.93 & -1.33 \\ 0.08 & -0.02 & -1.33 & 1.33 \end{bmatrix}$
RFS Method for Chain-Like Systems	$\begin{bmatrix} 13.60 & 0 & 0 & 0 \\ 0 & 12.74 & 0 & 0 \\ 0 & 0 & 14.68 & 0 \\ 0 & 0 & 0 & 13.67 \end{bmatrix}$	$\begin{bmatrix} 119.17 & -59.31 & 0 & 0 \\ -59.31 & 80.42 & -21.11 & 0 \\ 0 & -21.11 & \mathbf{397.79} & -376.68 \\ 0 & 0 & -376.68 & \mathbf{376.68} \end{bmatrix}$	$\begin{bmatrix} 2.73 & -1.32 & 0 & 0 \\ -1.32 & 2.76 & -1.44 & 0 \\ 0 & -1.44 & 2.95 & -1.51 \\ 0 & 0 & -1.51 & 1.51 \end{bmatrix}$
Model Updating Method	$\begin{bmatrix} 13.73 & 0.53 & -0.13 & 0.34 \\ 0.56 & 12.99 & 0.66 & -0.13 \\ -0.43 & 1.07 & 13.17 & 2.28 \\ 0.27 & -0.16 & 1.44 & 10.84 \end{bmatrix}$	$\begin{bmatrix} 54.92 & -9.71 & -34.79 & 10.80 \\ -31.46 & 51.52 & 15.28 & -46.07 \\ 25.58 & -83.75 & \mathbf{327.39} & -295.90 \\ -18.87 & 54.36 & -293.76 & \mathbf{323.73} \end{bmatrix}$	$\begin{bmatrix} 3.18 & -1.85 & 0.17 & 0.07 \\ -1.75 & 3.38 & -1.70 & -0.01 \\ 0.10 & -1.47 & 2.62 & -1.22 \\ 0.03 & -0.14 & -1.01 & 1.12 \end{bmatrix}$
Sub-Space Method	$\begin{bmatrix} 14.86 & 0.13 & 0.27 & -0.42 \\ -0.03 & 14.29 & 0.11 & -0.03 \\ 0.06 & 0.34 & 14.49 & 0.17 \\ -0.19 & -0.16 & 0.43 & 14.30 \end{bmatrix}$	$\begin{bmatrix} 87.93 & -24.87 & -86.41 & 49.44 \\ -27.47 & 45.98 & 22.36 & -42.95 \\ -0.65 & -80.53 & \mathbf{453.49} & -429.76 \\ -22.58 & 85.22 & -394.62 & \mathbf{431.57} \end{bmatrix}$	$\begin{bmatrix} 3.50 & -2.11 & 0.34 & -0.02 \\ -2.08 & 3.89 & -2.04 & 0.07 \\ 0.37 & -1.98 & 3.40 & -1.68 \\ -0.12 & 0.08 & -1.69 & 1.64 \end{bmatrix}$
Iterative PEM Method	$\begin{bmatrix} 14.72 & 0.29 & -0.19 & -0.10 \\ 0.13 & 14.30 & 0.34 & 0.00 \\ 0.25 & 0.82 & 14.96 & 0.02 \\ -0.32 & -0.11 & 1.08 & 14.06 \end{bmatrix}$	$\begin{bmatrix} 44.01 & -7.69 & -23.05 & 1.12 \\ -15.72 & 41.06 & -18.23 & -11.80 \\ -2.17 & -70.85 & \mathbf{395.98} & -386.26 \\ -8.31 & 50.06 & -375.62 & \mathbf{419.98} \end{bmatrix}$	$\begin{bmatrix} 3.45 & -2.05 & 0.23 & 0.06 \\ -2.05 & 3.84 & -1.98 & 0.04 \\ 0.36 & -1.94 & 3.38 & -1.68 \\ -0.15 & 0.08 & -1.52 & 1.51 \end{bmatrix}$

Partial Instrumentation Recordings (Model Order Reduction)

For this scenario, it is assumed that only time-history records obtained from the accelerometers on the top two floors are available. Tables IV.4 and IV.5 present the obtained mass, damping and stiffness matrices using partial instrumentation recordings for case 1 and 4, respectively. Comprehensive results for all case studies are tabulated and presented in Appendix A. Similar to the results from full instrumentation data, other than elements corresponding to the MR damper in the damping matrix (bolded values), no significant change is detected in other structural dynamic matrices throughout the experiment. For all methods, the identified values in the damping matrix corresponding to the location of MR damper (diagonal terms) monotonically increase as the input current to the MR damper is intensified which is a sign of change in this location. However, there is much less agreement among the identified matrices from different system identification methods probably due to short length of recordings.

IV.4.2 Identified Classical Frequencies and Damping Values

To extract the classical frequencies, damping values, and mode-shapes of the structure, the state-space representation of the system should be constructed using relationships given in Equation IV.36. The modal properties of the system can then be derived using the Equations III.4 to III.8. Figure IV.9 schematically illustrates the four identified frequencies and corresponding mode-shapes of the tested building structure in the excitation direction for case 0.

Tables IV.6 and IV.7 present four extracted classical frequencies and corresponding damping values of the structure using full instrumentation recordings for cases 0 and 4, respectively. Comprehensive results for all case studies are tabulated and presented in Appendix A. As shown in these

Table IV.4: Identified mass, damping, and stiffness matrices of the system, using partial instrumentation recordings: Case 1

Method \ Matrix	**M**	**C**	$\mathbf{K}_{(\times 10^{-5})}$
Linear System Method	$\begin{bmatrix} 9.00 & 1.00 \\ 0.85 & 12.83 \end{bmatrix}$	$\begin{bmatrix} \mathbf{243.18} & -199.32 \\ -191.80 & \mathbf{236.73} \end{bmatrix}$	$\begin{bmatrix} 1.10 & -0.84 \\ -1.45 & 1.40 \end{bmatrix}$
Sym. Linear System Method	$\begin{bmatrix} 9.00 & 1.00 \\ 1.00 & 10.77 \end{bmatrix}$	$\begin{bmatrix} \mathbf{243.18} & -199.32 \\ -199.32 & \mathbf{222.34} \end{bmatrix}$	$\begin{bmatrix} 1.10 & -0.84 \\ -0.84 & 0.86 \end{bmatrix}$
RFS Method for Chain-Like Systems	$\begin{bmatrix} 14.93 & 0.00 \\ 0.00 & 13.65 \end{bmatrix}$	$\begin{bmatrix} \mathbf{296.55} & -227.11 \\ -227.11 & \mathbf{227.11} \end{bmatrix}$	$\begin{bmatrix} 1.64 & -1.29 \\ -1.29 & 1.29 \end{bmatrix}$
Model Updating Method	$\begin{bmatrix} 9.02 & 0.96 \\ 0.84 & 12.88 \end{bmatrix}$	$\begin{bmatrix} \mathbf{250.66} & -194.03 \\ -192.14 & \mathbf{233.61} \end{bmatrix}$	$\begin{bmatrix} 1.11 & -0.85 \\ -1.46 & 1.41 \end{bmatrix}$
Sub-Space Method	$\begin{bmatrix} 14.77 & -3.04 \\ 0.34 & 11.33 \end{bmatrix}$	$\begin{bmatrix} \mathbf{276.80} & -274.35 \\ -177.99 & \mathbf{213.74} \end{bmatrix}$	$\begin{bmatrix} 2.36 & -1.91 \\ -1.35 & 1.29 \end{bmatrix}$
Iterative PEM Method	$\begin{bmatrix} 17.70 & 0.10 \\ 0.26 & 14.68 \end{bmatrix}$	$\begin{bmatrix} \mathbf{322.95} & -290.92 \\ -221.23 & \mathbf{269.75} \end{bmatrix}$	$\begin{bmatrix} 2.38 & -1.86 \\ -1.77 & 1.69 \end{bmatrix}$

Table IV.5: Identified mass, damping, and stiffness matrices of the system, using partial instrumentation recordings: Case 4

Method \ Matrix	**M**	**C**	$\mathbf{K}_{(\times 10^{-5})}$
Linear System Method	$\begin{bmatrix} 10.56 & 1.72 \\ 1.10 & 11.72 \end{bmatrix}$	$\begin{bmatrix} \mathbf{356.80} & -346.07 \\ -331.42 & \mathbf{393.60} \end{bmatrix}$	$\begin{bmatrix} 1.21 & -0.93 \\ -1.19 & 1.19 \end{bmatrix}$
Sym. Linear System Method	$\begin{bmatrix} 10.56 & 1.72 \\ 1.72 & 11.34 \end{bmatrix}$	$\begin{bmatrix} \mathbf{356.80} & -346.07 \\ -346.07 & \mathbf{389.24} \end{bmatrix}$	$\begin{bmatrix} 1.21 & -0.93 \\ -0.93 & 0.97 \end{bmatrix}$
RFS Method for Chain-Like Systems	$\begin{bmatrix} 15.04 & 0.00 \\ 0.00 & 13.59 \end{bmatrix}$	$\begin{bmatrix} \mathbf{454.52} & -404.18 \\ -404.18 & \mathbf{404.18} \end{bmatrix}$	$\begin{bmatrix} 1.73 & -1.37 \\ -1.37 & 1.37 \end{bmatrix}$
Model Updating Method	$\begin{bmatrix} 10.57 & 1.70 \\ 1.09 & 11.76 \end{bmatrix}$	$\begin{bmatrix} \mathbf{356.71} & -345.17 \\ -331.40 & \mathbf{393.89} \end{bmatrix}$	$\begin{bmatrix} 1.22 & -0.94 \\ -1.20 & 1.20 \end{bmatrix}$
Sub-Space Method	$\begin{bmatrix} 15.98 & 0.02 \\ -0.48 & 12.01 \end{bmatrix}$	$\begin{bmatrix} \mathbf{365.85} & -405.81 \\ -340.41 & \mathbf{411.16} \end{bmatrix}$	$\begin{bmatrix} 2.15 & -1.73 \\ -1.45 & 1.41 \end{bmatrix}$
Iterative PEM Method	$\begin{bmatrix} 17.11 & 0.27 \\ 0.21 & 15.05 \end{bmatrix}$	$\begin{bmatrix} \mathbf{449.51} & -481.20 \\ -405.32 & \mathbf{495.60} \end{bmatrix}$	$\begin{bmatrix} 2.29 & -1.83 \\ -1.72 & 1.68 \end{bmatrix}$

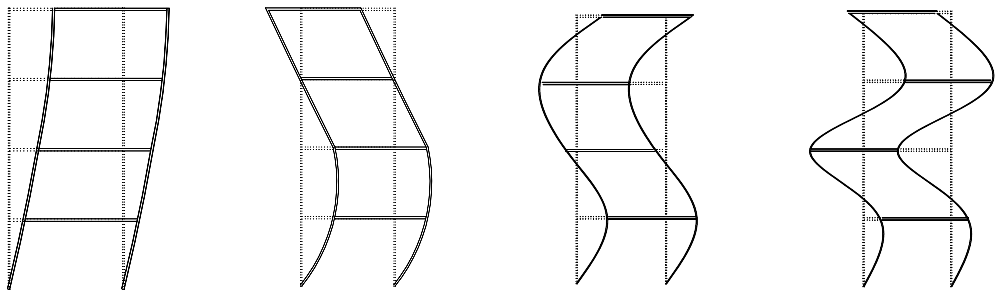

(a) $f_1 \simeq 5.6Hz$ (b) $f_2 \simeq 16.6Hz$ (c) $f_3 \simeq 26.5Hz$ (d) $f_4 \simeq 35.8Hz$

Figure IV.9: Four identified frequencies and corresponding mode-shapes of the tested building structure in the excitation direction for Case 0.

tables, there is a reasonable agreement among the obtained values from different system identification methods. It is also noticeable that the nonlinear behavior of the MR damper is mainly manifested in the damping value of the third dominant mode of the system. As shown in Figure IV.9, the top two floors (location of the MR damper) have the highest participation in the third mode of the system.

Table IV.8 to IV.9 show two identified classical frequencies and corresponding damping values of the structure using partial instrumentation recordings for case 1 to 4, respectively. Note that the two identified modes using partial instrumentation recordings correspond to the first and the third dominant modes of the structure. This is due to the fact the third floor of the structure is minimally excited by the second dominant mode of the system (see Figure IV.9). This reveals one of main potential disadvantages of model order reduction in system identification applications. Again, the increasing damping value of the second identified mode (third mode of the structure) shows a significant change in the damping properties of the system.

Table IV.6: Identified frequencies and damping ratios: Case 0

Method \ Mode	$f_1(Hz)$	$\zeta_1(\%)$	$f_2(Hz)$	$\zeta_2(\%)$	$f_3(Hz)$	$\zeta_3(\%)$	$f_4(Hz)$	$\zeta_4(\%)$
Linear System Method	5.62	1.623	16.70	1.324	26.56	1.165	35.89	0.765
Sym. Linear System Method	5.72	2.024	16.51	1.479	26.81	1.083	35.73	0.759
RFS Method for Chain-Like Systems	5.70	0.279	17.66	0.740	26.18	0.998	32.82	1.564
Model Updating Method	5.62	1.604	16.69	1.369	26.57	1.141	35.90	0.771
Sub-Space Method	5.65	1.768	16.65	1.114	26.54	1.065	35.83	0.629
Iterative PEM Method	5.64	1.497	16.58	0.781	26.38	0.794	35.75	0.560

Table IV.7: Identified frequencies and damping ratios: Case 4

Method \ Mode	$f_1(Hz)$	$\zeta_1(\%)$	$f_2(Hz)$	$\zeta_2(\%)$	$f_3(Hz)$	$\zeta_3(\%)$	$f_4(Hz)$	$\zeta_4(\%)$
Linear System Method	5.55	1.974	16.68	5.003	25.60	11.894	34.64	5.119
Sym. Linear System Method	5.50	1.750	16.50	6.248	26.87	13.504	35.18	4.881
RFS Method for Chain-Like Systems	5.54	0.829	16.76	4.897	24.79	11.194	30.09	6.340
Model Updating Method	5.46	2.045	16.68	5.017	25.61	11.895	34.64	5.111
Sub-Space Method	5.42	2.193	16.70	4.296	25.95	13.149	34.59	4.262
Iterative PEM Method	5.45	1.829	16.51	4.776	25.66	11.010	34.63	4.097

Table IV.8: Identified frequencies and damping ratios (partial instrumentation): Case 1

Method \ Mode	$f_1(Hz)$	$\zeta_1(\%)$	$f_2(Hz)$	$\zeta_2(\%)$
Linear System Method	5.44	4.751	24.68	14.740
Sym. Linear System Method	5.50	4.489	23.05	16.992
RFS Method for Chain-Like Systems	5.39	3.337	22.10	12.327
Model Updating Method	5.42	5.534	24.70	14.651
Sub-Space Method	5.41	3.206	24.65	10.505
Iterative PEM Method	5.44	3.668	24.68	11.122

Table IV.9: Identified frequencies and damping ratios (partial instrumentation): Case 4

Method \ Mode	$f_1(Hz)$	$\zeta_1(\%)$	$f_2(Hz)$	$\zeta_2(\%)$
Linear System Method	5.45	3.888	24.30	24.089
Sym. Linear System Method	5.51	3.630	23.62	26.115
RFS Method for Chain-Like Systems	5.47	2.572	22.73	20.373
Model Updating Method	5.45	3.965	24.36	23.921
Sub-Space Method	5.41	3.346	24.43	17.548
Iterative PEM Method	5.39	3.649	24.50	18.695

IV.4.3 Restoring Forces in Chain-Like System

To evaluate the dependence of the restoring forces on basis functions, the parameters of Equation IV.29 is evaluated by means of the method developed by Masri and Caughey (1979). The approach uses information about the state variables of non-linear systems to express the system characteristics in terms of two-dimensional Chebyshev polynomials as follows:

$$\mathbf{G}(z', \dot{z'}) = \sum_{i=0}^{m} \sum_{j=0}^{n} C_{ij} \mathbf{T}_i(z') \mathbf{T}_j(\dot{z'}) \tag{IV.44}$$

in which $\mathbf{T_i}$ represents the i^{th} Chebyshev polynomial of the first kind and z' and $\dot{z'}$ are the displacement and velocity vectors, normalized through the following equation:

$$z' = \frac{z - \frac{z_{max} + z_{min}}{2}}{\frac{z_{max} - z_{min}}{2}} \tag{IV.45}$$

The orthogonal nature of the Chebyshev polynomials and their equal ripple characteristics make them convenient to use in least-squares approximations.

The fidelity of the method is first evaluated using the synthetic data obtained from two analytical models. The first case is a linear 4-DOF system while a nonlinear damper is added to the second model between the 3^{rd} and 4^{th} DOFs. The nonlinearity is assumed to be proportional to the odd powers of velocity and displacement and their products as follows:

$$\begin{aligned}&\mathbf{M}\ddot{\mathbf{x}}(t)+\mathbf{C}\dot{\mathbf{x}}(t)+\mathbf{K}\mathbf{x}(t)\\&+\mathbf{f}_{NL}\left(\mathbf{x}(t),\mathbf{x}^3(t),\dot{\mathbf{x}}(t),\dot{\mathbf{x}}^3(t),\mathbf{x}(t)\dot{\mathbf{x}}(t),\mathbf{x}^3(t)\dot{\mathbf{x}}(t),\mathbf{x}(t)\dot{\mathbf{x}}^3(t),\mathbf{x}^3(t)\dot{\mathbf{x}}^3(t)\right)=\mathbf{f}(t)\end{aligned} \tag{IV.46}$$

Tables IV.10 and IV.11 present the corresponding parameters of the Chebyshev polynomials in the approximation of the inter-story restoring forces for the linear and nonlinear cases, respectively. Comparison of the two tables shows that the values in the last row of Table IV.11 identify the damping (increase in the value corresponding to $\dot{z}$) and its nonlinearity (non-zero values for odd powers of $\dot{z}$ and z and their products) between the 3^{rd} and 4^{th} DOF of the system.

For the experimental data, Table IV.12 to IV.16 illustrate the corresponding parameters of Chebyshev polynomials of each basis function in the inter-story restoring forces for case 0 to 4, respectively. As shown in these tables, the inter-story forces are primarily determined by the relative displacement in each floor with much less dependence upon other basis functions. The high values representating the relative displacement for the restoring forces in the first three floors show no significant change throughout the experiment while the contribution of the corresponding parameter for the restoring force in the 4^{th} floor gradually decreases during the experiment. Meanwhile, the contribution of the relative velocity of the 4^{th} floor (where nonlinear damper is employed) increases as the current in the MR damper is intensified. The nonlinearity in the system, imposed by MR damper, is also identified by gradual escalation in contribution of z^3 and $\dot{z}^3$. Note that

Table IV.10: Corresponding parameters of basis functions in restoring forces using Chebyshev polynomials: Analytical Linear System

$\mathbf{G_i}$	$\mathbf{z}$	$\mathbf{\dot{z}}$	$\mathbf{z^2}$	$\mathbf{\dot{z}^2}$	$\mathbf{z^3}$	$\mathbf{\dot{z}^3}$	$\mathbf{z\dot{z}}$	$\mathbf{z^2\dot{z}}$	$\mathbf{z\dot{z}^2}$	$\mathbf{z^2\dot{z}^2}$	$\mathbf{z^3\dot{z}}$	$\mathbf{z\dot{z}^3}$	$\mathbf{z^3\dot{z}^2}$	$\mathbf{z^2\dot{z}^3}$	$\mathbf{z^3\dot{z}^3}$	1
$\mathbf{G_1}$	425.82	0.00	-0.23	-0.08	-4.44	-0.01	-0.51	-0.01	-4.56	0.12	0.62	0.38	4.50	0.04	-0.52	-0.03
$\mathbf{G_2}$	400.50	-0.30	0.31	0.13	-4.03	0.20	-3.65	0.52	-5.66	-0.22	3.48	7.79	6.03	-0.27	-8.18	0.39
$\mathbf{G_3}$	319.88	0.03	0.02	-0.01	1.29	0.02	4.55	-0.01	-2.15	-0.03	-4.39	-1.70	2.81	0.00	1.50	-0.08
$\mathbf{G_4}$	292.20	$\mathbf{0.06}$	-0.26	-0.06	$\mathbf{5.49}$	$\mathbf{-0.03}$	$\mathbf{-1.90}$	0.14	0.00	0.11	$\mathbf{2.21}$	$\mathbf{2.30}$	0.94	-0.06	$\mathbf{-2.55}$	-0.09

Table IV.11: Corresponding parameters of basis functions in restoring forces using Chebyshev polynomials: Analytical Nonlinear System

$\mathbf{G_i}$	$\mathbf{z}$	$\mathbf{\dot{z}}$	$\mathbf{z^2}$	$\mathbf{\dot{z}^2}$	$\mathbf{z^3}$	$\mathbf{\dot{z}^3}$	$\mathbf{z\dot{z}}$	$\mathbf{z^2\dot{z}}$	$\mathbf{z\dot{z}^2}$	$\mathbf{z^2\dot{z}^2}$	$\mathbf{z^3\dot{z}}$	$\mathbf{z\dot{z}^3}$	$\mathbf{z^3\dot{z}^2}$	$\mathbf{z^2\dot{z}^3}$	$\mathbf{z^3\dot{z}^3}$	1
$\mathbf{G_1}$	329.43	-0.03	-0.01	-0.03	-7.00	0.12	0.92	0.05	2.32	-0.02	-0.65	-1.08	-4.13	-0.05	0.82	-0.02
$\mathbf{G_2}$	295.83	-0.02	-0.04	0.00	-4.90	0.05	-0.03	-0.09	-2.61	-0.02	0.10	0.10	3.46	0.12	-0.19	-0.05
$\mathbf{G_3}$	267.80	0.09	0.24	0.25	-1.60	-0.05	-0.07	-0.22	-2.42	-0.46	0.07	0.08	2.91	0.30	-0.08	-0.12
$\mathbf{G_4}$	182.48	$\mathbf{155.83}$	-0.47	0.03	$\mathbf{68.75}$	$\mathbf{-10.42}$	$\mathbf{-25.29}$	13.01	-1.55	0.25	$\mathbf{12.48}$	$\mathbf{30.31}$	-2.33	-34.11	$\mathbf{-14.14}$	0.03

Table IV.12: Corresponding parameters of basis functions in restoring forces using Chebyshev polynomials: Case 0

$\mathbf{G_i}$	$\mathbf{z'}$	$\dot{\mathbf{z}}'$	$\mathbf{z'^2}$	$\dot{\mathbf{z}}'^2$	$\mathbf{z'^3}$	$\dot{\mathbf{z}}'^3$	$\mathbf{z'}\dot{\mathbf{z}}'$	$\mathbf{z'^2}\dot{\mathbf{z}}'$	$\mathbf{z'}\dot{\mathbf{z}}'^2$	$\mathbf{z'^2}\dot{\mathbf{z}}'^2$	$\mathbf{z'^3}\dot{\mathbf{z}}'$	$\mathbf{z'}\dot{\mathbf{z}}'^3$	$\mathbf{z'^3}\dot{\mathbf{z}}'^2$	$\mathbf{z'^2}\dot{\mathbf{z}}'^3$	$\mathbf{z'^3}\dot{\mathbf{z}}'^3$	1
$\mathbf{G_1}$	225.25	1.13	-4.07	-1.37	6.88	-1.32	-20.57	-2.32	10.49	3.02	21.01	17.84	-12.19	2.78	-18.83	1.82
$\mathbf{G_2}$	249.91	0.06	-0.36	-0.11	-5.49	0.08	-2.94	0.03	-3.56	0.21	2.99	3.24	3.13	-0.05	-3.31	0.15
$\mathbf{G_3}$	275.74	-0.02	0.54	0.06	11.41	0.23	-0.27	-0.03	-6.82	-0.25	1.40	2.14	1.39	0.13	-2.75	-0.28
$\mathbf{G_4}$	290.05	**0.04**	-1.90	-0.37	21.36	**0.01**	0.40	-0.08	6.72	0.74	-0.20	-0.39	-10.24	0.07	0.21	0.99

Table IV.13: Corresponding parameters of basis functions in restoring forces using Chebyshev polynomials: Case 1

$\mathbf{G_i}$	$\mathbf{z'}$	$\dot{\mathbf{z}}'$	$\mathbf{z'^2}$	$\dot{\mathbf{z}}'^2$	$\mathbf{z'^3}$	$\dot{\mathbf{z}}'^3$	$\mathbf{z'}\dot{\mathbf{z}}'$	$\mathbf{z'^2}\dot{\mathbf{z}}'$	$\mathbf{z'}\dot{\mathbf{z}}'^2$	$\mathbf{z'^2}\dot{\mathbf{z}}'^2$	$\mathbf{z'^3}\dot{\mathbf{z}}'$	$\mathbf{z'}\dot{\mathbf{z}}'^3$	$\mathbf{z'^3}\dot{\mathbf{z}}'^2$	$\mathbf{z'^2}\dot{\mathbf{z}}'^3$	$\mathbf{z'^3}\dot{\mathbf{z}}'^3$	1
$\mathbf{G_1}$	304.22	2.29	1.03	1.04	-13.76	-1.37	53.57	-3.18	-38.83	-0.75	-50.03	-22.86	27.14	1.77	26.53	-0.88
$\mathbf{G_2}$	299.25	1.05	-0.03	0.56	-7.22	-0.43	0.93	0.13	-22.37	-0.89	0.47	-0.01	23.29	-0.63	-1.10	-0.07
$\mathbf{G_3}$	296.72	0.23	-8.55	-0.30	52.20	-1.17	7.14	1.83	-14.07	-0.13	-7.01	-3.09	10.50	0.10	4.07	4.34
$\mathbf{G_4}$	150.17	**24.93**	-14.36	-0.55	40.56	**−19.85**	-11.19	-4.76	59.59	0.49	9.50	12.00	-59.86	6.38	-10.29	7.25

Table IV.14: Corresponding parameters of basis functions in restoring forces using Chebyshev polynomials: Case 2

$\mathbf{G_i}$	$\mathbf{z'}$	$\dot{\mathbf{z}}'$	$\mathbf{z'^2}$	$\dot{\mathbf{z}}'^2$	$\mathbf{z'^3}$	$\dot{\mathbf{z}}'^3$	$\mathbf{z'}\dot{\mathbf{z}}'$	$\mathbf{z'^2}\dot{\mathbf{z}}'$	$\mathbf{z'}\dot{\mathbf{z}}'^2$	$\mathbf{z'^2}\dot{\mathbf{z}}'^2$	$\mathbf{z'^3}\dot{\mathbf{z}}'$	$\mathbf{z'}\dot{\mathbf{z}}'^3$	$\mathbf{z'^3}\dot{\mathbf{z}}'^2$	$\mathbf{z'^2}\dot{\mathbf{z}}'^3$	$\mathbf{z'^3}\dot{\mathbf{z}}'^3$	1
$\mathbf{G_1}$	272.46	0.29	0.18	-0.38	-20.96	0.30	9.62	-1.06	-14.00	-0.18	-2.03	6.89	11.58	0.03	-9.96	0.14
$\mathbf{G_2}$	251.78	1.14	-0.01	0.24	-17.67	-0.50	-0.10	-0.45	2.70	-0.52	0.13	-0.04	3.97	0.34	0.02	0.01
$\mathbf{G_3}$	224.09	0.07	-3.59	-0.21	13.26	-0.16	-0.43	0.23	-33.56	0.56	2.02	3.56	41.05	0.06	-5.05	1.76
$\mathbf{G_4}$	173.39	**35.86**	-4.24	-0.14	73.81	**−23.52**	1.13	-5.30	33.61	0.11	-0.99	-1.88	-32.68	5.10	1.67	2.16

Table IV.15: Corresponding parameters of basis functions in restoring forces using Chebyshev polynomials: Case 3

$\mathbf{G_i}$	$\mathbf{z'}$	$\dot{\mathbf{z}}'$	$\mathbf{z'^2}$	$\dot{\mathbf{z}}'^2$	$\mathbf{z'^3}$	$\dot{\mathbf{z}}'^3$	$\mathbf{z'}\dot{\mathbf{z}}'$	$\mathbf{z'^2}\dot{\mathbf{z}}'$	$\mathbf{z'}\dot{\mathbf{z}}'^2$	$\mathbf{z'^2}\dot{\mathbf{z}}'^2$	$\mathbf{z'^3}\dot{\mathbf{z}}'$	$\mathbf{z'}\dot{\mathbf{z}}'^3$	$\mathbf{z'^3}\dot{\mathbf{z}}'^2$	$\mathbf{z'^2}\dot{\mathbf{z}}'^3$	$\mathbf{z'^3}\dot{\mathbf{z}}'^3$	1
$\mathbf{G_1}$	344.73	2.62	1.12	0.71	-25.75	-2.71	30.00	-3.81	-27.79	-2.22	-26.55	-8.60	19.15	3.91	12.71	-0.37
$\mathbf{G_2}$	300.94	0.83	-0.35	0.03	-28.69	-0.16	2.54	-0.16	-7.56	-0.27	-2.22	-2.44	9.29	-0.25	2.02	0.22
$\mathbf{G_3}$	305.91	0.16	-8.12	0.45	4.51	-0.42	3.94	0.45	-30.79	-0.38	-4.57	-3.05	38.61	0.38	3.67	3.91
$\mathbf{G_4}$	218.00	**51.92**	-7.02	-0.32	45.52	**−33.11**	-2.15	-4.32	13.82	-1.18	2.62	-0.14	-7.87	1.56	-0.56	3.95

Table IV.16: Corresponding parameters of basis functions in restoring forces using Chebyshev polynomials: Case 4

$\mathbf{G_i}$	$\mathbf{z'}$	$\dot{\mathbf{z}}'$	$\mathbf{z'^2}$	$\dot{\mathbf{z}}'^2$	$\mathbf{z'^3}$	$\dot{\mathbf{z}}'^3$	$\mathbf{z'}\dot{\mathbf{z}}'$	$\mathbf{z'^2}\dot{\mathbf{z}}'$	$\mathbf{z'}\dot{\mathbf{z}}'^2$	$\mathbf{z'^2}\dot{\mathbf{z}}'^2$	$\mathbf{z'^3}\dot{\mathbf{z}}'$	$\mathbf{z'}\dot{\mathbf{z}}'^3$	$\mathbf{z'^3}\dot{\mathbf{z}}'^2$	$\mathbf{z'^2}\dot{\mathbf{z}}'^3$	$\mathbf{z'^3}\dot{\mathbf{z}}'^3$	1
$\mathbf{G_1}$	269.45	-0.06	-1.49	-1.36	-11.00	0.67	6.04	0.09	-3.19	1.30	-3.20	2.97	-2.58	-1.20	-1.45	1.11
$\mathbf{G_2}$	255.08	0.50	-0.27	-0.07	-29.11	-0.03	0.13	0.20	-10.21	-0.60	-0.07	0.06	15.59	-0.39	-0.09	0.33
$\mathbf{G_3}$	270.07	0.28	-15.19	-0.32	15.14	-0.72	-1.70	0.86	-41.95	0.83	2.11	3.33	50.41	0.04	-3.88	7.56
$\mathbf{G_4}$	176.71	**62.44**	-9.73	-1.72	56.70	**−39.62**	3.40	-14.65	10.00	3.32	-0.18	-6.36	-7.17	10.38	3.17	4.91

the negative sign of parameters corresponding to $\dot{z}^3$ shows nonlinear softening with respect to the velocity whereas the positive sign of parameters for to z^3 is a sign of nonlinear hardening with respect to the displacement.

IV.5 Concluding Remarks

Based on evaluation of the results from six different system identification methods using experimentally recorded data from a 4-story model building, the following conclusions can be made:

(i). All six methods could successfully identify, locate and quantify the increasing damping imposed to the system by MR damper throughout the experiment when using full instrumentation recordings. The identified values in the damping matrix corresponding to the location of the MR damper (between the third and fourth floors) monotonically increase as the input current to the MR damper is intensified.

(ii). Identified system matrices from different methods were in acceptable agreement with each other when using full instrumentation recordings. However, identified mass values by Subspace and Iterative PEM methods are generally higher ($8\% \sim 13\%$) than real measured values in the lab. For other four system identification methods, the identified mass values are very close to measured mass in all case studies except for case 0, where these values are less ($14\% \sim 16\%$) than real values. The identified of the stiffness of floors by RFS method is generally less ($15\% \sim 20\%$) than corresponding identified values by other five methods.

(iii). Identified system matrices using partial instrumentation recordings were in less agreement with each other due to the short length of recordings; however, all identification methods could successfully detect the change in the damping properties of the system.

(iv). In addition, the RFS method could identify the nonlinearity of the damping in the system and its behavior (softening or hardening) with respect to different vibrational signatures of the structure.

Chapter V

IDENTIFICATION OF NONLINEAR STRUCTURAL MODELS USING ARTIFICIAL NEURAL NETWORKS

V.1 Introduction

THIS chapter explores the potential of using artificial neural networks for the detection of changes in the characteristics of the structure-unknown non-linear dynamic systems.

V.1.1 Background

An Artificial Neural Network (ANN) or simply Neural Network (NN) is a mathematical or computational model of an interconnected group of artificial neurons, that mimics the behavior of biological nervous systems to model complex relationships between inputs and outputs or find patterns in data. A neural network processes information using a connectionist approach to computation and adapts its structure based on external or internal information that flows through the network. Neural networks have been extensively employed to solve problems in numerous fields of engineering and science and have opened up new possibilities in the various domains such as signal processing, control systems, robotics, pattern recognition, speech recognition, medicine, business and financial analysis, and gaming.

Of particular relevance to the field of SHM, there has been increasing interest in recent decades toward using neural networks for the identification of mathematical models of physical structures on the basis of experimental measurements. Non-parametric identification methods can be used when the model structure is not clearly known. These methods try to provide the parameters of a mathematical model which fits the input/output data rather than to identify the physical parameters of the system. Some inherent properties of artificial neural network models such as computational-efficiency, fault-tolerance, and adaptation make them a superior tool for this purpose in comparison to traditional computational models. Furthermore, a neural network with proper architecture can can treat both linear and nonlinear systems with the same formulation. This is a plausible property when dealing with civil engineering structure where nonlinearity is usually present.

These potentials have motivated many researchers to study neural network based approaches for signature analysis of the system response in system identification and damage detection fields. Kudva et al. (1992) applied a BP neural network to detect and localize large area damage in an analytical plate model. Wu et al. (1992) trained a Back-Propagation (BP) Neural Network to detect individual member damage (loss of stiffness) from the measured response of a three-story building modeled by a two-dimensional ”shear building” driven by earthquake excitation. Masri et al. (1993) developed a procedure based on the use of ANN for the identification of nonlinear dynamic systems and applied it to the damped Duffing oscillator under deterministic excitation. Worden et al. (1993) trained a three-hidden-layer BP neural network to identify damage in a twenty-member framework structure using simulated data and later tested it on an experimental model of the same geometry. Elkordy et al. (1993) proposed a structural damage diagnostic system based on a BP Neural Networks using both experimental and analytical data. They concluded that NN could diagnose complicated damage patterns and handle noisy and partially incomplete data sets. Szewczyk and Hajela (1994) formulated detection of damage in analytical models of frame and truss structures as an inverse problem and utilized a modified Counter-Propagation (CP) Neural Networks to solve it. Stephens and VanLuchene (1994) used a single-layer BP neural network to identify damage and condition assessment in multistory buildings using response data from an experimental one-tenth scale reinforced concrete structure. Tsou and Shen (1994) developed an on-line damage identification methodology for damage characterization (location and severity) of two spring-mass systems through a BP neural network. The neural network was constructed by three multi-layer sub-nets and used to identify the map from the change in modal frequencies to the change in the spring stiffness values. Rhim and Lee (1995) examined the potential of using a Multi-Layer Perceptron (MLP) artificial neural network in conjunction with system identification techniques to detect and characterize the damage in composite structures. Pandey and Barai (1995) compared a two-hidden-layer to a single-layer BP neural network architecture for damage detection of steel-truss bridge structures through mapping from various nodal time histories to changes in stiffness. A non-parametric neural network-based approach is presented by Masri et al. (2000) for the detection of changes in the characteristics of structure-unknown systems. They showed that proposed damage detection methodology was robust in detecting relatively small changes in the structural parameters, even in presence of noise in vibration measurements. A structural damage detection method based on parameter identification using an iterative neural network (NN) technique was proposed by Chang et al. (2000) and verified both numerically and experimentally using a clamped-clamped T beam. Zang and Imregun (2001) studied a structural damage detection using measured frequency response functions (FRFs) as input data to artificial neural networks. Zapico et al. (2001) studied a vibration-based procedure for damage assessment in a two-storey steel frame and steel-concrete composite floors structure using neural networks. Two natural frequencies and mode shapes were used as inputs to the neural network, and three different definitions of damage (sections, bars and floors) were predicted as outputs. Zubaydi et al. (2002) used neural network for damage identification in the side shell of a ship's structure. The input to the network was the auto-correlation function of the vibration response of the structure while the output was a single function formed by adding together the damping and a part of the restoring forces. The function was used to identify, quantify, and locate the damage in the model. Wu et al. (2002) introduced a decentralized parametric damage detection approach based on neural networks. Yam et al. (2003) studied a vibration-based damage detection for composite structures using wavelet transform and neural network identification. Kao and Hung (2003) introduced a methodology to detect structural damage via free vibration responses generated by approximating artificial neural networks. The extent of changes to the system was assessed through comparing the periods and amplitudes of the free vibration responses of the damaged and undamaged states. Quantification and localisation of damage in beam-like structures for location and severity prediction of damage in beam-like structures was studied and experimentally validated by Sahin and Shenoi (2003) by using a combination of global (changes in natural frequencies) and local (curvature mode shapes) vibration-based analysis data as input in artificial neural networks. Maity and Saha (2004) used neural networks for damage assessment in structure from changes in static parameter. They applied the idea on a simple cantilever beam, where strain and displacement were used as possible candidates for damage identification by a BP neural network. A neural networks-based damage detection method using the modal properties was studied by Lee et al. (2005) for modelling errors in the baseline finite element model of bridges. In this model, the differences or the ratios of the mode shape components between before and after damage were used as the input to the neural networks since they were found to be less sensitive to the modelling errors than the mode shapes themselves. Fang et al. (2005) explored the structural damage detection using frequency response functions (FRFs) as input data to the back-propagation neural network (BPNN). Bakhary et al. (2007) proposed a statistical approach to take into account the effect of uncertainties in developing an ANN model for damage detection purposes. In this model, the probability of damage existence (PDE) was calculated based on the probability density function of the existence of undamaged and damaged states. Jiang and Adeli (2007) developed a non-parametric system identification-based approach for damage detection of high-rise building structures subjected to seismic excitations using the dynamic fuzzy wavelet neural network (WNN) model. The model could work for a partially instrumented system, where the structure was divided into a series of sub-structures around a few pre-selected instrumented floors. Li et al. (2008) proposed a damage identification method based on the combination of artificial neural network, Dempster-Shafer (D-S) evidence theory-based information fusion and the Shannon entropy, to form a weighted and selective information fusion technique to reduce the impact of uncertainties on damage identification. Comprehensive literature reviews on the subject of using neural networks in damage identification and health monitoring of structural systems can be found in Doebling et al. (1996), Adeli (2001), and Sohn et al. (2004).

V.1.2 Scope

An overview of the concept behind the approach is presented in Section V.2. Three different neural network architectures for the identification method are proposed. In Section V.3, the usefulness of the approach for the detection of structural changes is demonstrated in a physical systems for four different levels of imposed nonlinear damping. Two formulations of error between actual and predicted output are presented and the correlation between the level of change and predic-

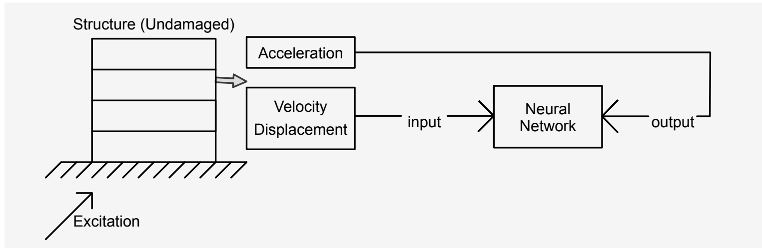

(a) Training stage

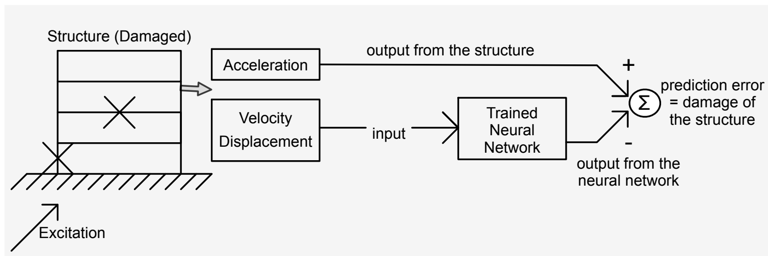

(b) Detection stage

Figure V.1: Schematic diagram of damage detection using neural networks. (Nakamura et al. (1998))

tion errors are studied. The potential advantages as well as limitations of the methodology are discussed. The concluding remarks are highlighted in Section V.4.

V.2 Formulation

V.2.1 Methodology

Figure V.1 shows the schematic diagram of the neural network based approach for the damage detection. The overall procedure is conducted in two steps:

(i). **Training stage**: As shown in Figure V.1(a), a neural network is trained by the data obtained from the undamaged structure.

(ii). **Detection stage**: As illustrated in Figure V.1(b), the trained network is fed input data, which is the same input to the system (reference structure) and the output from the network and

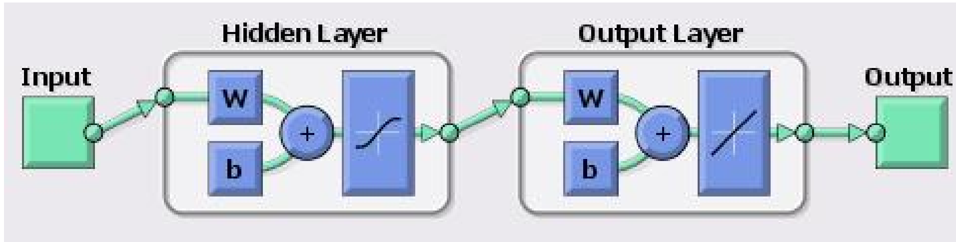

Figure V.2: Diagram of the neural network in MATLAB® (Adapted from the software manual).

the output from the system are compared to each other.

If the network is well trained, both the intact system and the network should have reasonably matching outputs. However, if the properties of the system have changed, the output from the trained network will deviate from the system output, resulting in a quantitative measure of the changes (error) in the physical system relative to undamaged condition. Using this methodology, changes (damage) in the system can be detected just by observing the output error of the trained network. It is worth to note that the proposed approach requires the training the neural network only once for the reference system. The scheme is appealing for field implementation due to its simplicity; however, attributing the quantified of the changes in the neural network output with respect to changes in the physical system parameters will still be a challenging issue.

V.2.2 Neural Network Architecture

The **nftool** module in the Neural Network Toolbox of MATLAB® was employed for this study. The neural network used is a two-layer feed-forward network with sigmoid hidden neurons and linear output neurons (Figure V.2). The network will be trained with Levenberg-Marquardt back-propagation algorithm, unless there is not enough memory, in which case scaled conjugate gradient back-propagation (trainscg) will be used. According to the software manual, “the network can fit multi-dimensional mapping problems arbitrarily well, given consistent data and enough

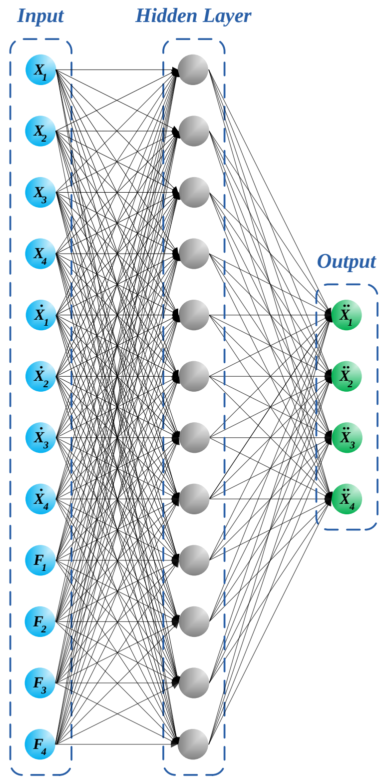

Figure V.3: Neural Network (NN) with Input of Measured Displacements, Velocities, and Excitations and Output of System Accelerations.

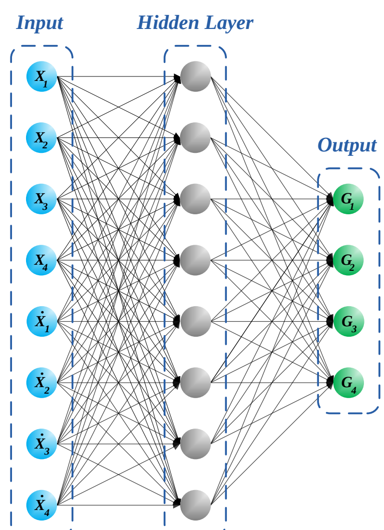

Figure V.4: Neural Network (NN) with Input of Measured Relative Displacements, and Relative Velocities, and Output of Restoring Forces on All Stories

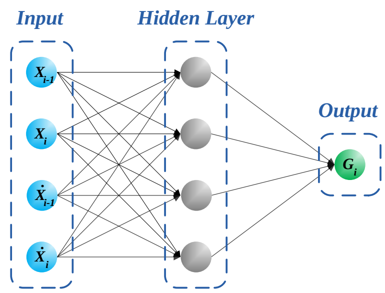

Figure V.5: Neural Network (NN) with Input of Measured Relative Displacements, and Relative Velocities, and Output of Restoring Forces on Each Story

neurons in its hidden layer."

A significant feature of the present study is the development of a sufficiently general neural network approach which will be adequate to handle linear as well as nonlinear system without any modifications. Two different architectures for the neural network are considered. As shown in Figure V.3, the first system model approximates the unknown function $\mathbf{H}$ in the equation $\ddot{\mathbf{x}} = \mathbf{H}(\mathbf{x}, \dot{\mathbf{x}}, \mathbf{f})$. This function will be approximated by a neural network whose outputs are the four system accelerations, while the inputs to the network are the four force excitations, displacements and velocities recorded on all floors. This model can be easily incorporated with a numerical differential equation solution (e.g., Runge-Kutta method) for prediction and control purposes (Masri et al. (2000)). The representative neural network used in this study has 12 input and 4 output nodes with 12 hidden neurons.

One classification of the non-destructive evaluation (NDE) of structural systems is local vs global methods or, alternatively, micro or macro methods (Masri et al. (1996)). Global methods attempt to simultaneously assess the condition of the whole system, whereas local methods are designed to provide information about a relatively small region of the structure by using local measurements. The two approaches are complementary to each other, with the optimum choice of method highly dependent on the scope of the problem at hand and the nature of the sensor network.

The topology of the experimental model building which can be modeled as a chain-like system also provides the opportunity to develop and investigate global and local NDE methods. In the second model studied herein, the relative displacement and the relative velocity of floors are selected as the input to the network and the restoring force is selected as the output of the network. For this model, two different scenarios are studied. In the first case (Figure V.4), all the input data are fed to a single neural network to predict four restoring forces in the floors. In the second case (Figure V.5), four neural networks are trained, each individual representing a physical system corresponding to a specific storey of the building. The number of neurons in the hidden layer of the neural network are selected as 8 and 4 for global and local models, respectively.

V.2.3 Performance Criteria

To evaluate the performance of the proposed method, two definitions of error are used to measure the deviation of predicted output of the neural network models ($\hat{Y}$) from the corresponding actual data (Y).

(i). Root Mean Square (**RMS**): A normalized error which is the average squared difference between outputs and targets. Lower values are better. Zero means no error.

$$RMS = \sqrt{\frac{\sum_{i=1}^{N}\left(Y_i - \hat{Y}_i\right)^2}{\sum_{i=1}^{N} Y_i^2}} \tag{V.1}$$

(ii). Regression value (**R**): R measures the correlation between outputs and targets. An R value of one means a close relationship, while zero shows a random relationship. For ease of comparison, the value of $1 - R$ is measured and presented in the study.

$$1 - R = 1.0 - \frac{\sum_{i=1}^{N}\left(Y_i - \bar{Y}_i\right)\left(\hat{Y}_i - \bar{\hat{Y}}_i\right)}{\sqrt{\sum_{i=1}^{N}\left(Y_i - \bar{Y}_i\right)^2 \sum_{i=1}^{N}\left(\hat{Y}_i - \bar{\hat{Y}}_i\right)^2}} \tag{V.2}$$

V.3 Results and Discussion

V.3.1 Performance in Detection of Change

As explained in previous section, the measured data from case 0 (no MR damper) was used to train the neural network. Then the network was used as a model for prediction of the system's responses in cases 1 to 4, where various levels of nonlinearity were induced to the system by the installed MR damper between the third and the fourth floors. To evaluate the trained network performance, the previously two discussed indices, Root Mean Square (**RMS**) and Regression (**1 - R**) errors between the output of the network and the corresponding actual data, were calculated for the training data set itself (case 0), as well as the recorded data after imposing nonlinearity to the system (cases 1 to 4).

It is worth pointing out that the network size is an important factor in the final performance. If the net is too small, then it is not able to store all the training patterns, due to an insufficient number of parameters. On the other hand, if the net is too large, then it does not "generalize", meaning it tends to simply store the training patterns rather than performing interpolation. For the application presented here, number of neurons in the hidden layer of each neural network is selected to meet these criteria. The results for all three neural network based approaches are illustrated in Figure V.6. Each of the panels shown in this Figure V.6 corresponds to a bar chart of the output error for

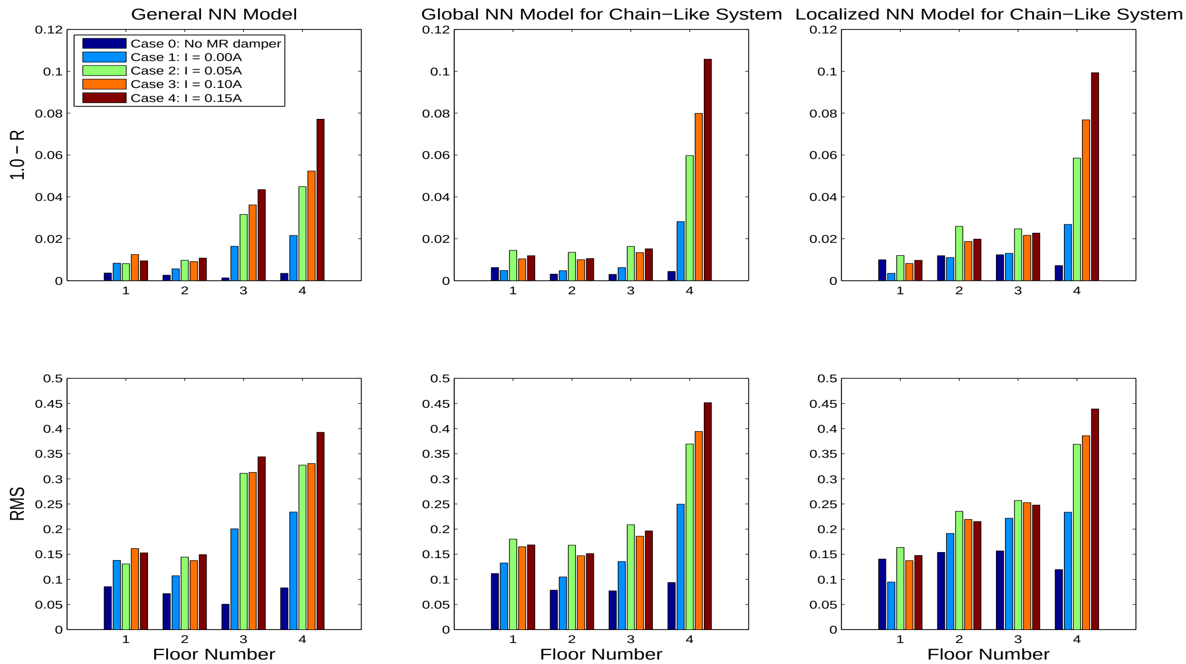

Figure V.6: Performance of different neural networks models for detection of change in the system.

different floors throughout the experiment. For example, the first panel shown on the top of LHS exhibits the output **1 - R** error for the general neural network model that predicts the acceleration of the floors. The abscissa shows the floor number. At each floor, the first bar illustrates the error for case 0 and the rest of the bars show the corresponding error for cases 1 to 4 in the same order. Therefore, the height of the bars shown in the panel is directly proportional to the extent of the deviation error between the measured system response and the predictions on the basis of the behavior of the reference model. Three major observations in these plot are conspicuous:

(i). Damage Localization: All three approaches clearly indicate higher values of error for both **RMS** and **1 - R** where the MR is installed (between the third and fourth floors) in cases 1 to 4.

(ii). Damage Quantification: The value of errors are ascending as the increase of current in the

MR damper introduces higher levels of nonlinearity to the system. Thus, both qualitatively and quantitatively, it is seen that as the extent of the parameter changes is increased, a corresponding increase in the deviation error of the network is observed.

(iii). For a given measured and predicted data sets in each case study, **RMS** generally gives higher values of discrepancy while **1 - R** index shows higher relative sensitivity toward change in the system.

Note that both approaches which model the structure as a chain-like system are more successful in pinpointing the location of change (fourth floor) compared to the general neural network method. This behavior is attributable to the fact that no extra information about the physical system was given to the net in the first approach, other than the input/output sequences, and that no model of the system was assumed during the learning phase; whereas the neural networks that predict the inter-story restoring forces of the building are actually benefiting from a prior information about the topology of the system.

Without any knowledge of the characteristics of the structure being identified, the accuracy of a well-trained neural network can be quantitatively gauged by means of its output performance indices. In other words, dimensionless deviation errors (such as **RMS** or **1 - R**) can be reliably used as an straight-forward index to select an appropriate network for authentic representation of the reference system. The results also indicate that, by selecting a threshold level relative to the deviation error associated with the undamaged system response, all the well-trained networks can be utilized to provide a sensitive indicator of the presence of potentially serious damage in the system being monitored.

V.3.2 General Neural Network Model Combined with ODE Solvers

The general neural network model of this study can be easily incorporated with a numerical differential equation solution (e.g., Runge-Kutta method) for prediction and control purposes. For a system with the governing equations of motion in the form of:

$$\mathbf{m}\ddot{\mathbf{x}}(t) + G(\dot{\mathbf{x}}(t), \mathbf{x}(t)) = \mathbf{f}(t) \tag{V.3}$$

, which can be rewritten as:

$$\ddot{\mathbf{x}}(t) = \frac{1}{\mathbf{m}}(\mathbf{f}(t) - G(\dot{\mathbf{x}}(t), \mathbf{x}(t))) = H(\dot{\mathbf{x}}(t), \mathbf{x}(t), \mathbf{f}(t)) \tag{V.4}$$

the trained neural network can replace function H to predict the response of the system. This procedure is schematically shown in Figure V.7. After training five neural network for all the linear and nonlinear cases, the predicted response of the structure on all floors are numerically computed in the manner discussed above and plotted versus the corresponding measured data. The results are illustrated in Figures V.8 to V.12 for cases 0 to 4, respectively. The **ode45** solver in MATLAB® which implements fourth-fifth-order formulas of the Runge-Kutta-Fehlberg method was employed for this study. The accuracy of the predictions is so high as to make the two distinct curves in each of the plots practically indistinguishable. This also reveals that the neural network predictor gives promising results for both linear and nonlinear systems. It should be noted that the predicted response will include the effects of both the network identification errors as well as error propagation effects associated with the computational scheme (Runge-Kutta) used to obtain the numerical solution.

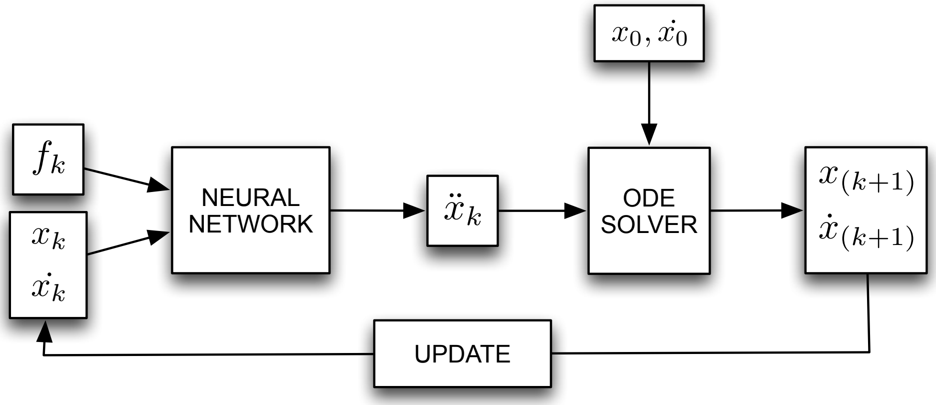

Figure V.7: General neural network model combined with an ODE solver to predict the response of the system.

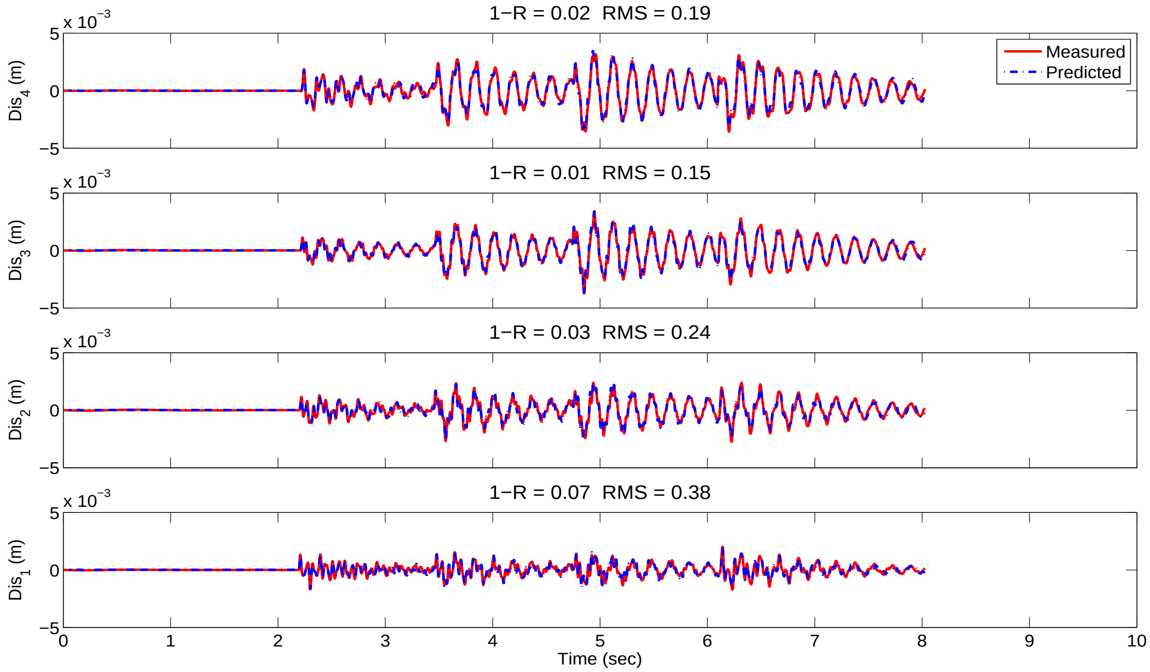

Figure V.8: Measured vs. predicted displacement of the structure at each floor for Case 0 using RK4.5

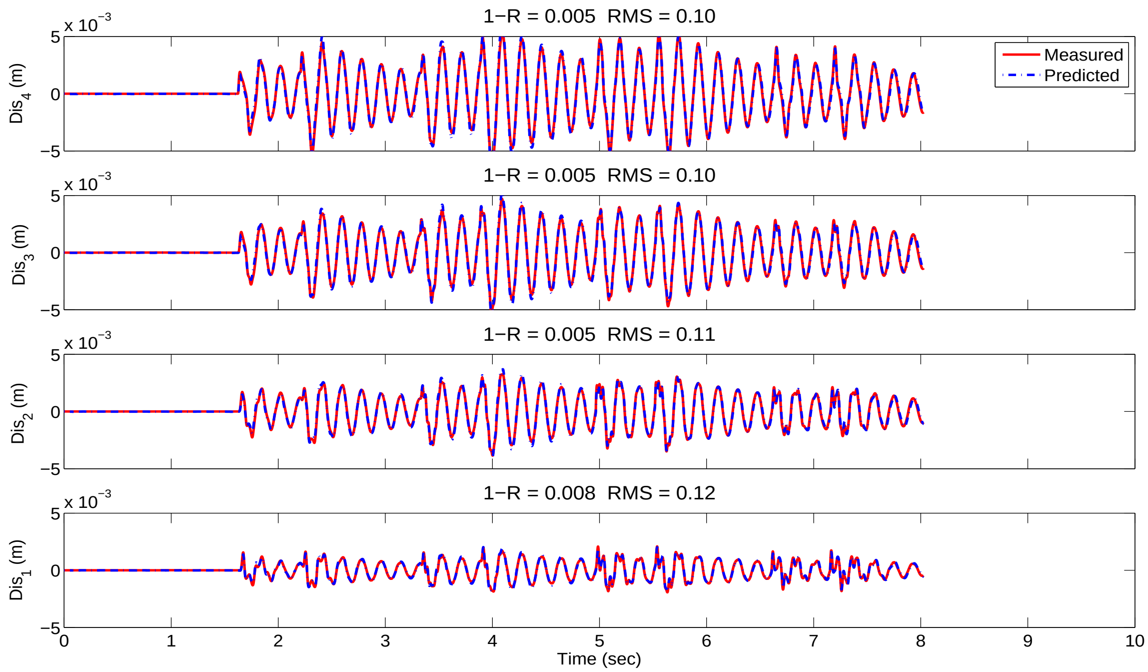

Figure V.9: Measured vs. predicted displacement of the structure at each floor for Case 1 using RK4.5

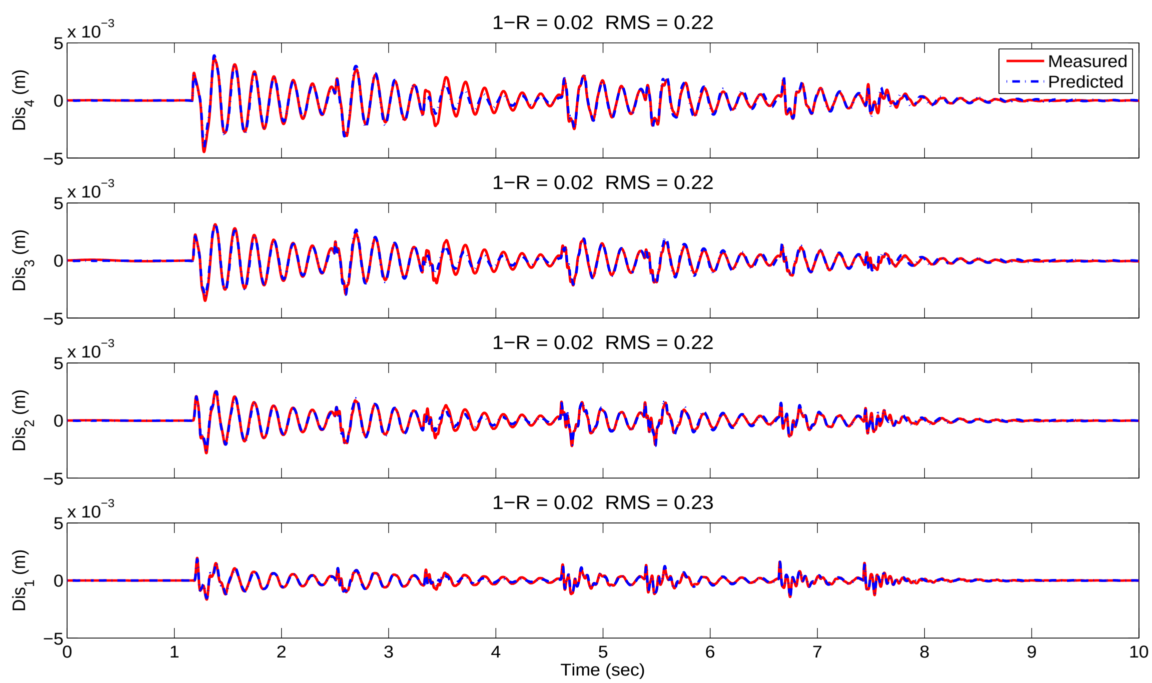

Figure V.10: Measured vs. predicted displacement of the structure at each floor for Case 2 using RK4.5

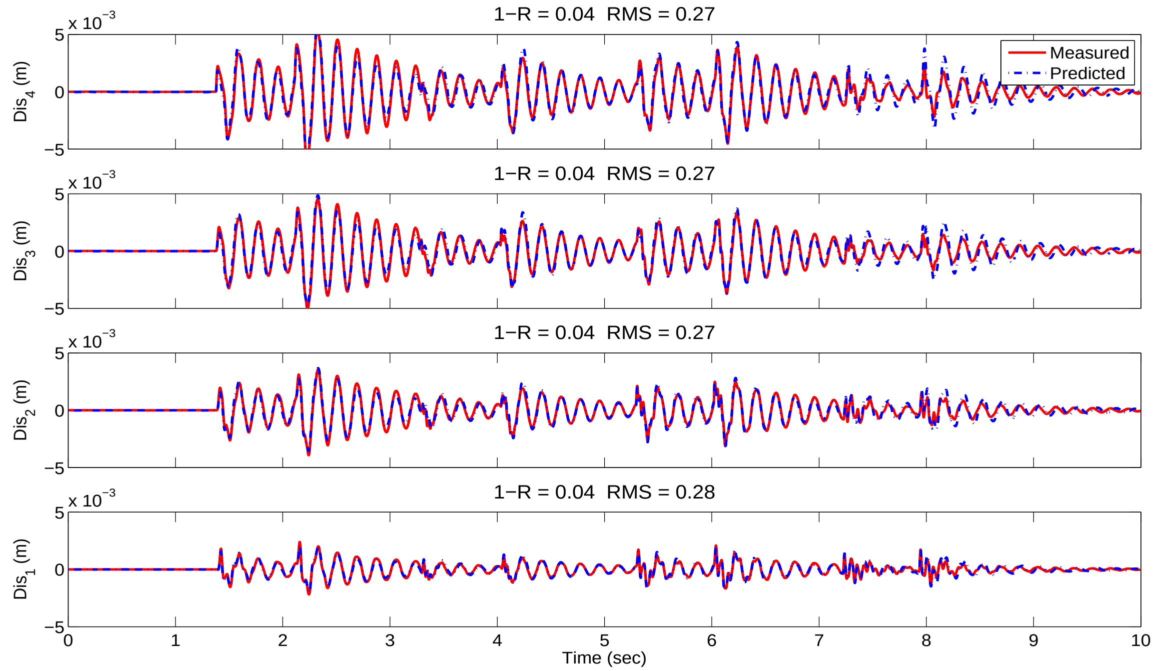

Figure V.11: Measured vs. predicted displacement of the structure at each floor for Case 3 using RK4.5

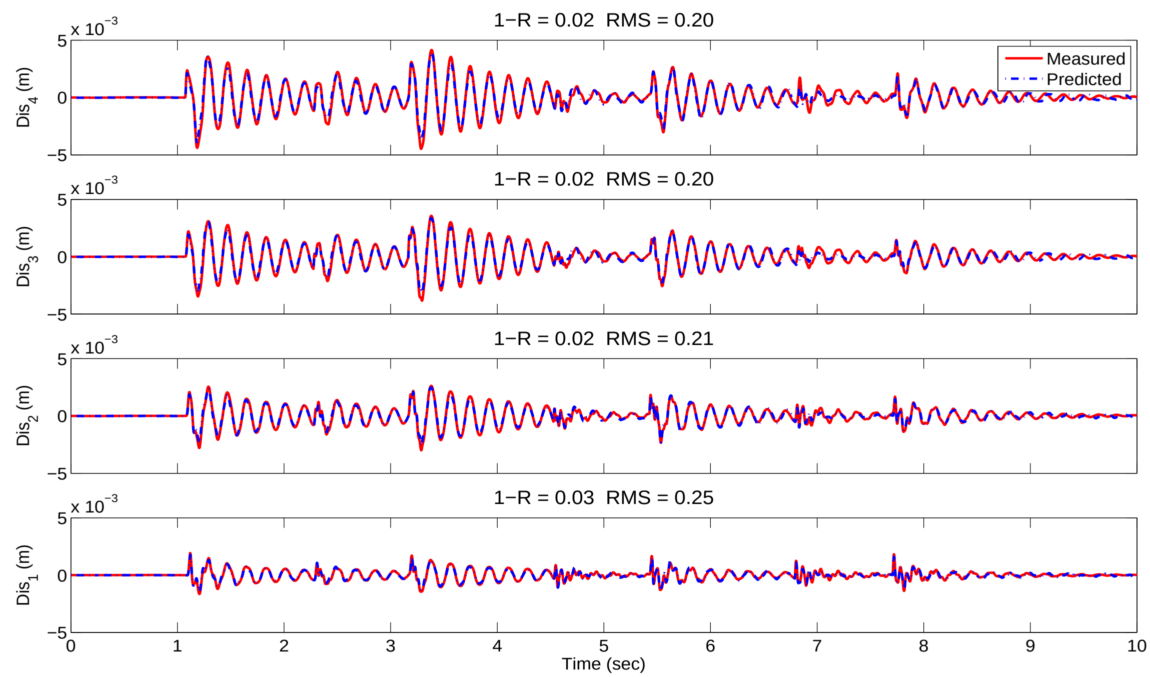

Figure V.12: Measured vs. predicted displacement of the structure at each floor for Case 4 using RK4.5

V.3.3 Estimation of Structural Mass for Chain-Like Systems

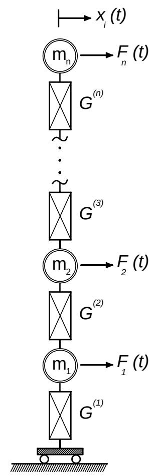

Figure V.13: Model of a MDOF chain-like system.

As discussed in previous chapter, for the MDOF chain-like structure shown in Figure V.13 which consists of n elements, each with a lumped mass m_i, the nonlinear restoring function $G^{(i)}$ at each floor can be calculated as:

$$\mathbf{G}^{(\mathbf{i})}(\mathbf{z}_i, \dot{\mathbf{z}}_i) = \sum_{j=i}^{n} (\mathbf{F_j}(t) - m_j \ddot{\mathbf{x}}_\mathbf{j}) \qquad i = 1, 2, ..., n \tag{V.5}$$

where $\mathbf{z}_i$ and $\dot{\mathbf{z}}_i$ are the relative displacement and velocity between two consecutive floors, respectively. Thus, starting from the tip of the chain, one can sequentially determine the time-histories of all the inter-story restoring forces within the chain. However, as shown in Equation V.5, this will require knowing the mass either through measuring the structural masses at the floors or calculating them based on design information. The objective of the study reported herein is to combine a neural network that predicts the restoring forces from given displacement and velocities of the floor with an optimization package to eliminate the requirement of knowing the structural mass.

First, restoring forces will be computed based on an arbitrary estimation of mass at each floor. Then, a neural network will be trained to predict these restoring forces from the measured velocities and displacements. If the assumed masses deviate from accurate values, there will be a poor relationship between the relative displacement and velocity at each floor and the corresponding calculated restoring force. This will consequently result in a poor-trained neural network that reflect itself in high values of performance criteria (**RMS** or **1 - R**). Therefore, a cost function based on these errors can be defined and optimized by adjusting the assumed structural masses to archive a well-trained neural network:

$$J(\underset{\sim}{\alpha}) = \sum_{i=1}^{n} \mathbf{W_i} \times \mathbf{RMS_i} \tag{V.6}$$

As shown in Equation V.6, the importance of accuracy of the estimated values for each floor can also manifested with weights ($\mathbf{W_i}$) in the cost function. The final optimized set of values will represent the actual mass of each floor in the structure. Figure V.14 shows a graphical interpretation of the process. The mass of the experimental structure under investigation is estimated using the proposed method and representative result of optimization process is shown in Figure V.15. Initial population is randomly selected from a uniform distribution in the range of $0 \sim 25kg$ and equal weights for all floors are considered in the definition of the cost function. Note that estimated final values are in close agreement with the measured structural mass of each floor in the lab ($52.4/4 = 13.1kg$).

The results of estimated structural mass for cases 0 to 4 are tabulated in Table V.1 and also illustrated in a bar plot format in Figure V.16. As shown in this figure, the final estimated values in all

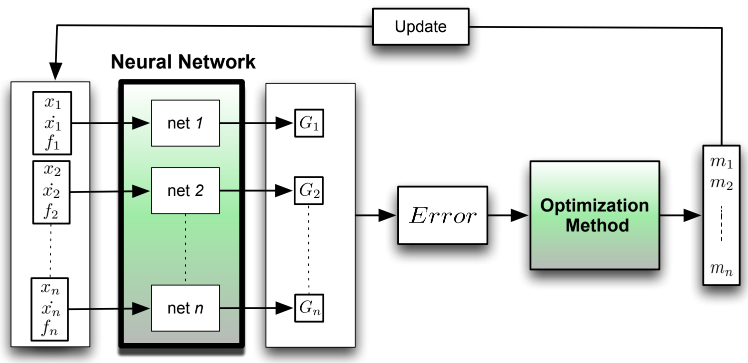

Figure V.14: Flowchart of structural mass estimation for chain-like systems using optimization methods.

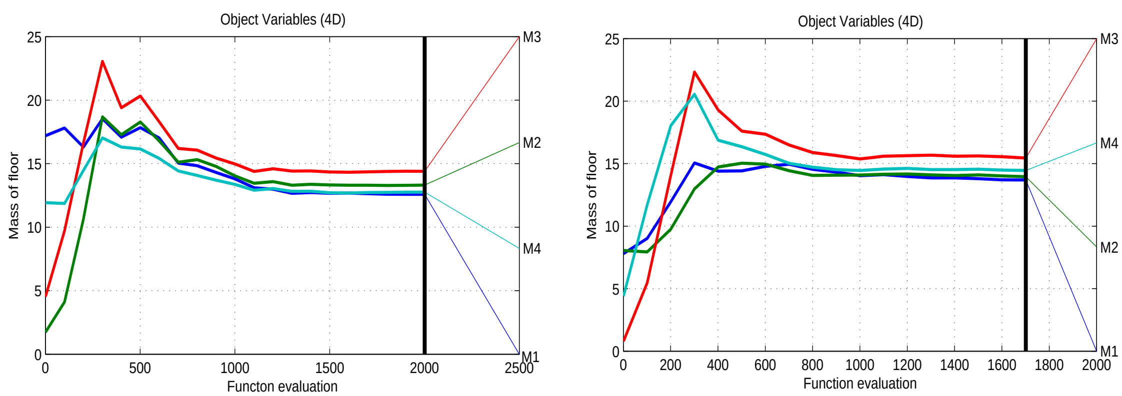

(a) Case 0

(b) Case 3

Figure V.15: Estimation of mass of the floors using CMA-ES for Case 0 and Case 3. Initial population is randomly selected from on a uniform distribution in the range of $0 \sim 25kg$ and equal weights for all floors are considered in the definition of the cost function.

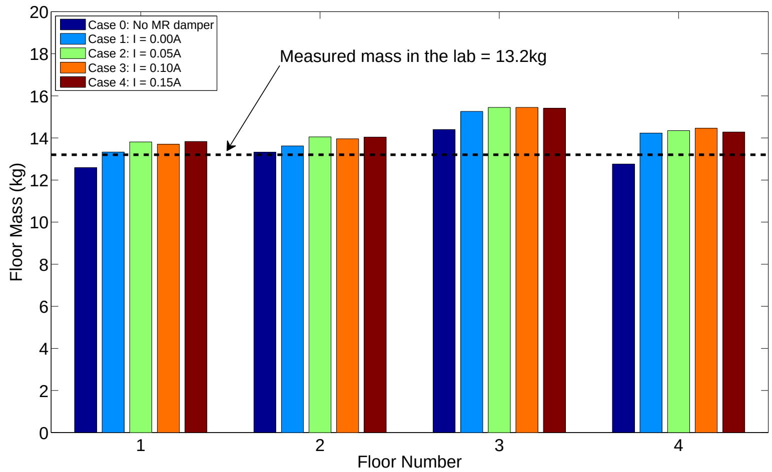

Figure V.16: Estimated mass of the floors using CMA-ES for Cases 0 to 4.

Table V.1: Estimated mass of the floors using CMA-ES for Cases 0 to 4 (M$_{measured} = 13.2kg$).

Floor Number	**Mass (kg)**				
	Case 0	**Case 1**	**Case 2**	**Case 3**	**Case 4**
1^{st} Floor	12.59	13.33	13.81	13.70	13.83
2^{nd} Floor	13.32	13.62	14.05	13.96	14.04
3^{rd} Floor	14.40	15.26	15.45	15.45	15.41
4^{th} Floor	12.76	14.23	14.35	14.46	14.28

floors are very close the actual measured structural mass for all linear and nonlinear cases. The deviation of these values from the actual measured mass of each floor in the lab is bounded to just $-5\% \sim 16\%$. This is highly superior and more consistent when compared to the estimation of structural mass by other system identification methods in the previous chapter.

V.4 Concluding Remarks

A time-domain non-parametric approach using artificial neural networks is presented for the detection of changes in the characteristics of structure-unknown systems. The neural network is trained, using vibration measurements from a "healthy" (reference) structure. The trained network is subsequently fed with vibration measurements data from the slightly damaged (changed) structure to monitor its health. The method requires no detailed knowledge about the topology or the nature of the underlying structure, or of the failure modes of the system. This is a significant advantage since the method can potentially cope with unforeseen failure scenarios. However, a major disadvantage of the approach is that detectable changes can not be directly attributable to a specific failure mode, but simply indicate that damage has occurred. For systems with certain topologies (e.g., chain-like systems), the method can also provide useful information about the damaged region of the structure. The approach is applied to recorded data from the 4-story experimental model building that was studied in the previous chapter.

Through this study, it is shown that the proposed non-parametric approach is capable of providing a relatively sensitive indicator of changes (damage) in the structural parameters and can be utilized as a high-fidelity tool for assessing the condition of structures. A technique based on combination of neural networks with optimization methods to estimate the structural mass of the floors in chain-like systems is also proposed. Results of the study show that the estimated final values are in close agreement with the measured structural mass of each floor in the lab.

Chapter VI

Conclusion

THE main goal of the study reported herein is to investigate and evaluate different vibration-signature-based methods for system identification, damage detection and health monitoring of civil structures. A brief introduction to Structural Health Monitoring is presented in the first chapter. The following chapter reports the performance of two stochastic methods of global optimization for a subset of well-known benchmark functions. The application of these methods in finite element model updating approaches for damage detection purposes is investigated in Chapter 3. The case study is a quarter-scale, two-span bridge system, experimentally tested at the University of Nevada, Reno. Chapter 4 reports the performance of different system identification approaches for experimentally recorded data of a 1/20 scale 4-story building equipped with smart devices of magneto-rheological (MR) damper. This case study is also studied in Chapter 5 to investigate the application of artificial neural networks for the identification of nonlinear structural models.

Considering the promising performance of various system identification and damage detection methods and approaches under discussion, the general conclusions from this study are useful in providing guidelines for the application of vibration-signature-based methods to real-world problems, especially in the implementation of structural health monitoring for complex, nonlinear distributed systems.

VI.1 Overview of dissertation

VI.1.1 Chapter II

In the second chapter, the performance of two global optimization methods are numerically investigated on a subset of well-known test functions. The global optimization algorithms under discussion were Genetic Algorithm (**ga** modules in MATLAB®) and an evolutionary strategy called CMA-ES. A suit of five standard test functions with a search space of dimensionality $n = 5, 10, 25, 50, 100$ was considered to study the effects of the problem-order on the performance of the optimization methods. In addition, the effects of population size on the performance of evolutionary methods are investigated for a subset of population sizes of $Pop = 5, 10, 25, 50, 100, 250, 500, 1000$. For each case, an ensemble of 100 simulations was generated to reach a reliable statistical data set. Based on the comparison of these results, the following conclusions can be made:

- Evolutionary stochastic optimization methods are generally successful in solving high-dimensional problems.
- As expected, both optimization methods require significantly more function evaluations to reach the solution for higher problem-orders.
- Increasing the population size significantly improves the performance of these methods at the expense of higher number of function evaluations. The study shows that the optimal population size takes a wide range of values, depending on the cost function. For a given

objective function, the optimum population size may be tuned through calibration process with the help of a statistical analysis.

- For multi-modal functions, CMA-ES shows better performance than GA in the sense that it returns smaller final function value with less average number of required function evaluations to reach the solution. For instance, while CMA-ES outperform GA on Ackley and Rastrigin functions (as shown in Figures II.7 and II.8), it significantly falls behind GA on Rosenbrock function. Noting that Rosenbrock is the only uni-modal non-separable test function of this study, this indicates that the performance of these optimization packages varies with the topography of the functions. This conclusion also agrees with the findings of the developers of CMA-ES, reported in Hansen and Kern (2004).

VI.1.2 Chapter III

The underlying objective of the study in chapter 3 is to evaluate the performance of two global optimization methods in the finite element model updating approaches for damage detection in dispersed structural systems, which usually deals with minimization of a complex, non-linear, non-convex, high-dimensional cost function. The case study was a two-span reinforced concrete bridge, experimentally tested at the University of Nevada, Reno. The Subspace method for system identification was used to extract the modal parameters (natural frequencies, mode shapes, and modal damping) of the bridge system. A NASTRAN® computer model was developed based on the previous SAP2000 model provided by the NEES@Reno team, and validated with the system identification results from the measured data. A simple on-line damage detection method, using an ARMA model, was proposed and employed to trigger the finite element model updating process. Two scenarios, assuming the availability of limited or large number of sensors were investigated for the finite element model updating procedure. The feasibility of the proposed finite element model updating algorithm to accurately detect, localize, and quantify the damage in the columns of the tested bridge throughout the experiment was investigated and validated by comparison to experimental measurements and visual inspections.

Based on the comparison of the results from the application of the finite element model updating algorithm under discussion with the strain gauge measurements and visual observations, the following conclusions can be made:

(i). The simple ARMA model proposed for preliminary on-line damage detection can significantly increase the efficacy of the model updating process.

(ii). The finite element model updating algorithm presented and applied in this study could accurately detect and quantify the overall damage in the tested bridge bents throughout the experiment.

(iii). The proposed method also showed very promising results for damage detection in the system using output-only data. This reveals the potential of the technique to provide a useful tool for SHM purposes in conjunction with promising methods for the identification of modal properties using available ambient vibration data.

(iv). The finite element model updating algorithm used in this study was shown to be robust and accurate to detect, localize and quantify the damage in the columns in synthetic simulations; however, the experimental results could not be completely validated. The reliability of these results highly depends upon the accuracy of the identified (equivalent) modal properties of the (damaged, nonlinear) structure in different stages of the experiment.

(v). Detected damage values are highly correlated ($\rho_{cmaes} = 0.956, \rho_{ga} = 0.946$) with the damage index developed by Park and Ang (1985), which is a practical measure of damage based on dissipated hysteretic energy and ductility demand.

(vi). Both CMA-ES and GA converge to pretty close global minimums; however, GA may take more computational effort to reach the solution, especially for higher-order problem.

VI.1.3 Chapter IV

Based on evaluation of the results from six different system identification methods using experimentally recorded data from a 4-story model building, the following conclusions can be made:

(i). Identified system matrices from different methods were in acceptable agreement with each other when using full instrumentation recordings.

(ii). All six methods could successfully identify, locate and quantify the increasing damping imposed on the system by the MR damper throughout the experiment, when using full instrumentation recordings. The identified values in the damping matrix corresponding to the location of the MR damper (between the third and fourth floors) monotonically increase as the input current to the MR damper is intensified.

(iii). Identified system matrices using partial instrumentation recordings were in less agreement with each other due to the short length of recordings; however, all identification methods could successfully detect the change in the damping properties of the system.

(iv). In addition, the RFS method could identify the nonlinearity of the damping in the system and its behavior (softening or hardening) with respect to different vibrational signatures of the structure.

VI.1.4 Chapter V

In chapter 5, a time-domain non-parametric approach using artificial neural networks is presented for the detection of changes in the characteristics of structure-unknown systems. The neural network is trained, using vibration measurements from a "healthy" (reference) structure. The trained network is subsequently fed with vibration measurements data from the slightly damaged (changed) structure to monitor its health. The method requires no detailed knowledge about the topology or the nature of the underlying structure, or of the failure modes of the system. This is a significant advantage since the method can potentially cope with unforeseen failure scenarios. However, a major disadvantage of the approach is that detectable changes can not be directly attributable to a specific failure mode, but simply indicate that damage may have occurred. For systems with certain topologies (e.g., chain-like systems), the method can also provide useful information about the damaged region(s) of the structure. The approach is applied to recorded data from the 4-story experimental model building that was studied in the previous chapter.

Through this study, it is shown that the proposed non-parametric approach is capable of providing a relatively sensitive indicator of changes (damage) in the structural parameters, and can be utilized as a high-fidelity tool for assessing the condition of structures. A technique based on combination of neural networks with optimization methods to estimate the structural mass of the floors in chain-like systems is also proposed. Results of the study show that the estimated final mass values are in close agreement with the measured structural mass of each floor in the lab.

BIBLIOGRAPHY

Adeli, H. 2001. Neural networks in civil engineering: 19892000. *Computer-Aided Civil and Infrastructure Engineering*, 16(2):126–142.

Adeli, H. and Cheng, N. 1994a. Augmented lagrangian genetic algorithm for structural optimization. *Journal of Aerospace Engineering*, 7(1):104–118.

Adeli, H. and Cheng, N. 1994b. Concurrent genetic algorithms for optimization of large structures. *Journal of Aerospace Engineering*, 7(3):276–296.

Adeli, H. and Jiang, X. 2006. Dynamic fuzzy wavelet neural network model for structural system identification. *Journal of Structural Engineering*, 132(1):102 – 111.

Akimoto, Y., Nagata, Y., Ono, I., and Kobayashi, S. 2012. Theoretical foundation for cma-es from information geometry perspective. *Algorithmica*, 64:698–716.

Allen, M., Sumali, H., and Epp, D. 2008. Piecewise-linear restoring force surfaces for semi-nonparametric identification of nonlinear systems. *Nonlinear Dynamics*, 54:123–135.

Andersen, P., Brincker, R., Peeters, B., De Roeck, G., Hermans, L., and Kramer, C. 1999. Comparison of system identification methods using ambient bridge test data. volume 1, pages 1035 – 1041, Kissimmee, FL, USA.

Atalla, M. and Inman, D. 1998. On model updating using neural networks. *Mechanical Systems and Signal Processing*, 12(1):135 – 161.

Bai, E.-W. 2010. Frequency domain identification of hammerstein models. In Giri, F. and Bai, E.-W., editors, *Block-oriented Nonlinear System Identification*, volume 404 of *Lecture Notes in Control and Information Sciences*, pages 161–180. Springer London.

Bakhary, N., Hao, H., and Deeks, A. J. 2007. Damage detection using artificial neural network with consideration of uncertainties. *Engineering Structures*, 29(11):2806 – 2815.

Baruch, M. 1978. Optimization procedure to correct stiffness and flexibility matrices using vibration tests. 16(11):1208 – 1210.

Belendez, A., Pascual, C., Neipp, C., Belendez, T., and Hernandez, A. 2008. An equivalent linearization method for conservative nonlinear oscillators. *International Journal of Nonlinear Sciences and Numerical Simulation*, 9(1):9–17.

Bellizzi, S. and Defilippi, M. 2003. Non-linear mechanical systems identification using linear systems with random parameters. *Mechanical Systems and Signal Processing*, 17(1):203 – 210.

Bellizzi, S., Guillemain, P., and Kronland-Martinet, R. 2001. Identification of coupled non-linear modes from free vibration using time-frequency representations. *Journal of Sound and Vibration*, 243(2):191 – 213.

Berman, A. and Flannelly, W. 1971. Theory of incomplete models of dynamic structures. *AIAA Journal*, 9(8):1481–1487.

Bouc, R. 1994. The power spectral density of response for a strongly non-linear random oscillator. *Journal of Sound and Vibration*, 175(3):317 – 331.

Brownjohn, J. 2007. Structural health monitoring of civil infrastructure. *Philosophical Transactions of the Royal Society A: Mathematical, Physical and Engineering Sciences*, 365:589 – 622.

Bruckner, A. and Lin, Y. 1987. Generalization of the equivalent linearization method for non-linear random vibration problems. *International Journal of Non-Linear Mechanics*, 22(3):227 – 235.

Caughey, T. 1963. Equivalent linearization techniques. *Journal of the Acoustical Society of America*, 35(11):1706 – 1711.

Chandrashekhar, M. and Ganguli, R. 2009. Structural Damage Detection Using Modal Curvature and Fuzzy Logic. *Structural Health Monitoring*, 8(4):267–282.

Chang, C. C., Chang, T. Y. P., Xu, Y. G., and Wang, M. L. 2000. Structural damage detection using an iterative neural network. *Journal of Intelligent Material Systems and Structures*, 11(1):32–42.

Chang, P. C., Flatau, A., and Liu, S. C. 2003. Review Paper: Health Monitoring of Civil Infrastructure. *Structural Health Monitoring*, 2(3):257–267.

Chassiakos, A. and Masri, S. 1996. Modelling unknown structural systems through the use of neural networks. *Earthquake Engineering and Structural Dynamics*, 25(2):117 – 128.

Chatterjee, A. and Vyas, N. S. 2004. Non-linear parameter estimation in multi-degree-of-freedom systems using multi-input volterra series. *Mechanical Systems and Signal Processing*, 18(3):457 – 489.

Chen, C.-W. 2009. Modeling and control for nonlinear structural systems via a nn-based approach. *Expert Systems with Applications*, 36(3, Part 1):4765 – 4772.

Chen, S. and Billings, S. A. 1992. Neural networks for nonlinear dynamic system modelling and identification. *International Journal of Control*, 56:319–346.

Cheung, S. and Beck, J. 2009. Bayesian model updating using hybrid monte carlo simulation with application to structural dynamic models with many uncertain parameters. *Journal of Engineering Mechanics*, 135(4):243–255.

Chu, M., Datta, B., Lin, W.-W., and Xu, S. 2008. Spillover phenomenon in quadratic model updating. *AIAA Journal*, 46(2):420 – 428.

Cornwell, P., Farrar, C., Doebling, S., and Sohn, H. 1999. Environmental variability of modal properties. *Experimental Techniques*, 23(6):45–48.

De Cock, K. and De Moor, B. 2003. *Subspace Identification Methods: In Contribution to Section 5.5, "Control Systems Robotics and Automation"*. Encyclopedia of Life Support Systems (EOLSS), Developed under the Auspices of the UNESCO, Eolss Publishers, Oxford ,UK, http://www.eolss.net.

Dippery, K. and Smith, S. 1998. Optimal control approach to nonlinear system identification. volume 1, pages 637 – 643, Santa Barbara, CA, USA.

Doebling, S., Farrar, C., and Prime, M. 1998. Summary review of vibration-based damage identification methods. *Shock and Vibration Digest*, 30(2):91 – 105.

Doebling, S., R. Farrar, C., Prime, M., and Shevitz, D. 1996. Damage identification and health monitoring of structural and mechanical systems from changes in their vibration characteristics: A literature review. Technical Report LA-13070-MS, Los Alamos National Laboratory, Los Alamos, New Mexico.

Duym, S. and Schoukens, J. 1995. Design of excitation signals for the restoring force surface method. *Mechanical Systems and Signal Processing*, 9(2):139 – 158.

Elkordy, M., Chang, K., and Lee, G. 1993. Neural networks trained by analytically simulated damage states. *Journal of Computing in Civil Engineering*, 7(2):130–145.

Fang, X., Luo, H., and Tang, J. 2005. Structural damage detection using neural network with learning rate improvement. *Computers & Structures*, 83(2526):2150 – 2161.

Farhat, C. and Hemez, F. M. 1993. Updating finite element dynamic models using an element-by-element sensitivity methodology. *Aiaa Journal*, 31:1702–1711.

Farrar, C. R. and Worden, K. 2007. An introduction to structural health monitoring. *Philosophical Transactions of the Royal Society A: Mathematical, Physical and Engineering Sciences*, 365(1851):303–315.

Feijoo, J. V., Worden, K., and Stanway, R. 2004. System identification using associated linear equations. *Mechanical Systems and Signal Processing*, 18(3):431 – 455.

Friswell, M. and Mottershead, J. 1995. *Finite Element Model Updating in Structural Dynamics*. Springer.

Fritzen, C., Jennewein, D., and Kiefer, T. 1998. Damage detection based on model updating methods. *Mechanical Systems and Signal Processing*, 12(1):163 – 186.

Ghanem, R. and Romeo, F. 2001. A wavelet-based approach for model and parameter identification of non-linear systems. *International Journal of Non-Linear Mechanics*, 36(5):835 – 859.

Gifford, S. 1989. *Volterra series analysis of nonlinear structures*. PhD thesis.

Hansen, N. and Kern, S. 2004. Evaluating the CMA evolution strategy on multimodal test functions. In *Parallel Problem Solving from Nature PPSN VIII*, volume 3242 of *LNCS*, pages 282–291. Springer.

Haroon, M., Adams, D. E., and Luk, Y. W. 2005. A technique for estimating linear parameters using nonlinear restoring force extraction in the absence of an input measurement. *Journal of Vibration and Acoustics*, 127(5):483–492.

He, X., Moaveni, B., Conte, J., Elgamal, A., and Masri, S. 2008. Modal identification study of vincent thomas bridge using simulated wind-induced ambient vibration data. *Computer-Aided Civil and Infrastructure Engineering*, 23(5):373–388.

Hemez, F. and Doebling, S. 2001. Review and assessment of model updating for nonlinear, transient dynamics. *Mechanical Systems and Signal Processing*, 15(1):45 – 74.

Hera, A. and Hou, Z. 2004. Application of wavelet approach for asce structural health monitoring benchmark studies. *Journal of Engineering Mechanics*, 130(1):96–104.

Hou, Z., Noori, M., and Amand, R. S. 2000. Wavelet-based approach for structural damage detection. *Journal of Engineering Mechanics*, 126(7):677–683.

Iwan, W. D. 1973. A generalization of the concept of equivalent linearization. *International Journal of Non-Linear Mechanics*, 8(3):279 – 287.

Iwan, W. D. and Mason, A. 1980. Equivalent linearization for systems subjected to non-stationary random excitation. *International Journal of Non-Linear Mechanics*, 15(2):71 – 82.

Jaishi, B. and Ren, W. 2005. Structural finite element model updating using ambient vibration test results. *Journal of Structural Engineering*, 131(4):617 – 628.

Jezequel, L. 1997. *New Advances in Modal Synthesis of Large Structures: Non-linear Damped and Non-deteministic Cases*. A.A. Balkema.

Jiang, X. and Adeli, H. 2007. Pseudospectra, music, and dynamic wavelet neural network for damage detection of highrise buildings. *International Journal for Numerical Methods in Engineering*, 71(5):606–629.

Johnson, N., Saiidi, M., , and Sanders, D. 2006. Large-scale experimental and analytical studies of a two-span reinforced concrete bridge system. Technical Report CCEER-06-02, Center for Civil Engineering Earthquake Research, Department of Civil Engineering, University of Nevada, Reno, Nevada.

Kao, C. and Hung, S.-L. 2003. Detection of structural damage via free vibration responses generated by approximating artificial neural networks. *Computers & Structures*, 81(2829):2631 – 2644.

Kareem, A. and Kijewski, T. 2002. Time-frequency analysis of wind effects on structures. *Journal of Wind Engineering and Industrial Aerodynamics*, 90(12-15):1435 – 1452. Fifth Asia-Pacific Conference on Wind Engineering.

Kerschen, G., Golinval, J., and Worden, K. 2001. Theoretical and experimental identification of a non-linear beam. *Journal of Sound and Vibration*, 244(4):597 – 613.

Kerschen, G. and Golinval, J.-C. 2005. Generation of accurate finite element models of nonlinear systems application to an aeroplane-like structure. *Nonlinear Dynamics*, 39:129–142.

Kerschen, G., Worden, K., Vakakis, A. F., and Golinval, J.-C. 2006. Past, present and future of nonlinear system identification in structural dynamics. *Mechanical Systems and Signal Processing*, 20(3):505 – 592.

Khan, A. and Vyas, N. 2001. Nonlinear bearing stiffness parameter estimation in flexible rotor-bearing systems using volterra and wiener approach. *Probabilistic Engineering Mechanics*, 16(2):137 – 157.

Kim, S., Pakzad, S., Culler, D., Demmel, J., Fenves, G., Glaser, S., and Turon, M. 2007. Health monitoring of civil infrastructures using wireless sensor networks. pages 254–263.

Kitada, Y. 1998. Identification of nonlinear structural dynamic systems using wavelets. *Journal of Engineering Mechanics*, 124(10):1059 – 1066.

Ko, J. and Ni, Y. 2005. Technology developments in structural health monitoring of large-scale bridges. *Engineering Structures*, 27(12):1715 – 1725.

Kosmatopoulos, E., Smyth, A., Masri, S., and Chassiakos, A. 2001. Robust adaptive neural estimation of restoring forces in nonlinear structures. *Journal of Applied Mechanics*, 68(6):880–893.

Kudva, J. N., Munir, N., and Tan, P. W. 1992. Damage detection in smart structures using neural networks and finite-element analyses. *Smart Materials and Structures*, 1(2):108–112.

Kyprianou, A., Worden, K., and Panet, M. 2001. Identification of hysteretic systems using the differential evolution algorithm. *Journal of Sound and Vibration*, 248(2):289 – 314.

Lee, J. J., Lee, J. W., Yi, J. H., Yun, C. B., and Jung, H. Y. 2005. Neural networks-based damage detection for bridges considering errors in baseline finite element models. *Journal of Sound and Vibration*, 280(3-5):555 – 578.

Leontaritis, I. J. and Billings, S. A. 1985a. Input-output parametric models for non-linear systems Part I: deterministic non-linear systems. *International Journal of Control*, 41(2):303–328.

Leontaritis, I. J. and Billings, S. A. 1985b. Input-output parametric models for non-linear systems part II: stochastic non-linear systems. *International Journal of Control*, 41(2):329–344.

Levin, R. and Lieven, N. 1998. Dynamic finite element model updating using simulated annealing and genetic algorithms. *Mechanical Systems and Signal Processing*, 12(1):91 – 120.

Li, H., Bao, Y., and Ou, J. 2008. Structural damage identification based on integration of information fusion and shannon entropy. *Mechanical Systems and Signal Processing*, 22(6):1427 – 1440. Special Issue: Mechatronics.

Ljung, L. 1986. *System Identification: Theory for the User*. Prentice-Hall, Inc.

Maity, D. and Saha, A. 2004. Damage assessment in structure from changes in static parameter using neural networks. *Sadhana*, 29:315–327.

Masri, S. and Caughey, T. 1979. A nonparametric identification technique for nonlinear dynamic problems. *Journal of Applied Mechanics*, 46(2):433–447.

Masri, S., Chassiakos, A., and Caughey, T. 1992. Structure-unknown non-linear dynamic systems: identification through neural networks. *Smart Materials and Structures*, 1(1):45–56.

Masri, S., Chassiakos, A., and Caughey, T. 1993. Identification of nonlinear dynamic systems using neural networks. *Journal of Applied Mechanics*, 60(1):123–133.

Masri, S., Ghanem, R., Govindan, R., and Nayeri, R. 2008. A decentralized procedure for structural health monitoring of uncertain nonlinear systems provided with dense active sensor arrays. *Smart Materials and Structures*, 17(4):045024 (15 pp.).

Masri, S., Miller, R., Saud, A., and Caughey, T. 1987a. Identification of nonlinear vibrating structures: Part i - formulation. *Journal of Applied Mechanics, Transactions ASME*, 54(4):918 – 922.

Masri, S., Miller, R., Saud, A., and Caughey, T. 1987b. Identification of nonlinear vibrating structures: Part ii - applications. *Journal of Applied Mechanics, Transactions ASME*, 54(4):923 – 929.

Masri, S., Nakamura, M., Chassiakos, A., and Caughey, T. 1996. Neural network approach to detection of changes in structuralparameters. *Journal of Engineering Mechanics*, 122(4):350–360.

Masri, S., Sassi, H., and Caughey, T. 1982. Nonparametric identification of nearly arbitrary nonlinear systems. *Journal of Applied Mechanics*, 49(3):619–628.

Masri, S., Smyth, A., Chassiakos, A., Caughey, T., and Hunter, N. 2000. Application of neural networks for detection of changes in nonlinear systems. *Journal of Engineering Mechanics*, 126(7):666 – 676.

Meyer, S. and Link, M. 2003. Modelling and updating of local non-linearities using frequency response residuals. *Mechanical Systems and Signal Processing*, 17(1):219 – 226.

Mohammad, K., Worden, K., and Tomlinson, G. 1992. Direct parameter estimation for linear and non-linear structures. *Journal of Sound and Vibration*, 152(3):471 – 499.

Muto, M. and Beck, J. 2008. Bayesian updating and model class selection for hysteretic structural models using stochastic simulation. *Journal of Vibration and Control*, 14(1-2):7 – 34.

Nakamura, M., Masri, S., Chassiakos, A., and Caughey, T. 1998. A method for non-parametric damage detection through the use of neural networks. *Earthquake Engineering and Structural Dynamics*, 27(9):997–1010.

Narendra, K. and Parthasarathy, K. 1990. Identification and control of dynamical systems using neural networks. *Neural Networks, IEEE Transactions on*, 1(1):4 –27.

Nayeri, R. 2007. *Analytical and Experimental Studies in System Identification and Modeling for Structural Control and Health Monitoring*. Phd dissertation, University of Southern California.

Nayeri, R., Masri, S., Ghanem, R., and Nigbor, R. 2008. A novel approach for the structural identification and monitoring of a full-scale 17-story building based on ambient vibration measurements. *Smart Materials and Structures*, 17(2):025006 (19 pp.).

Nayfeh, A. 1985. Parametric identification of nonlinear dynamic systems. *Computers & Structures*, 20(1-3):487 – 493. Special Issue: Advances and Trends in Structures and Dynamics.

Ni, Y., Zhou, H., Chan, K., and Ko, J. 2008. Modal flexibility analysis of cable-stayed ting kau bridge for damage identification. *Computer-Aided Civil and Infrastructure Engineering*, 23(3):223–236.

Ostermeier, A., Gawelczyk, A., , and Hansen, N. 1994. A derandomized approach to self-adaptation of evolution strategies. *Evolutionary Computation*, 2(4):369 – 380.

Pai, P., Huang, L., Hu, J., and Langewisch, D. 2008. Time-frequency method for nonlinear system identification and damage detection. *Structural Health Monitoring*, 7(2):103 – 127.

Pandey, P. and Barai, S. 1995. Multilayer perceptron in damage detection of bridge structures. *Computers & Structures*, 54(4):597 – 608.

Park, Y. and Ang, A. 1985. Mechanistic seismic damage model for reinforced concrete. *Journal of Structural Engineering*, 111(4):722 – 739.

Peeters, B. and De Roeck, G. 2001. One-year monitoring of the z24-bridge: environmental effects versus damage events. *Earthquake Engineering and Structural Dynamics*, 30(2):149–171.

Peeters, B. and Roeck, G. D. 2001. Stochastic system identification for operational modal analysis: A review. *Journal of Dynamic Systems, Measurement, and Control*, 123(4):659–667.

Peifer, M., Timmer, J., and Voss, H. 2003. Non-parametric identification of non-linear oscillating systems. *Journal of Sound and Vibration*, 267(5):1157 – 1167.

Pintelon, R. and Schoukens, J. 2001. *System identification: a frequency domain approach*. IEEE Press.

Platten, M., Wright, J., Dimitriadis, G., and Cooper, J. 2009. Identification of multi-degree of freedom non-linear systems using an extended modal space model. *Mechanical Systems and Signal Processing*, 23(1):8 – 29. Special Issue: Non-linear Structural Dynamics.

Proppe, C., Pradlwarter, H., and Schuller, G. 2003. Equivalent linearization and monte carlo simulation in stochastic dynamics. *Probabilistic Engineering Mechanics*, 18(1):1 – 15.

Rhim, J. and Lee, S. W. 1995. A neural network approach for damage detection and identification of structures. *Computational Mechanics*, 16:437–443.

Rice, H. 1995. Identification of weakly non-linear systems using equivalent linearization. *Journal of Sound and Vibration*, 185(3):473 – 481.

Rice, H. and Fitzpatrick, J. 1988. A generalised technique for spectral analysis of non-linear systems. *Mechanical Systems and Signal Processing*, 2(2):195 – 207.

Roberts, J., Dunne, J., and Debonos, A. 1995. A spectral method for estimation of non-linear system parameters from measured response. *Probabilistic Engineering Mechanics*, 10(4):199 – 207.

Roberts, J. and Spanos, P. 1990. *Random vibration and statistical linearization*. Wiley.

Rosenberg, R. 1962. The normal modes of nonlinear n-degree-of-freedom systems. *Journal of Applied Mechanics*, 29(1):7–14.

Rosenberg, R. 1966. On nonlinear vibrations of systems with many degrees of freedom. volume 9 of *Advances in Applied Mechanics*, pages 155 – 242. Elsevier.

Sahin, M. and Shenoi, R. 2003. Quantification and localisation of damage in beam-like structures by using artificial neural networks with experimental validation. *Engineering Structures*, 25(14):1785 – 1802.

Schetzen, M. 1980. *The Volterra and Wiener Theories of Nonlinear Systems*. John Wiley & Sons.

Schmidt, R. 1994. Updating non-linear components. *Mechanical Systems and Signal Processing*, 8(6):679 – 690.

Skolnik, D., Lei, Y., Yu, E., and Wallace, J. W. 2006. Identification, model updating, and response prediction of an instrumented 15-story steel-frame building. *Earthquake Spectra*, 22(3):781–802.

Socha, L. 2008. *Linearization methods for stochastic dynamic systems*. Lecture notes in physics. Springer Verlag.

Socha, L. and Soong, T. T. 1991. Linearization in analysis of nonlinear stochastic systems. *Applied Mechanics Reviews*, 44(10):399–422.

Sohn, H., Dzwonczyk, M., Straser, E. G., Kiremidjian, A. S., Law, K. H., and Meng, T. 1999. An experimental study of temperature effect on modal parameters of the alamosa canyon bridge. *Earthquake Engineering and Structural Dynamics*, 28(8):879–897.

Sohn, H., Farrar, C. R., Hemez, F. M., Shunk, D. D., Stinemates, D. W., Nadler, B. R., and Others 2004. A review of structural health monitoring literature: 1996 - 2001. *Los Alamos National Laboratory, Los Alamos, NM*.

Soize, C. and Le Fur, O. 1997. Modal identification of weakly non-linear multidimensional dynamical systems using a stochastic linearisation method with random coefficients. *Mechanical Systems and Signal Processing*, 11(1):37 – 49.

Spina, D., Valente, C., and Tomlinson, G. R. 1996. A new procedure for detecting nonlinearity from transient data using the gabor transform. *Nonlinear Dynamics*, 11:235–254.

Staszewski, W. J., Lee, B. C., Mallet, L., and Scarpa, F. 2004. Structural health monitoring using scanning laser vibrometry: I. lamb wave sensing. *Smart Materials and Structures*, 13(2):251–260.

Stephens, J. E. and VanLuchene, R. D. 1994. Integrated assessment of seismic damage in structures. *Computer-Aided Civil and Infrastructure Engineering*, 9(2):119–128.

Storer, D. and Tomlinson, G. 1993. Recent developments in the measurement and interpretation of higher order transfer functions from non-linear structures. *Mechanical Systems and Signal Processing*, 7(2):173 – 189.

Szemplinska-Stupnicka, W. 1979. The modified single mode method in the investigations of the resonant vibrations of non-linear systems. *Journal of Sound and Vibration*, 63(4):475 – 489.

Szemplinska-Stupnicka, W. 1983. non-linear normal modes and the generalized ritz method in the problems of vibrations of non-linear elastic continuous systems. *International Journal of Non-Linear Mechanics*, 18(2):149 – 165.

Szewczyk, Z. and Hajela, P. 1994. Damage detection in structures based on featuresensitive neural networks. *Journal of Computing in Civil Engineering*, 8(2):163–178.

Teughels, A., Maeck, J., and De Roeck, G. 2002. Damage assessment by finite element model updating using damage functions. *Computers and Structures*, 80(25):1869 – 1879.

Tsou, P. and Shen 1994. Structural damage detection and identification using neural networks. *AIAA J*, 32(1):176–183.

Wang, C. S., Wu, F., and Chang, F.-K. 2001. Structural health monitoring from fiber-reinforced composites to steel-reinforced concrete. *Smart Materials and Structures*, 10(3):548–552.

Wang, Y. June 2007. A wireless structural health monitoring system with multithreaded sensing devices: design and validation. *Structure 38; Infrastructure Engineering: Maintenance, Management, Life-Cycl*, 3:103–120.

Wen, Y. K. 1980. Equivalent linearization for hysteretic systems under random excitation. *Journal of Applied Mechanics*, 47(1):150–154.

Worden, K. 1990a. Data processing and experiment design for the restoring force surface method, part i: integration and differentiation of measured time data. *Mechanical Systems and Signal Processing*, 4(4):295 – 319.

Worden, K. 1990b. Data processing and experiment design for the restoring force surface method, part ii: Choice of excitation signal. *Mechanical Systems and Signal Processing*, 4(4):321 – 344.

Worden, K., Ball, A. D., and Tomlinson, G. R. 1993. Fault location in a framework structure using neural networks. *Smart Materials and Structures*, 2(3):189–200.

Wu, X., Ghaboussi, J., and Jr, J. G. 1992. Use of neural networks in detection of structural damage. *Computers & Structures*, 42(4):649 – 659.

Wu, Z., Xu, B., and Yokoyama, K. 2002. Decentralized parametric damage detection based on neural networks. *Computer-Aided Civil and Infrastructure Engineering*, 17(3):175–184.

Xu, B., He, J., Zhou, R., and Masri, S. 2010. Experimental study on a general data-based nonlinear identification approach for a mdof frame model structure. *AIP Conference Proceedings*, 1233:1070–1075.

Yam, L., Yan, Y., and Jiang, J. 2003. Vibration-based damage detection for composite structures using wavelet transform and neural network identification. *Composite Structures*, 60(4):403 – 412.

Yuen, K. and Beck, J. 2003. Updating properties of nonlinear dynamical systems with uncertain input. *Journal of Engineering Mechanics*, 129(1):9 – 20.

Zang, C. and Imregun, M. 2001. Structural damage detection using artificial neural networks and measured frf data reduced via principal component projection. *Journal of Sound and Vibration*, 242(5):813 – 827.

Zapico, J. L., Worden, K., and Molina, F. J. 2001. Vibration-based damage assessment in steel frames using neural networks. *Smart Materials and Structures*, 10(3):553–559.

Zimmerman, D. and Kaouk, K. 1994. Structural damage detection using a minimum rank update theory. *Transactions of the ASME. Journal of Vibration and Acoustics*, 116(2):222 – 231.

Zubaydi, A., Haddara, M., and Swamidas, A. 2002. Damage identification in a ship's structure using neural networks. *Ocean Engineering*, 29(10):1187 – 1200.

Appendix A

Table A.1: Identified mass, damping, and stiffness matrices of the system: Case 0

Method \ Matrix	**M**	**C**	$\mathbf{K}_{(\times 10^{-5})}$
Linear System Method	$\begin{bmatrix} 11.10 & 0.74 & -0.17 & 0.71 \\ 0.63 & 11.99 & 0.27 & 0.29 \\ -0.63 & 0.49 & 12.83 & 0.58 \\ 0.88 & 0.54 & 0.55 & 11.67 \end{bmatrix}$	$\begin{bmatrix} 42.74 & -2.85 & -16.22 & -4.11 \\ -8.20 & 29.61 & -9.55 & -7.29 \\ -15.17 & -7.47 & \mathbf{48.23} & 5.33 \\ -0.96 & -3.69 & -8.70 & \mathbf{12.05} \end{bmatrix}$	$\begin{bmatrix} 2.60 & -1.44 & 0.02 & 0.14 \\ -1.63 & 3.27 & -1.80 & 0.11 \\ 0.06 & -1.72 & 3.08 & -1.45 \\ 0.15 & 0.07 & -1.58 & 1.43 \end{bmatrix}$
Sym. Linear System Method	$\begin{bmatrix} 11.10 & 0.74 & -0.17 & 0.71 \\ 0.74 & 11.06 & 0.38 & 0.30 \\ -0.17 & 0.38 & 12.13 & 0.53 \\ 0.71 & 0.30 & 0.53 & 10.44 \end{bmatrix}$	$\begin{bmatrix} 42.74 & -2.85 & -16.22 & -4.11 \\ -2.85 & 29.60 & -10.26 & -6.55 \\ -16.22 & -10.26 & \mathbf{48.45} & 5.80 \\ -4.11 & -6.55 & 5.80 & \mathbf{9.61} \end{bmatrix}$	$\begin{bmatrix} 2.60 & -1.44 & 0.02 & 0.14 \\ -1.44 & 2.96 & -1.64 & 0.09 \\ 0.02 & -1.64 & 2.97 & -1.39 \\ 0.14 & 0.09 & -1.39 & 1.25 \end{bmatrix}$
RFS Method for Chain-Like Systems	$\begin{bmatrix} 11.34 & 0 & 0 & 0 \\ 0 & 11.15 & 0 & 0 \\ 0 & 0 & 13.06 & 0 \\ 0 & 0 & 0 & 12.55 \end{bmatrix}$	$\begin{bmatrix} 39.60 & -20.83 & 0 & 0 \\ -20.83 & 47.78 & -26.95 & 0 \\ 0 & -26.95 & \mathbf{38.05} & -11.10 \\ 0 & 0 & -11.10 & \mathbf{11.10} \end{bmatrix}$	$\begin{bmatrix} 2.53 & -1.27 & 0 & 0 \\ -1.27 & 2.79 & -1.52 & 0 \\ 0 & -1.52 & 3.07 & -1.55 \\ 0 & 0 & -1.55 & 1.55 \end{bmatrix}$
Model Updating Method	$\begin{bmatrix} 11.12 & 0.72 & -0.21 & 0.74 \\ 0.60 & 11.94 & 0.28 & 0.30 \\ -0.65 & 0.52 & 12.83 & 0.59 \\ 0.85 & 0.51 & 0.54 & 11.65 \end{bmatrix}$	$\begin{bmatrix} 44.00 & -2.63 & -16.23 & -3.96 \\ -7.94 & 29.87 & -10.59 & -7.57 \\ -15.03 & -6.55 & \mathbf{47.25} & 4.83 \\ -2.66 & -2.71 & -7.56 & \mathbf{11.69} \end{bmatrix}$	$\begin{bmatrix} 2.60 & -1.44 & 0.01 & 0.14 \\ -1.63 & 3.26 & -1.80 & 0.11 \\ 0.05 & -1.71 & 3.08 & -1.45 \\ 0.15 & 0.07 & -1.58 & 1.43 \end{bmatrix}$
Sub-Space Method	$\begin{bmatrix} 14.93 & 0.13 & -0.56 & -0.28 \\ 0.01 & 14.10 & 0.02 & -0.17 \\ -0.29 & 0.03 & 13.81 & -0.04 \\ -0.15 & -0.10 & 0.02 & 12.56 \end{bmatrix}$	$\begin{bmatrix} 49.99 & -2.91 & -21.66 & -4.20 \\ -10.07 & 29.36 & -10.09 & -7.75 \\ -16.39 & -7.61 & \mathbf{50.46} & 7.16 \\ -2.36 & -3.02 & -5.95 & \mathbf{12.07} \end{bmatrix}$	$\begin{bmatrix} 3.60 & -2.14 & 0.25 & 0.06 \\ -2.10 & 3.98 & -2.13 & 0.09 \\ 0.23 & -2.05 & 3.49 & -1.64 \\ -0.01 & 0.14 & -1.77 & 1.60 \end{bmatrix}$
Iterative PEM Method	$\begin{bmatrix} 14.50 & 0.10 & -0.50 & -0.18 \\ 0.05 & 14.09 & 0.18 & 0.02 \\ -0.25 & 0.10 & 14.15 & -0.14 \\ 0.11 & 0.04 & 0.09 & 12.78 \end{bmatrix}$	$\begin{bmatrix} 46.97 & -6.92 & -26.79 & 1.39 \\ -16.36 & 24.06 & -5.17 & -6.10 \\ 0.41 & -8.17 & \mathbf{34.47} & 11.28 \\ -5.53 & 0.99 & -0.64 & \mathbf{6.06} \end{bmatrix}$	$\begin{bmatrix} 3.47 & -2.08 & 0.26 & 0.05 \\ -2.06 & 3.92 & -2.13 & 0.12 \\ 0.24 & -2.07 & 3.56 & -1.69 \\ 0.03 & 0.13 & -1.78 & 1.61 \end{bmatrix}$

Table A.2: Identified mass, damping, and stiffness matrices of the system: Case 1

Method \ Matrix	**M**	**C**	$\mathbf{K}_{(\times 10^{-5})}$
Linear System Method	$\begin{bmatrix} 13.33 & 0.54 & -0.08 & 0.20 \\ 0.65 & 13.04 & 0.52 & -0.08 \\ -0.31 & 0.71 & 13.78 & 0.96 \\ 0.18 & 0.01 & 0.72 & 12.46 \end{bmatrix}$	$\begin{bmatrix} 40.48 & -10.81 & -18.84 & 1.86 \\ -19.33 & 38.01 & -4.70 & -16.75 \\ 10.47 & -18.08 & \mathbf{207.38} & -200.01 \\ -9.18 & 4.53 & -170.12 & \mathbf{217.96} \end{bmatrix}$	$\begin{bmatrix} 3.09 & -1.82 & 0.22 & 0.04 \\ -1.76 & 3.46 & -1.82 & 0.04 \\ 0.16 & -1.73 & 3.10 & -1.48 \\ 0.02 & 0.04 & -1.50 & 1.41 \end{bmatrix}$
Sym. Linear System Method	$\begin{bmatrix} 13.33 & 0.54 & -0.08 & 0.20 \\ 0.54 & 13.18 & 0.51 & -0.09 \\ -0.08 & 0.51 & 13.95 & 0.99 \\ 0.20 & -0.09 & 0.99 & 12.65 \end{bmatrix}$	$\begin{bmatrix} 40.48 & -10.81 & -18.84 & 1.86 \\ -10.81 & 35.78 & -8.75 & -14.54 \\ -18.84 & -8.75 & \mathbf{220.23} & -209.24 \\ 1.86 & -14.54 & -209.24 & \mathbf{255.56} \end{bmatrix}$	$\begin{bmatrix} 3.09 & -1.82 & 0.22 & 0.04 \\ -1.82 & 3.53 & -1.84 & 0.04 \\ 0.22 & -1.84 & 3.20 & -1.51 \\ 0.04 & 0.04 & -1.51 & 1.42 \end{bmatrix}$
RFS Method for Chain-Like Systems	$\begin{bmatrix} 13.01 & 0 & 0 & 0 \\ 0 & 12.02 & 0 & 0 \\ 0 & 0 & 14.06 & 0 \\ 0 & 0 & 0 & 13.68 \end{bmatrix}$	$\begin{bmatrix} 129.46 & -65.23 & 0 & 0 \\ -65.23 & 94.96 & -29.74 & 0 \\ 0 & -29.74 & \mathbf{241.53} & -211.79 \\ 0 & 0 & -211.79 & \mathbf{211.79} \end{bmatrix}$	$\begin{bmatrix} 2.59 & -1.24 & 0 & 0 \\ -1.24 & 2.59 & -1.35 & 0 \\ 0 & -1.35 & 2.66 & -1.31 \\ 0 & 0 & -1.31 & 1.31 \end{bmatrix}$
Model Updating Method	$\begin{bmatrix} 13.34 & 0.54 & -0.07 & 0.20 \\ 0.66 & 13.03 & 0.52 & -0.08 \\ -0.31 & 0.72 & 13.78 & 0.96 \\ 0.17 & 0.02 & 0.73 & 12.47 \end{bmatrix}$	$\begin{bmatrix} 41.06 & -11.49 & -17.25 & 0.78 \\ -18.30 & 37.49 & -4.38 & -17.46 \\ 11.23 & -18.00 & \mathbf{207.31} & -200.32 \\ -9.36 & 4.85 & -170.14 & \mathbf{217.65} \end{bmatrix}$	$\begin{bmatrix} 3.09 & -1.82 & 0.22 & 0.04 \\ -1.75 & 3.45 & -1.81 & 0.04 \\ 0.16 & -1.73 & 3.10 & -1.48 \\ 0.02 & 0.04 & -1.50 & 1.41 \end{bmatrix}$
Sub-Space Method	$\begin{bmatrix} 14.37 & 0.18 & -0.08 & -0.21 \\ -0.01 & 13.92 & 0.19 & 0.00 \\ 0.07 & -0.16 & 14.83 & 0.57 \\ -0.11 & 0.14 & 0.51 & 13.93 \end{bmatrix}$	$\begin{bmatrix} 48.30 & -11.34 & -34.94 & 11.55 \\ -14.27 & 35.53 & -0.27 & -18.18 \\ -3.04 & -5.84 & \mathbf{256.83} & -253.10 \\ 1.29 & 3.05 & -206.75 & \mathbf{256.06} \end{bmatrix}$	$\begin{bmatrix} 3.38 & -2.06 & 0.32 & 0.00 \\ -2.04 & 3.83 & -2.04 & 0.09 \\ 0.41 & -2.20 & 3.59 & -1.68 \\ -0.07 & 0.18 & -1.79 & 1.62 \end{bmatrix}$
Iterative PEM Method	$\begin{bmatrix} 14.40 & 0.11 & -0.34 & -0.07 \\ 0.10 & 14.00 & 0.14 & 0.03 \\ 0.12 & 0.33 & 14.84 & -0.18 \\ -0.21 & 0.11 & 0.52 & 14.33 \end{bmatrix}$	$\begin{bmatrix} 24.58 & -6.35 & -0.49 & -14.84 \\ -11.91 & 34.75 & -24.27 & 2.46 \\ 22.11 & -18.21 & \mathbf{224.38} & -228.63 \\ -25.81 & 4.69 & -176.41 & \mathbf{236.86} \end{bmatrix}$	$\begin{bmatrix} 3.40 & -2.07 & 0.29 & 0.03 \\ -2.04 & 3.88 & -2.10 & 0.11 \\ 0.36 & -2.08 & 3.58 & -1.74 \\ -0.09 & 0.18 & -1.84 & 1.67 \end{bmatrix}$

Table A.3: Identified mass, damping, and stiffness matrices of the system: Case 2

Method \ Matrix	**M**	**C**	$\mathbf{K}_{(\times 10^{-5})}$
Linear System Method	$\begin{bmatrix} 13.49 & 0.62 & -0.01 & 0.17 \\ 0.56 & 13.37 & 1.00 & -0.28 \\ -0.21 & 1.26 & 12.40 & 1.98 \\ 0.12 & -0.20 & 1.45 & 11.58 \end{bmatrix}$	$\begin{bmatrix} 53.16 & -5.17 & -27.80 & -1.10 \\ -25.52 & 60.35 & 5.76 & -43.92 \\ 0.96 & -59.57 & \mathbf{249.99} & -217.35 \\ -4.34 & 32.58 & -218.71 & \mathbf{265.50} \end{bmatrix}$	$\begin{bmatrix} 3.10 & -1.81 & 0.23 & 0.01 \\ -1.83 & 3.48 & -1.66 & -0.07 \\ 0.11 & -1.37 & 2.46 & -1.14 \\ 0.02 & -0.12 & -1.14 & 1.21 \end{bmatrix}$
Sym. Linear System Method	$\begin{bmatrix} 13.49 & 0.62 & -0.01 & 0.17 \\ 0.62 & 13.34 & 1.02 & -0.29 \\ -0.01 & 1.02 & 13.11 & 2.14 \\ 0.17 & -0.29 & 2.14 & 12.22 \end{bmatrix}$	$\begin{bmatrix} 53.16 & -5.17 & -27.80 & -1.10 \\ -5.17 & 54.47 & -1.61 & -39.23 \\ -27.80 & -1.61 & \mathbf{263.18} & -252.55 \\ -1.10 & -39.23 & -252.55 & \mathbf{322.71} \end{bmatrix}$	$\begin{bmatrix} 3.10 & -1.81 & 0.23 & 0.01 \\ -1.81 & 3.46 & -1.66 & -0.07 \\ 0.23 & -1.66 & 2.74 & -1.23 \\ 0.01 & -0.07 & -1.23 & 1.28 \end{bmatrix}$
RFS Method for Chain-Like Systems	$\begin{bmatrix} 13.53 & 0 & 0 & 0 \\ 0 & 12.59 & 0 & 0 \\ 0 & 0 & 14.38 & 0 \\ 0 & 0 & 0 & 13.78 \end{bmatrix}$	$\begin{bmatrix} 128.56 & -69.26 & 0 & 0 \\ -69.26 & 81.18 & -11.92 & 0 \\ 0 & -11.92 & \mathbf{286.35} & -274.43 \\ 0 & 0 & -274.43 & \mathbf{274.43} \end{bmatrix}$	$\begin{bmatrix} 2.73 & -1.33 & 0 & 0 \\ -1.33 & 2.79 & -1.46 & 0 \\ 0 & -1.46 & 2.96 & -1.50 \\ 0 & 0 & -1.50 & 1.50 \end{bmatrix}$
Model Updating Method	$\begin{bmatrix} 13.49 & 0.63 & -0.00 & 0.16 \\ 0.56 & 13.37 & 1.01 & -0.28 \\ -0.21 & 1.27 & 12.38 & 1.97 \\ 0.11 & -0.20 & 1.43 & 11.57 \end{bmatrix}$	$\begin{bmatrix} 53.78 & -4.56 & -28.06 & -0.85 \\ -26.03 & 60.42 & 4.47 & -43.49 \\ 0.83 & -59.81 & \mathbf{248.76} & -216.25 \\ -4.50 & 32.25 & -218.88 & \mathbf{265.58} \end{bmatrix}$	$\begin{bmatrix} 3.10 & -1.81 & 0.23 & 0.01 \\ -1.83 & 3.47 & -1.66 & -0.07 \\ 0.11 & -1.36 & 2.45 & -1.14 \\ 0.02 & -0.11 & -1.14 & 1.21 \end{bmatrix}$
Sub-Space Method	$\begin{bmatrix} 14.37 & 0.13 & 0.25 & 0.14 \\ 0.03 & 15.12 & 0.24 & 0.00 \\ 0.13 & 0.14 & 14.69 & -0.17 \\ 0.02 & -0.12 & 0.04 & 14.19 \end{bmatrix}$	$\begin{bmatrix} 81.84 & -4.86 & -55.67 & 11.61 \\ -15.03 & 44.60 & 3.18 & -29.93 \\ -7.38 & -60.62 & \mathbf{325.13} & -301.52 \\ -22.36 & 46.78 & -263.30 & \mathbf{329.88} \end{bmatrix}$	$\begin{bmatrix} 3.39 & -2.09 & 0.36 & -0.01 \\ -2.21 & 4.12 & -2.15 & 0.06 \\ 0.41 & -2.07 & 3.45 & -1.67 \\ -0.05 & 0.12 & -1.80 & 1.67 \end{bmatrix}$
Iterative PEM Method	$\begin{bmatrix} 14.31 & -0.13 & 0.12 & 0.41 \\ 0.30 & 14.86 & -0.07 & -0.47 \\ 1.00 & 0.68 & 13.50 & -2.18 \\ -0.30 & -0.80 & 0.64 & 14.41 \end{bmatrix}$	$\begin{bmatrix} 44.91 & -1.09 & -30.67 & 6.48 \\ -21.46 & 42.52 & 6.28 & -36.78 \\ 15.02 & -60.34 & \mathbf{322.61} & -319.47 \\ -13.81 & 37.14 & -278.96 & \mathbf{340.93} \end{bmatrix}$	$\begin{bmatrix} 3.40 & -2.14 & 0.34 & 0.04 \\ -2.11 & 4.04 & -2.09 & 0.03 \\ 0.50 & -1.87 & 3.34 & -1.76 \\ -0.01 & -0.09 & -1.62 & 1.64 \end{bmatrix}$

Table A.4: Identified mass, damping, and stiffness matrices of the system: Case 3

Method \ Matrix	**M**	**C**	$\mathbf{K}_{(\times 10^{-5})}$
Linear System Method	$\begin{bmatrix} 13.47 & 0.48 & -0.04 & 0.20 \\ 0.47 & 13.08 & 0.63 & -0.01 \\ -0.22 & 0.89 & 13.18 & 1.51 \\ 0.16 & -0.02 & 1.55 & 12.02 \end{bmatrix}$	$\begin{bmatrix} 45.54 & -3.45 & -25.91 & -1.95 \\ -26.90 & 49.65 & 8.00 & -30.50 \\ 18.48 & -59.54 & \mathbf{291.05} & -279.24 \\ -12.06 & 38.94 & -263.11 & \mathbf{309.75} \end{bmatrix}$	$\begin{bmatrix} 3.11 & -1.85 & 0.24 & 0.03 \\ -1.79 & 3.44 & -1.78 & 0.03 \\ 0.17 & -1.58 & 2.80 & -1.33 \\ 0.00 & -0.08 & -1.17 & 1.23 \end{bmatrix}$
Sym. Linear System Method	$\begin{bmatrix} 13.47 & 0.48 & -0.04 & 0.20 \\ 0.48 & 13.27 & 0.63 & -0.02 \\ -0.04 & 0.63 & 13.70 & 1.63 \\ 0.20 & -0.02 & 1.63 & 12.45 \end{bmatrix}$	$\begin{bmatrix} 45.54 & -3.45 & -25.91 & -1.95 \\ -3.45 & 43.02 & -3.36 & -23.77 \\ -25.91 & -3.36 & \mathbf{303.63} & -313.37 \\ -1.95 & -23.77 & -313.37 & \mathbf{386.18} \end{bmatrix}$	$\begin{bmatrix} 3.11 & -1.85 & 0.24 & 0.03 \\ -1.85 & 3.52 & -1.81 & 0.03 \\ 0.24 & -1.81 & 3.04 & -1.42 \\ 0.03 & 0.03 & -1.42 & 1.37 \end{bmatrix}$
RFS Method for Chain-Like Systems	$\begin{bmatrix} 13.61 & 0 & 0 & 0 \\ 0 & 12.70 & 0 & 0 \\ 0 & 0 & 14.69 & 0 \\ 0 & 0 & 0 & 13.91 \end{bmatrix}$	$\begin{bmatrix} 131.99 & -67.39 & 0 & 0 \\ -67.39 & 91.48 & -24.08 & 0 \\ 0 & -24.08 & \mathbf{352.23} & -328.15 \\ 0 & 0 & -328.15 & \mathbf{328.15} \end{bmatrix}$	$\begin{bmatrix} 2.70 & -1.30 & 0 & 0 \\ -1.30 & 2.72 & -1.42 & 0 \\ 0 & -1.42 & 2.88 & -1.45 \\ 0 & 0 & -1.45 & 1.45 \end{bmatrix}$
Model Updating Method	$\begin{bmatrix} 13.47 & 0.48 & -0.03 & 0.19 \\ 0.48 & 13.09 & 0.63 & -0.01 \\ -0.22 & 0.88 & 13.17 & 1.51 \\ 0.16 & -0.00 & 1.56 & 12.02 \end{bmatrix}$	$\begin{bmatrix} 45.54 & -3.05 & -25.65 & -2.78 \\ -26.78 & 50.26 & 7.91 & -30.69 \\ 18.20 & -59.00 & \mathbf{290.68} & -278.81 \\ -12.00 & 40.20 & -264.02 & \mathbf{309.19} \end{bmatrix}$	$\begin{bmatrix} 3.11 & -1.85 & 0.24 & 0.03 \\ -1.79 & 3.44 & -1.78 & 0.03 \\ 0.17 & -1.58 & 2.80 & -1.33 \\ -0.01 & -0.07 & -1.17 & 1.23 \end{bmatrix}$
Sub-Space Method	$\begin{bmatrix} 14.67 & 0.01 & 0.02 & -0.75 \\ -0.01 & 14.33 & 0.03 & 0.02 \\ 0.02 & 0.47 & 14.80 & 1.03 \\ -0.14 & -0.33 & 0.59 & 13.54 \end{bmatrix}$	$\begin{bmatrix} 72.37 & -16.02 & -90.74 & 55.60 \\ -24.14 & 41.57 & 17.06 & -33.18 \\ -17.62 & -39.37 & \mathbf{419.28} & -409.60 \\ 15.36 & 36.53 & -378.25 & \mathbf{425.72} \end{bmatrix}$	$\begin{bmatrix} 3.44 & -2.08 & 0.35 & -0.03 \\ -2.09 & 3.92 & -2.10 & 0.10 \\ 0.35 & -2.05 & 3.45 & -1.65 \\ -0.07 & 0.10 & -1.65 & 1.57 \end{bmatrix}$
Iterative PEM Method	$\begin{bmatrix} 14.67 & -0.37 & -0.38 & -0.19 \\ -0.08 & 14.59 & 0.19 & 0.05 \\ 0.48 & 0.07 & 15.53 & -0.32 \\ -0.27 & 0.19 & 0.43 & 14.50 \end{bmatrix}$	$\begin{bmatrix} 9.72 & 44.68 & -78.85 & 30.51 \\ 17.40 & -22.12 & 71.58 & -60.23 \\ -41.37 & -5.38 & \mathbf{319.90} & -340.25 \\ -6.89 & 34.06 & -332.61 & \mathbf{394.66} \end{bmatrix}$	$\begin{bmatrix} 3.42 & -2.09 & 0.25 & 0.06 \\ -2.01 & 3.77 & -1.95 & 0.05 \\ 0.26 & -1.96 & 3.56 & -1.78 \\ -0.05 & 0.14 & -1.78 & 1.66 \end{bmatrix}$

Table A.5: Identified mass, damping, and stiffness matrices of the system: Case 4

Method \ Matrix	**M**	**C**	$\mathbf{K}_{(\times 10^{-5})}$
Linear System Method	$\begin{bmatrix} 13.72 & 0.53 & -0.14 & 0.37 \\ 0.55 & 13.00 & 0.67 & -0.12 \\ -0.43 & 1.06 & 13.17 & 2.27 \\ 0.27 & -0.16 & 1.43 & 10.84 \end{bmatrix}$	$\begin{bmatrix} 54.46 & -9.98 & -36.75 & 12.84 \\ -32.06 & 52.49 & 15.33 & -46.34 \\ 25.80 & -84.01 & \mathbf{326.03} & -295.32 \\ -19.19 & 55.89 & -295.02 & \mathbf{323.97} \end{bmatrix}$	$\begin{bmatrix} 3.17 & -1.85 & 0.16 & 0.08 \\ -1.75 & 3.39 & -1.70 & -0.01 \\ 0.10 & -1.47 & 2.62 & -1.22 \\ 0.03 & -0.14 & -1.01 & 1.12 \end{bmatrix}$
Sym. Linear System Method	$\begin{bmatrix} 13.72 & 0.53 & -0.14 & 0.37 \\ 0.53 & 13.26 & 0.67 & -0.14 \\ -0.14 & 0.67 & 13.68 & 2.53 \\ 0.37 & -0.14 & 2.53 & 11.93 \end{bmatrix}$	$\begin{bmatrix} 54.46 & -9.98 & -36.75 & 12.84 \\ -9.98 & 47.69 & 1.55 & -38.42 \\ -36.75 & 1.55 & \mathbf{337.10} & -342.98 \\ 12.84 & -38.42 & -342.98 & \mathbf{424.73} \end{bmatrix}$	$\begin{bmatrix} 3.17 & -1.85 & 0.16 & 0.08 \\ -1.85 & 3.50 & -1.74 & -0.02 \\ 0.16 & -1.74 & 2.93 & -1.33 \\ 0.08 & -0.02 & -1.33 & 1.33 \end{bmatrix}$
RFS Method for Chain-Like Systems	$\begin{bmatrix} 13.60 & 0 & 0 & 0 \\ 0 & 12.74 & 0 & 0 \\ 0 & 0 & 14.68 & 0 \\ 0 & 0 & 0 & 13.67 \end{bmatrix}$	$\begin{bmatrix} 119.17 & -59.31 & 0 & 0 \\ -59.31 & 80.42 & -21.11 & 0 \\ 0 & -21.11 & \mathbf{397.79} & -376.68 \\ 0 & 0 & -376.68 & \mathbf{376.68} \end{bmatrix}$	$\begin{bmatrix} 2.73 & -1.32 & 0 & 0 \\ -1.32 & 2.76 & -1.44 & 0 \\ 0 & -1.44 & 2.95 & -1.51 \\ 0 & 0 & -1.51 & 1.51 \end{bmatrix}$
Model Updating Method	$\begin{bmatrix} 13.73 & 0.53 & -0.13 & 0.34 \\ 0.56 & 12.99 & 0.66 & -0.13 \\ -0.43 & 1.07 & 13.17 & 2.28 \\ 0.27 & -0.16 & 1.44 & 10.84 \end{bmatrix}$	$\begin{bmatrix} 54.92 & -9.71 & -34.79 & 10.80 \\ -31.46 & 51.52 & 15.28 & -46.07 \\ 25.58 & -83.75 & \mathbf{327.39} & -295.90 \\ -18.87 & 54.36 & -293.76 & \mathbf{323.73} \end{bmatrix}$	$\begin{bmatrix} 3.18 & -1.85 & 0.17 & 0.07 \\ -1.75 & 3.38 & -1.70 & -0.01 \\ 0.10 & -1.47 & 2.62 & -1.22 \\ 0.03 & -0.14 & -1.01 & 1.12 \end{bmatrix}$
Sub-Space Method	$\begin{bmatrix} 14.86 & 0.13 & 0.27 & -0.42 \\ -0.03 & 14.29 & 0.11 & -0.03 \\ 0.06 & 0.34 & 14.49 & 0.17 \\ -0.19 & -0.16 & 0.43 & 14.30 \end{bmatrix}$	$\begin{bmatrix} 87.93 & -24.87 & -86.41 & 49.44 \\ -27.47 & 45.98 & 22.36 & -42.95 \\ -0.65 & -80.53 & \mathbf{453.49} & -429.76 \\ -22.58 & 85.22 & -394.62 & \mathbf{431.57} \end{bmatrix}$	$\begin{bmatrix} 3.50 & -2.11 & 0.34 & -0.02 \\ -2.08 & 3.89 & -2.04 & 0.07 \\ 0.37 & -1.98 & 3.40 & -1.68 \\ -0.12 & 0.08 & -1.69 & 1.64 \end{bmatrix}$
Iterative PEM Method	$\begin{bmatrix} 14.72 & 0.29 & -0.19 & -0.10 \\ 0.13 & 14.30 & 0.34 & 0.00 \\ 0.25 & 0.82 & 14.96 & 0.02 \\ -0.32 & -0.11 & 1.08 & 14.06 \end{bmatrix}$	$\begin{bmatrix} 44.01 & -7.69 & -23.05 & 1.12 \\ -15.72 & 41.06 & -18.23 & -11.80 \\ -2.17 & -70.85 & \mathbf{395.98} & -386.26 \\ -8.31 & 50.06 & -375.62 & \mathbf{419.98} \end{bmatrix}$	$\begin{bmatrix} 3.45 & -2.05 & 0.23 & 0.06 \\ -2.05 & 3.84 & -1.98 & 0.04 \\ 0.36 & -1.94 & 3.38 & -1.68 \\ -0.15 & 0.08 & -1.52 & 1.51 \end{bmatrix}$

Table A.6: Identified mass, damping, and stiffness matrices of the system, using partial instrumentation recordings: Case 1

Method \ Matrix	**M**	**C**	$\mathbf{K}_{(\times 10^{-5})}$
Linear System Method	$\begin{bmatrix} 9.00 & 1.00 \\ 0.85 & 12.83 \end{bmatrix}$	$\begin{bmatrix} \mathbf{243.18} & -199.32 \\ -191.80 & \mathbf{236.73} \end{bmatrix}$	$\begin{bmatrix} 1.10 & -0.84 \\ -1.45 & 1.40 \end{bmatrix}$
Sym. Linear System Method	$\begin{bmatrix} 9.00 & 1.00 \\ 1.00 & 10.77 \end{bmatrix}$	$\begin{bmatrix} \mathbf{243.18} & -199.32 \\ -199.32 & \mathbf{222.34} \end{bmatrix}$	$\begin{bmatrix} 1.10 & -0.84 \\ -0.84 & 0.86 \end{bmatrix}$
RFS Method for Chain-Like Systems	$\begin{bmatrix} 14.93 & 0.00 \\ 0.00 & 13.65 \end{bmatrix}$	$\begin{bmatrix} \mathbf{296.55} & -227.11 \\ -227.11 & \mathbf{227.11} \end{bmatrix}$	$\begin{bmatrix} 1.64 & -1.29 \\ -1.29 & 1.29 \end{bmatrix}$
Model Updating Method	$\begin{bmatrix} 9.02 & 0.96 \\ 0.84 & 12.88 \end{bmatrix}$	$\begin{bmatrix} \mathbf{250.66} & -194.03 \\ -192.14 & \mathbf{233.61} \end{bmatrix}$	$\begin{bmatrix} 1.11 & -0.85 \\ -1.46 & 1.41 \end{bmatrix}$
Sub-Space Method	$\begin{bmatrix} 14.77 & -3.04 \\ 0.34 & 11.33 \end{bmatrix}$	$\begin{bmatrix} \mathbf{276.80} & -274.35 \\ -177.99 & \mathbf{213.74} \end{bmatrix}$	$\begin{bmatrix} 2.36 & -1.91 \\ -1.35 & 1.29 \end{bmatrix}$
Iterative PEM Method	$\begin{bmatrix} 17.70 & 0.10 \\ 0.26 & 14.68 \end{bmatrix}$	$\begin{bmatrix} \mathbf{322.95} & -290.92 \\ -221.23 & \mathbf{269.75} \end{bmatrix}$	$\begin{bmatrix} 2.38 & -1.86 \\ -1.77 & 1.69 \end{bmatrix}$

Table A.7: Identified mass, damping, and stiffness matrices of the system, using partial instrumentation recordings: Case 2

Method \ Matrix	**M**	**C**	$\mathbf{K}_{(\times 10^{-5})}$
Linear System Method	$\begin{bmatrix} 9.55 & 1.38 \\ 1.01 & 12.41 \end{bmatrix}$	$\begin{bmatrix} \mathbf{302.81} & -278.96 \\ -252.23 & \mathbf{320.27} \end{bmatrix}$	$\begin{bmatrix} 1.16 & -0.89 \\ -1.36 & 1.34 \end{bmatrix}$
Sym. Linear System Method	$\begin{bmatrix} 9.55 & 1.38 \\ 1.38 & 11.17 \end{bmatrix}$	$\begin{bmatrix} \mathbf{302.81} & -278.96 \\ -278.96 & \mathbf{317.53} \end{bmatrix}$	$\begin{bmatrix} 1.16 & -0.89 \\ -0.89 & 0.92 \end{bmatrix}$
RFS Method for Chain-Like Systems	$\begin{bmatrix} 14.78 & 0.00 \\ 0.00 & 13.70 \end{bmatrix}$	$\begin{bmatrix} \mathbf{369.14} & -307.79 \\ -307.79 & \mathbf{307.79} \end{bmatrix}$	$\begin{bmatrix} 1.76 & -1.40 \\ -1.40 & 1.40 \end{bmatrix}$
Model Updating Method	$\begin{bmatrix} 9.56 & 1.38 \\ 1.00 & 12.44 \end{bmatrix}$	$\begin{bmatrix} \mathbf{303.96} & -279.68 \\ -252.59 & \mathbf{320.79} \end{bmatrix}$	$\begin{bmatrix} 1.17 & -0.90 \\ -1.37 & 1.34 \end{bmatrix}$
Sub-Space Method	$\begin{bmatrix} 15.89 & -0.08 \\ -0.25 & 12.10 \end{bmatrix}$	$\begin{bmatrix} \mathbf{299.48} & -315.93 \\ -247.97 & \mathbf{315.58} \end{bmatrix}$	$\begin{bmatrix} 2.20 & -1.75 \\ -1.50 & 1.45 \end{bmatrix}$
Iterative PEM Method	$\begin{bmatrix} 17.43 & 0.18 \\ 0.07 & 15.09 \end{bmatrix}$	$\begin{bmatrix} \mathbf{372.44} & -374.36 \\ -304.21 & \mathbf{391.21} \end{bmatrix}$	$\begin{bmatrix} 2.40 & -1.89 \\ -1.83 & 1.76 \end{bmatrix}$

Table A.8: Identified mass, damping, and stiffness matrices of the system, using partial instrumentation recordings: Case 3

Method \ Matrix	**M**	**C**	$\mathbf{K}_{(\times 10^{-5})}$
Linear System Method	$\begin{bmatrix} 9.60 & 1.02 \\ 1.10 & 12.64 \end{bmatrix}$	$\begin{bmatrix} \mathbf{323.17} & -298.93 \\ -309.31 & \mathbf{371.76} \end{bmatrix}$	$\begin{bmatrix} 1.03 & -0.79 \\ -1.32 & 1.30 \end{bmatrix}$
Sym. Linear System Method	$\begin{bmatrix} 9.60 & 1.02 \\ 1.02 & 11.36 \end{bmatrix}$	$\begin{bmatrix} \mathbf{323.17} & -298.93 \\ -298.93 & \mathbf{343.00} \end{bmatrix}$	$\begin{bmatrix} 1.03 & -0.79 \\ -0.79 & 0.82 \end{bmatrix}$
RFS Method for Chain-Like Systems	$\begin{bmatrix} 15.88 & 0.00 \\ 0.00 & 13.78 \end{bmatrix}$	$\begin{bmatrix} \mathbf{437.65} & -377.82 \\ -377.82 & \mathbf{377.82} \end{bmatrix}$	$\begin{bmatrix} 1.70 & -1.33 \\ -1.33 & 1.33 \end{bmatrix}$
Model Updating Method	$\begin{bmatrix} 9.85 & 0.95 \\ 1.03 & 12.74 \end{bmatrix}$	$\begin{bmatrix} \mathbf{346.98} & -315.60 \\ -302.65 & \mathbf{363.48} \end{bmatrix}$	$\begin{bmatrix} 1.03 & -0.78 \\ -1.34 & 1.32 \end{bmatrix}$
Sub-Space Method	$\begin{bmatrix} 16.53 & 0.32 \\ 0.46 & 15.10 \end{bmatrix}$	$\begin{bmatrix} \mathbf{457.98} & -430.65 \\ -374.14 & \mathbf{442.64} \end{bmatrix}$	$\begin{bmatrix} 1.86 & -1.45 \\ -1.70 & 1.65 \end{bmatrix}$
Iterative PEM Method	$\begin{bmatrix} 16.81 & 0.38 \\ 0.25 & 16.07 \end{bmatrix}$	$\begin{bmatrix} \mathbf{442.44} & -438.23 \\ -432.21 & \mathbf{512.71} \end{bmatrix}$	$\begin{bmatrix} 1.81 & -1.40 \\ -1.84 & 1.79 \end{bmatrix}$

Table A.9: Identified mass, damping, and stiffness matrices of the system, using partial instrumentation recordings: Case 4

Method \ Matrix	**M**	**C**	$\mathbf{K}_{(\times 10^{-5})}$
Linear System Method	$\begin{bmatrix} 10.56 & 1.72 \\ 1.10 & 11.72 \end{bmatrix}$	$\begin{bmatrix} \mathbf{356.80} & -346.07 \\ -331.42 & \mathbf{393.60} \end{bmatrix}$	$\begin{bmatrix} 1.21 & -0.93 \\ -1.19 & 1.19 \end{bmatrix}$
Sym. Linear System Method	$\begin{bmatrix} 10.56 & 1.72 \\ 1.72 & 11.34 \end{bmatrix}$	$\begin{bmatrix} \mathbf{356.80} & -346.07 \\ -346.07 & \mathbf{389.24} \end{bmatrix}$	$\begin{bmatrix} 1.21 & -0.93 \\ -0.93 & 0.97 \end{bmatrix}$
RFS Method for Chain-Like Systems	$\begin{bmatrix} 15.04 & 0.00 \\ 0.00 & 13.59 \end{bmatrix}$	$\begin{bmatrix} \mathbf{454.52} & -404.18 \\ -404.18 & \mathbf{404.18} \end{bmatrix}$	$\begin{bmatrix} 1.73 & -1.37 \\ -1.37 & 1.37 \end{bmatrix}$
Model Updating Method	$\begin{bmatrix} 10.57 & 1.70 \\ 1.09 & 11.76 \end{bmatrix}$	$\begin{bmatrix} \mathbf{356.71} & -345.17 \\ -331.40 & \mathbf{393.89} \end{bmatrix}$	$\begin{bmatrix} 1.22 & -0.94 \\ -1.20 & 1.20 \end{bmatrix}$
Sub-Space Method	$\begin{bmatrix} 15.98 & 0.02 \\ -0.48 & 12.01 \end{bmatrix}$	$\begin{bmatrix} \mathbf{365.85} & -405.81 \\ -340.41 & \mathbf{411.16} \end{bmatrix}$	$\begin{bmatrix} 2.15 & -1.73 \\ -1.45 & 1.41 \end{bmatrix}$
Iterative PEM Method	$\begin{bmatrix} 17.11 & 0.27 \\ 0.21 & 15.05 \end{bmatrix}$	$\begin{bmatrix} \mathbf{449.51} & -481.20 \\ -405.32 & \mathbf{495.60} \end{bmatrix}$	$\begin{bmatrix} 2.29 & -1.83 \\ -1.72 & 1.68 \end{bmatrix}$

Table A.10: Identified frequencies and damping ratios: Case 0

Method \ Mode	$f_1(Hz)$	$\zeta_1(\%)$	$f_2(Hz)$	$\zeta_2(\%)$	$f_3(Hz)$	$\zeta_3(\%)$	$f_4(Hz)$	$\zeta_4(\%)$
Linear System Method	5.62	1.623	16.70	1.324	26.56	1.165	35.89	0.765
Sym. Linear System Method	5.72	2.024	16.51	1.479	26.81	1.083	35.73	0.759
RFS Method for Chain-Like Systems	5.70	0.279	17.66	0.740	26.18	0.998	32.82	1.564
Model Updating Method	5.62	1.604	16.69	1.369	26.57	1.141	35.90	0.771
Sub-Space Method	5.65	1.768	16.65	1.114	26.54	1.065	35.83	0.629
Iterative PEM Method	5.64	1.497	16.58	0.781	26.38	0.794	35.75	0.560

Table A.11: Identified frequencies and damping ratios: Case 1

Method \ Mode	$f_1(Hz)$	$\zeta_1(\%)$	$f_2(Hz)$	$\zeta_2(\%)$	$f_3(Hz)$	$\zeta_3(\%)$	$f_4(Hz)$	$\zeta_4(\%)$
Linear System Method	5.37	1.920	16.45	3.326	25.93	6.148	35.34	2.802
Sym. Linear System Method	5.46	1.629	16.38	3.856	26.09	7.093	35.39	2.724
RFS Method for Chain-Like Systems	5.45	0.867	16.25	4.109	23.93	7.443	30.03	5.073
Model Updating Method	5.39	1.891	16.46	3.348	25.92	6.125	35.32	2.809
Sub-Space Method	5.42	1.878	16.43	3.266	26.07	7.163	35.27	2.577
Iterative PEM Method	5.38	1.714	16.47	3.225	25.93	5.077	35.39	2.680

Table A.12: Identified frequencies and damping ratios: Case 2

Method \ Mode	$f_1(Hz)$	$\zeta_1(\%)$	$f_2(Hz)$	$\zeta_2(\%)$	$f_3(Hz)$	$\zeta_3(\%)$	$f_4(Hz)$	$\zeta_4(\%)$
Linear System Method	5.49	2.393	16.59	4.280	25.58	9.233	35.01	4.151
Sym. Linear System Method	5.50	1.690	16.53	5.706	25.84	10.256	35.42	3.741
RFS Method for Chain-Like Systems	5.56	0.807	16.71	3.914	24.76	8.530	30.65	5.310
Model Updating Method	5.44	2.380	16.56	4.287	25.56	9.246	34.99	4.149
Sub-Space Method	5.36	2.700	16.58	4.408	25.67	8.953	34.91	3.216
Iterative PEM Method	5.44	2.293	16.56	4.061	25.64	8.410	34.80	3.235

Table A.13: Identified frequencies and damping ratios: Case 3

Method \ Mode	$f_1(Hz)$	$\zeta_1(\%)$	$f_2(Hz)$	$\zeta_2(\%)$	$f_3(Hz)$	$\zeta_3(\%)$	$f_4(Hz)$	$\zeta_4(\%)$
Linear System Method	5.43	2.286	16.49	4.686	25.61	9.751	34.94	4.281
Sym. Linear System Method	5.36	1.824	16.40	5.915	26.16	11.079	35.23	3.836
RFS Method for Chain-Like Systems	5.54	0.885	16.52	4.819	24.36	10.117	29.98	6.074
Model Updating Method	5.42	2.284	16.50	4.694	25.58	9.773	34.93	4.275
Sub-Space Method	5.47	2.361	16.52	4.222	26.14	13.253	34.86	3.897
Iterative PEM Method	5.48	2.146	16.34	4.474	26.00	9.829	33.54	1.073

Table A.14: Identified frequencies and damping ratios: Case 4

Method \ Mode	$f_1(Hz)$	$\zeta_1(\%)$	$f_2(Hz)$	$\zeta_2(\%)$	$f_3(Hz)$	$\zeta_3(\%)$	$f_4(Hz)$	$\zeta_4(\%)$
Linear System Method	5.55	1.974	16.68	5.003	25.60	11.894	34.64	5.119
Sym. Linear System Method	5.50	1.750	16.50	6.248	26.87	13.504	35.18	4.881
RFS Method for Chain-Like Systems	5.54	0.829	16.76	4.897	24.79	11.194	30.09	6.340
Model Updating Method	5.46	2.045	16.68	5.017	25.61	11.895	34.64	5.111
Sub-Space Method	5.42	2.193	16.70	4.296	25.95	13.149	34.59	4.262
Iterative PEM Method	5.45	1.829	16.51	4.776	25.66	11.010	34.63	4.097

Table A.15: Identified frequencies and damping ratios (partial instrumentation): Case 1

Method \ Mode	$f_1(Hz)$	$\zeta_1(\%)$	$f_2(Hz)$	$\zeta_2(\%)$
Linear System Method	5.44	4.751	24.68	14.740
Sym. Linear System Method	5.50	4.489	23.05	16.992
RFS Method for Chain-Like Systems	5.39	3.337	22.10	12.327
Model Updating Method	5.42	5.534	24.70	14.651
Sub-Space Method	5.41	3.206	24.65	10.505
Iterative PEM Method	5.44	3.668	24.68	11.122

Table A.16: Identified frequencies and damping ratios (partial instrumentation): Case 2

Method \ Mode	$f_1(Hz)$	$\zeta_1(\%)$	$f_2(Hz)$	$\zeta_2(\%)$
Linear System Method	5.52	4.446	24.87	19.353
Sym. Linear System Method	5.51	4.273	23.54	22.180
RFS Method for Chain-Like Systems	5.49	2.992	23.03	15.681
Model Updating Method	5.47	4.506	24.93	19.320
Sub-Space Method	5.53	3.803	24.81	13.397
Iterative PEM Method	5.50	4.390	24.86	14.266

Table A.17: Identified frequencies and damping ratios (partial instrumentation): Case 3

Method \ Mode	$f_1(Hz)$	$\zeta_1(\%)$	$f_2(Hz)$	$\zeta_2(\%)$
Linear System Method	5.33	4.232	23.59	22.325
Sym. Linear System Method	5.29	4.996	21.64	24.565
RFS Method for Chain-Like Systems	5.45	2.902	22.04	19.130
Model Updating Method	5.44	4.193	23.37	22.577
Sub-Space Method	5.43	3.329	23.15	19.594
Iterative PEM Method	5.50	4.390	24.86	14.266

Table A.18: Identified frequencies and damping ratios (partial instrumentation): Case 4

Method \ Mode	$f_1(Hz)$	$\zeta_1(\%)$	$f_2(Hz)$	$\zeta_2(\%)$
Linear System Method	5.45	3.888	24.30	24.089
Sym. Linear System Method	5.51	3.630	23.62	26.115
RFS Method for Chain-Like Systems	5.47	2.572	22.73	20.373
Model Updating Method	5.45	3.965	24.36	23.921
Sub-Space Method	5.41	3.346	24.43	17.548
Iterative PEM Method	5.39	3.649	24.50	18.695